

Invited review

Glacial and gully erosion on Mars: A terrestrial perspective

Susan J. Conway ^{a,*}, Frances E.G. Butcher ^b, Tjalling de Haas ^{c,d}, Axel A.J. Deijns ^d, Peter M. Grindrod ^e, Joel M. Davis ^e

^a CNRS, UMR 6112 Laboratoire de Planétologie et Géodynamique, Université de Nantes, France
^b School of Physical Sciences, Open University, Milton Keynes MK7 6AA, UK
^c Department of Geography, Durham University, South Road, Durham DH1 3LE, UK
^d Faculty of Geoscience, Universiteit Utrecht, Heidelberglaan 2, 3584 CS Utrecht, the Netherlands
^e Department of Earth Sciences, The Natural History Museum, Cromwell Road, London SW7 5BD, UK



ARTICLE INFO

Article history:
 Received 30 December 2017
 Received in revised form 22 May 2018
 Accepted 22 May 2018
 Available online 24 May 2018

Keywords:
 Mars
 Martian gullies
 Viscous flow features
 Glacier-like forms
 Liquid water

ABSTRACT

The mid- to high latitudes of Mars host assemblages of landforms consistent with a receding glacial landscape on Earth. These landforms are postulated to have formed >5 Ma under a different climate regime when Mars' orbital obliquity was on average 10° higher than today. Here, we investigate the spatiotemporal relationship between gullies and glacial landforms, both common in the mid-latitudes. Gullies are kilometre-scale landforms with a source alcove, transportation channel, and depositional apron. The glacial landforms comprise (1) extant viscous flow features (VFF) that extend from the base of crater walls into the interior of crater floors and are widely interpreted as debris-covered glaciers containing extant ice, and (2) landforms such as arcuate ridges at the base of crater walls that have been interpreted as relicts of more recent, less extensive glacial advances focussed on crater walls. We measure headwall retreat associated with glacial landforms and date their host-craters to constrain minimum headwall retreat rates. We record headwall retreat rates up to ~10² m My⁻¹ for the youngest suite of glacial landforms, equivalent to erosion rates of wet-based glaciers on Earth and to headwall retreat rates associated with martian bedrock gully systems. We find extensive evidence for a single erosional episode dating 5–10 Ma, which postdates emplacement of the majority of VFF but seems to predate formation of the gullies. We propose that the wet-based glacial episode was associated with glaciation focussed on the crater walls rather than melting of the glacial ice deposits on the crater floors (VFF). This is consistent with our observations of crater wall morphologies, including the presence of arcuate ridges consistent with terrestrial glaciotectionic features that require liquid water to form, textural alteration of the eroded bedrock surface consistent with ice-segregation and frost-shattering, and the presence of downslope pasted-on terrain, tentatively interpreted here as glacial till deposits sourced from glacial erosion of the crater wall. The pasted-on terrain is usually interpreted as a thicker, latitude-dependant mantle located on sloping terrain formed from airfall of ice nucleated on dust, but we suggest that it has been reworked by glaciation and is predominantly glacial in origin. Although our results cannot substantiate that gullies are produced by meltwater, the discovery of this wet glacial event does provide evidence for widespread meltwater generation in Mars' recent history.

© 2018 Elsevier B.V. All rights reserved.

Contents

1.	Introduction	27
1.1.	The distribution of water ice on Mars	27
1.2.	Gullies and their relation to ice on Mars	28
1.3.	Objectives and structure	30
2.	Global distribution and thickness of pasted-on terrain	30
2.1.	Approach	30
2.2.	Pasted-on terrain	31
2.3.	Arcuate ridges and crater interior ice deposits	34
3.	Erosion of crater walls	36
3.1.	Approach	36
3.2.	Headwall retreat rate of glaciers and gullies	38

* Corresponding author.
 E-mail address: susan.conway@univ-nantes.fr (S.J. Conway).

4.	Glacial erosion	40
4.1.	Mechanisms of glacier erosion on earth	40
4.2.	Landscapes of glacial erosion and application to Mars	40
4.3.	Glaciation and erosion rates	45
5.	Gully-glacier interactions on Mars	51
6.	Conclusions	53
	Acknowledgements	53
	References	53

1. Introduction

The martian mid-latitudes are host to a suite of landforms that indicate significant geologically recent (10 s–100 s Ma) surface-atmosphere exchanges of water ice. This study focuses on two of the most common landforms: martian gullies and glacier-like forms. We examine the role they have played in landscape evolution over the last ten to hundreds of millions of years by using statistical analysis of topographic data. In this introduction, we first present a brief overview of the state of knowledge concerning the present and past distribution of ice and related landforms on Mars, then specify how martian gullies fit into this context and finally present the scope of the present study.

1.1. The distribution of water ice on Mars

Water ice is stable and exposed at the surface at the two polar caps of Mars, which each contain a volume of ice similar to the Greenland ice sheet on Earth – $\sim 10^6$ km³ (Plaut et al., 2007; Putzig et al., 2009; Bamber et al., 2013; Levy et al., 2014). Water vapour is contributed to the atmosphere by seasonal sublimation of the north polar cap, which has higher summer temperatures than the southern cap because of its lower altitude and higher atmospheric pressure (e.g., Richardson and Wilson, 2002). It also has a larger part of the water ice cap exposed at the surface compared to the south, where the rest of the surface is partially hidden by a perennial, thin, CO₂ ice layer and by surface debris (e.g., Thomas et al., 2000). Water vapour contributed to the atmosphere is redistributed across the planet and can be deposited as surface frosts down to the mid-latitudes (Svitek and Murray, 1990). Theoretical modelling predicts that ground ice on Mars should exist in diffusive equilibrium with the atmospheric water vapour – it should be cold trapped into the pores of the regolith (Mellon and Jakosky, 1993; Fisher, 2005). This idea is supported by observations from the Neutron and Gamma Ray Spectrometers on Mars Global Surveyor that found abundant hydrogen in the top metre of the regolith down to $\sim 50^\circ$ latitude in both hemispheres, which can be explained by an ice content of 4% to >64% in the regolith (Boynton et al., 2002; Feldman et al., 2004; Jakosky et al., 2005). This geophysical evidence is further supported by the observation of ubiquitous polygonally patterned ground in the same latitudinal band, consistent with thermal contraction cracks formed in ice-cemented soil over annual timescales (Mellon, 1997; Mangold, 2005; Levy et al., 2009a; Schon et al., 2012). A trench dug by the Phoenix lander at 68° N found excess and pore ice centimetres below the surface (as predicted by diffusive equilibrium models; Mellon et al., 2009), newly formed impact craters have exposed water ice in their ejecta at latitudes down to 39° N (Byrne et al., 2009; Dundas et al., 2014), and exposures of almost pure ice in eight ~ 800 -m-high scarps have been found at $\sim 55^\circ$ latitude (Dundas et al., 2018).

The latitude zone hosting ground ice is also an area that is smooth at scales of a kilometre (Kreslavsky and Head, 2000), as measured from elevation data from the Mars Orbiter Laser Altimeter (MOLA). This smoothing is partly attributed to the presence of the latitude-dependent mantle (LDM) – a deposit thought to consist of the remnants of an airfall deposit of ice nucleated on dust, where the dust forms a sublimation lag protecting the remaining deposits from

sublimation. Mustard et al. (2001) and Milliken et al. (2003) found that the LDM exhibited degraded or pitted textures at latitudes between 30 and 50° N and S, this change in texture coinciding with the change in surface roughness found from MOLA data (Kreslavsky and Head, 2000). The surface age of the LDM has been estimated at ~ 0.1 – 5 Ma and decreases in age with increasing latitude (Kostama et al., 2006; Levy et al., 2009b; Schon et al., 2012; Willmes et al., 2012). The LDM generally consists of alternating relatively ice- and dust-rich layers, indicating multiple generations of deposits formed under varying climatic conditions (Schon et al., 2009a). Various surface textures/draping deposits have been grouped under the term LDM, but we will argue below (see also Soare et al., 2017) that not all of these necessarily represent airfall dust-ice deposits. In total, LDM deposits cover 23% of the surface of Mars (Kreslavsky and Head, 2002) and are thought to contain 10^3 – 10^4 km³ of ice (Mustard et al., 2001; Kreslavsky and Head, 2002; Conway and Balme, 2014).

Another significant reservoir of ice on Mars are the viscous flow features (VFF) found in the martian mid-latitudes (e.g., Squyres, 1979; Milliken et al., 2003; Levy et al., 2014). They have a total estimated volume of 4.2×10^5 km³, which is $\sim 20\%$ of the total volume of the polar caps (Levy et al., 2014). We will use VFF as an umbrella term for a range of landforms thought to be similar to debris-covered glaciers on Earth. They include the following (illustrated in Fig. 1):

- Lobate debris aprons (LDA) – these are smooth aprons that extend from and encompass mesas. They can extend several to tens of kilometres from their mesa, and orbital radar observations have confirmed that they can be up to 1 km thick and contain >90% ice (Holt et al., 2008; Plaut et al., 2009). Their ages range from ~ 40 – 500 Ma (e.g., Mangold, 2003; Morgan et al., 2009; Baker et al., 2010; Hartmann et al., 2014) to ~ 1 Ga (e.g., Levy et al., 2007; Baker and Head, 2015; Berman et al., 2015). The LDAs are the largest reservoir of ice among the VFFs (Levy et al., 2014).
- Crater interior ice deposits, including concentric crater fill (CCF) – these deposits fill and smooth-over the floors of impact craters and are ubiquitous in the mid-latitudes (they number >9000; Levy et al., 2014). Levy et al. (2014) estimated that ice thicknesses can range up to 1.7 km. The surface of these fills often expresses lineations either concentric to the crater walls (in this case they are called CCF) or instead oriented in one direction (Dickson et al., 2012), and these orientations vary with latitude (pole-facing 30 – 45° and concentric $>45^\circ$). They have been dated to be as young as 10 Ma (Levy et al., 2009b) and as old as 700 Ma (Fassett et al., 2014). Crater interior ice deposits can cover part or all of the crater floor. Crater interior ice deposits are found in craters 2–72 km in diameter (Dickson et al., 2012) and represent the second largest reservoir of ice of the VFFs.
- Lineated valley fill (LVF) – these infill existing valleys, being particularly abundant near the martian dichotomy boundary. Their longitudinal ridges are thought to represent flow lines or lateral compression from convergence of LDA on opposite valley walls (e.g., Squyres, 1978, 1979; Carr, 2001). Age estimates for LVF are similar to those for LDA: 100–500 Ma (e.g., Morgan et al., 2009). The LVF represents the third largest reservoir of ice among the VFFs.

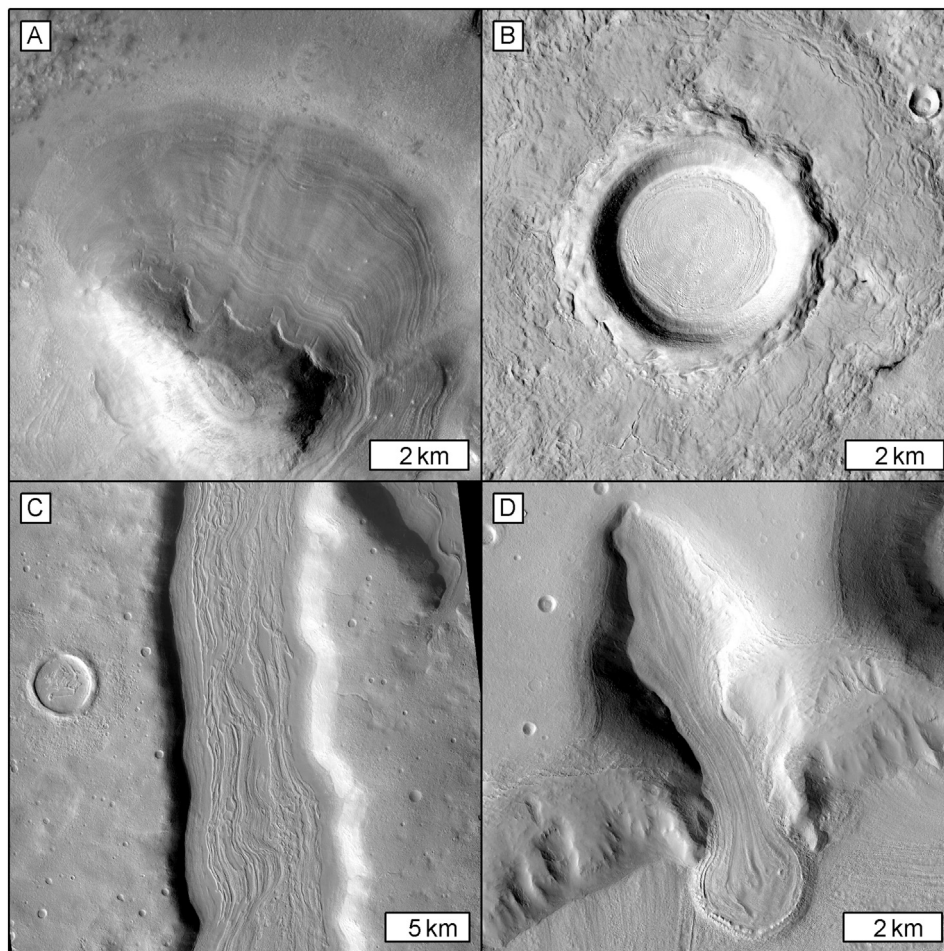


Fig. 1. Viscous flow features on Mars in local sinusoidal projections, north is up in all panels. (A) Lobate debris apron in Deuteronilus Mensae, CTX image F22_044466_2278. (B) Concentric crater fill in Utopia Planitia, CTX image P15_007067_2124. (C) Lineated valley fill in the Arabia Terra region, CTX image F06_038017_2202. (D) Glacier-like form in Protonilus Mensae, CTX image G03_019358_2225.

- GLF, glacier-like-forms – these landforms are the most similar in scale and form to terrestrial valley glaciers (Hubbard et al., 2011; Souness and Hubbard, 2012; Souness et al., 2012; Brough et al., 2016a). They usually originate from large alcoves in escarpments that can be on crater walls, valley walls, or mesas; are laterally confined to a valley/depression; and can extend out onto plains. The GLF are on average ~4 km long and ~1 km wide, and the largest examples are ~35 km long (Souness et al., 2012). We also include in this category lobate forms, such as those described in Milliken et al. (2003), Berman et al. (2009), and Hartmann et al. (2014), which are not topographically confined in their source area. Because of the lack of superposed craters, these landforms are generally assumed to have an age of 10–100 Ma and are thus younger than other VFF (Arfstrom and Hartmann, 2005; Berman et al., 2009; Hartmann et al., 2014; Hepburn et al., 2018).

Apart from occasional radar evidence for water ice under the debris cover of VFFs (Holt et al., 2008; Plaut et al., 2009), evidence for ice content is indirect and includes the presence of ablation textures (fractures, pitted surface, inverted/deformed impact craters, including *ring mold* craters) (Kress and Head, 2008), lineated surface topography thought to represent flow lines (e.g., Brough et al., 2016b), and depositional landforms (e.g., terminal moraines) (Head et al., 2010; Brough et al., 2016b) (Fig. 2). The VFFs are believed to behave like cold-based glaciers on Earth, where the ice is frozen to the bed and the flow is dominated by deformation of mass above by gravity-driven viscous creep (Mangold and Allemand, 2001; Pierce and Crown, 2003; Li et al., 2005; Karlsson et al.,

2015). Only in two locations have eskers been linked to VFF, providing evidence of basal glacial melting (Gallagher and Balme, 2015; Butcher et al., 2017). Rare supraglacial valleys have been attributed to transient supraglacial melting encouraged by focussing of solar radiation onto VFF surfaces from steep adjacent topography (Fassett et al., 2010).

The ice present in the ground (including LDM) and in VFF is believed to be in diffusive equilibrium with the atmosphere, yet insufficient water vapour can be mobilised at the present day to explain the presence of these large ice masses. The formation of VFF and LDM has been attributed to an increase in average orbital obliquity, leading to transfer of large amounts of ice to the mid-latitudes (Levrard et al., 2004, 2007; Madeleine et al., 2009). Mars' present axial obliquity is similar to that of the Earth (25°), but in the past 5 Ma has oscillated between 15° and 30° (with a periodicity of ~100 ka) and from 5 to 10 Ma between 28° and 45° (Laskar and Robutel, 1993; Laskar et al., 2004). Seasonal temperature asymmetries increase with obliquity: at high obliquity, polar regions receive increased insolation and the north polar cap is believed to have been completely destabilised around 4 Ma when the obliquity was on average higher (Levrard et al., 2007). The surface-atmosphere exchange in water ice and CO₂ becomes more intense at higher obliquity, and surface ice and ground ice are predicted to become stable even at equatorial latitudes.

1.2. Gullies and their relation to ice on Mars

The global distribution of martian gullies is spatially correlated with the distribution of water ice landforms described above. Gullies occur

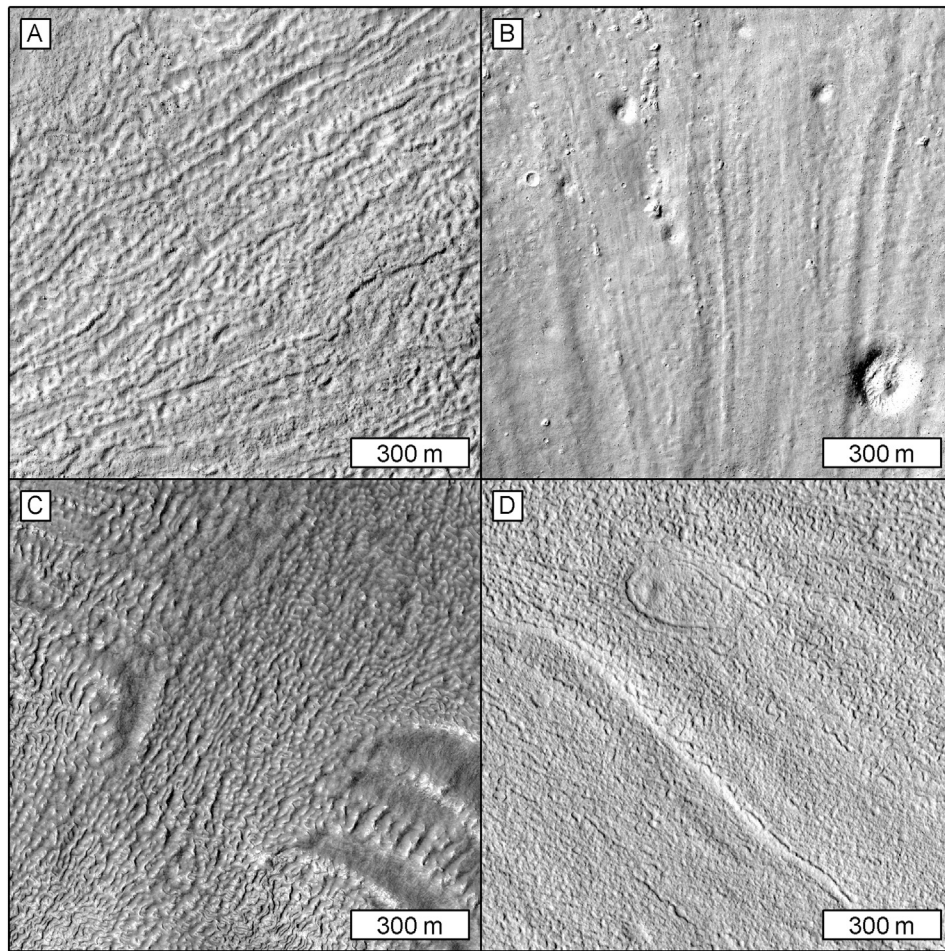


Fig. 2. Surface textures of viscous flow features on Mars at scales of 1:15,000. North is up in all panels and lighting is from the left (west). (A) Surface texture of crater interior ice deposits showing surface lineations comprising alternating discontinuous ridges and chains of elongated pits in HiRISE image ESP_028651_1370. (B) A ring-mold crater (bottom right) on the surface of a crater interior ice-deposit together with muted craters and normal craters, also showing surface lineations in HiRISE image ESP_046308_1425. (C) A lobate debris apron in Deuteronilus Mensae showing typical contorted raised and pitted surface patterns in HiRISE image ESP_018515_2225. (D) Lineated valley fill in the Acheron Fossae region with pitted and cracked textures and a deformed impact crater (the valley is oriented NW-SE) in HiRISE image ESP_016266_2165.

across the same range of latitudes as VFF, but they are less common where high concentrations of LDA and GLF occur and are only found in 12% of craters with interior ice deposits (Conway et al., 2018a). They are strongly linked to the presence of LDM (e.g., Levy et al., 2011; Dickson et al., 2015), although in the case of gullies the textures of this slope-side surficial deposit, into which they incise, are somewhat different to the LDM found in the plains; hence in this contribution we will refer to this unit using the term first coined by Christensen (2003) in relation to martian gullies: *pasted-on terrain*.

Gullies are typically kilometre-scale landforms found on steep slopes in the mid- to high latitudes of both hemispheres ($\sim 30^\circ$ to the polar caps; Harrison et al., 2015; Conway et al., 2017). They comprise a tributary source alcove, transport channel, and depositional apron (Malin and Edgett, 2000). They are found primarily on pole-facing slopes at latitudes between 30° and 40° and then mostly on equator-facing slopes poleward of 40° (but they can also occur on pole-facing slopes in this latitude interval). The relative lack of gullies in regions with no evidence for ground ice (between 30° N and 30° S), and their trends in orientation with latitude have led authors to conclude that changes in orbital obliquity are required to explain their present-day distribution (e.g., Costard et al., 2002; de Haas et al., 2015a). However, the process by which gullies form is under strong debate. Present-day activity in gullies is thought to be brought about via slope instability caused by sublimation of carbon dioxide (Diniaga et al., 2010; Dundas et al., 2010, 2012, 2015, 2017; Raack et al., 2015; Pasquon et al., 2016), and the distribution of surface carbon dioxide ice is strongly controlled by the presence of

(water) ground ice (Vincendon et al., 2010). However, whether such a process alone can explain the formation of the whole landform remains uncertain. In particular, equator-facing slopes at the present-day and in the past are not favourable locations for deposition, and thus sublimation, of CO_2 ice (Conway et al., 2018a). Formation by liquid water is consistent with the morphology and morphometry of gullies (e.g., Malin and Edgett, 2000; Conway and Balme, 2016), yet liquid water is a poor candidate to explain the present-day activity and can only be invoked under certain specific conditions in the past (Costard et al., 2002; Richardson and Mischna, 2005; Williams et al., 2008, 2009). Hence, understanding the interaction of gullies with other landforms in time and space has the potential to break this impasse.

Our knowledge on the timing of the activity and the overall age of gully systems is relatively limited. We know that gullies on martian dunes have such frequent and voluminous activity that their full-extent can be explained on a timescale of hundreds of years (Pasquon et al., 2017). Dundas et al. (2010, 2012) estimated that mid-latitude gullies (not formed in sand but in other materials, including bedrock and mantling materials) could be formed within the last few millions of years given the currently observed magnitude and frequency of their activity. Non-sand gullies also have morphological evidence for multiple episodes of activity – in one case authors have ascertained the age of part of a gully fan where other parts of the fan pre- and post-date the determined age of ~ 1.25 Ma (Schon et al., 2009b). Dickson et al. (2015) found common evidence of relict gullies, being exhumed from and buried by LDM (pasted-on terrain), showing that gully activity

must extend into epochs when this deposit was being formed/removed (estimated to be ~0.1–5 Ma; Kostama et al., 2006; Willmes et al., 2012).

De Haas et al. (2015b) found that gully alcoves had a similar size independent of the age of the host crater, and de Haas et al. (2018) proposed that gullies could have their erosion *reset* during glacial epochs. In the youngest craters where gullies are found emanating from well-defined bedrock alcoves cutback into the crater rim, de Haas et al. (2015b) estimated headwall retreat rates of 10^{-4} to 10^{-1} mm y^{-1} , which correspond to the backweathering rates experienced on rockwalls in Arctic, Nordic, and Alpine environments on Earth. De Haas et al. (2018) classed a crater as *glaciated* if it contained one or more of the following morphological features: arcuate ridges and/or spatulate depressions at the foot of the slope (Fig. 3; Arfstrom and Hartmann, 2005; Berman et al., 2005; Head et al., 2008; Hubbard et al., 2011; Jawin et al., 2018), floor-filling CCF indicated by concentric ridges and/or pitted textures within identifiable in-crater deposits (e.g., Levy et al., 2010; Dickson et al., 2012), or crater-scale downslope lobate features that diverge around obstacles on the crater floor and have longitudinal or transverse ridges and/or pitted textures on their surfaces (Fig. 2; e.g., Baker et al., 2010; Head et al., 2010). Several authors (e.g., Berman et al., 2005, 2009; Head et al., 2008; Hauber et al., 2011a; Schon and Head, 2011, 2012; Dickson et al., 2015; de Haas et al., 2018; Jawin et al., 2018) have suggested that these glacial landforms represent different stages of ice-deposition and removal (glacial-interglacial cycles) during martian obliquity cycles. The VFFs were able to form during glacial epochs when average obliquity was higher than today (>5 Ma). Since the last formation of VFF, LDM (pasted-on terrain) was deposited during smaller ice ages, which occurred during obliquity peaks in the present, lower-average obliquity regime (e.g., Mellon and Jakosky, 1995; Head et al., 2003; Madeleine et al., 2014). Many gullies that are present on Mars today have formed into VFF or LDM remnants (e.g., Dickson et al., 2015; de Haas et al., 2018), and thus their formation is strongly linked to VFF and LDM (pasted-on terrain).

Berman et al. (2005) and Head et al. (2008) noted that the rims of craters with arcuate ridges and gullies on their pole-facing walls had a lower elevation than equator-facing walls of the same craters. The model proposed by de Haas et al. (2018) hypothesises that evidence of

gully erosion (alcoves and channels) is removed from crater walls by glacial erosion and/or buried by glacial deposits after sublimation/melting. Further, Levy et al. (2016) estimated that VFF can be responsible for 10^{-5} – 10^{-4} mm y^{-1} of erosion. However, no study to date has attempted to directly assess the amount of erosion associated with the gullies and glacial landforms found on crater walls.

1.3. Objectives and structure

Here we use high resolution topographic data and dating of host craters to assess the amount and rate of erosion that these small-scale crater wall glaciers may have been responsible for and use analogy with glacial systems on Earth to assess by what mechanisms this erosion could have occurred. In our approach we use the consistency and coherence of the landforms and their spatial and topographic properties and relationships to go beyond analogy using the similarity of appearance of single landforms (Baker, 2014, 2017). We also compare to erosion rates in gullied craters without pasted-on terrain to assess whether glaciation is capable of erasing gullies on Mars.

This paper is structured as follows. First, we explore the link between the pasted-on terrain (into which gullies often incise) and glaciation by undertaking a global survey and highlighting key relationships and observations. Second, we undertake a detailed topographic analysis of a small subset of these craters and of gullied craters to ascertain the amount and rate of erosion of their walls and its link to previous glaciation. Third, we consider the morphological and topographical evidence gathered on Mars in light of the present knowledge of glacial erosion on Earth in order to build a coherent picture of the degradation of crater walls on Mars. Finally, we bring together knowledge from the martian literature to assess the consistency of our new hypothesis within the context of previous findings.

2. Global distribution and thickness of pasted-on terrain

2.1. Approach

We performed the majority of our morphological observations on NASA Mars Reconnaissance Orbiter High Resolution Imaging Science

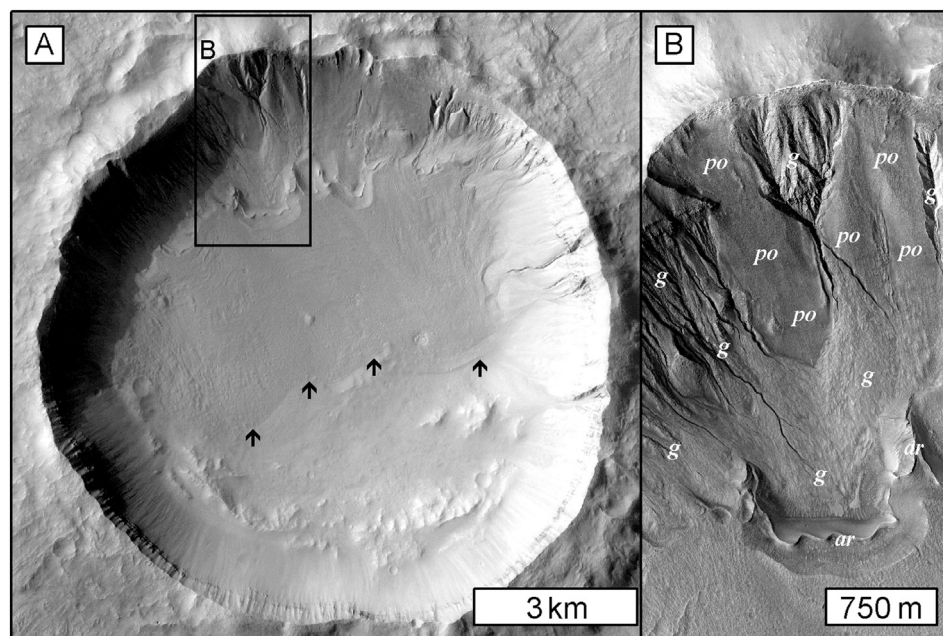


Fig. 3. Niquero Crater on Mars, an example with a crater interior ice deposit, arcuate ridges, pasted-on terrain and gullies. North is up in all panels. (A) Overview of crater in CTX image P03_002383_1417. Arrows indicate the southernmost extent of the crater interior ice-deposit. (B) Detail of gullies (labelled as 'g') and arcuate ridges (labelled as 'ar') within a spatulate depression with the presence of pasted-on terrain labelled as 'po'. HiRISE image ESP_030021_1410.

Experiment (MRO HiRISE) images at 25–50 cm/pixel taken up to April 2017. We used the [Harrison et al. \(2015\)](#) gully-distribution database as the basis for our initial survey, down-selecting to HiRISE images that were in the vicinity of gullies. Within this database we noted the occurrence of arcuate ridges associated with gully incisions and made observations on the nature of the pasted-on deposits associated with the gullies. We also searched for examples of craters without gullies but with pasted-on terrain and/or arcuate ridges by examining craters <10 km from the [Robbins and Hynek \(2012\)](#) database with (projection corrected) slopes of >20° derived from the MOLA-gridded data that had overlapping HiRISE images. We performed a random sample of this data set and many craters that do not have gullies but have pasted-on terrain and/or arcuate ridges will have been missed. Hence, this data set was not used to derive any global distribution statistics but to highlight pertinent relationships.

We recognised arcuate ridges in HiRISE images using the following criteria: a sinuous to highly arcuate ridge located at the foot of the crater wall and somewhat parallel to the crater rim ([Fig. 4A–C](#)). We identified pasted-on terrain as being a draping unit that smoothed the appearance of the crater wall at scales of ~1:25,000 with an upper lobate boundary ([Fig. 4D–F](#)). Gullies incised into this unit have a distinctive V-shaped cross section in their mid-section, and these gullies are often completely sourced within this unit, having a simple single elongate incision ([Fig. 4E](#); [Aston et al., 2011](#); [Conway and Balme, 2014](#)). It is worth noting that not all gullies have such V-shaped incisions. We previously performed measurements on HiRISE digital terrain models (DTM) and determined that the slopes of these incisions were on average 20° and ranged between 15° and 30° ([Conway and Balme, 2014](#)). Assuming a

20° slope, these incisions can be used as an estimate of the minimum depth of the pasted-on terrain simply by measuring the wall-length of the incision ([Conway et al., 2015](#)). We undertook a systematic survey of the incision wall-lengths in our HiRISE database in order to assess any trends in the thickness of pasted-on deposits with latitude. For craters hosting multiple gully systems, we measured the deepest incision because the depth of this incision should be closest to the total thickness of the pasted-on terrain.

2.2. Pasted-on terrain

The surface texture of the pasted-on terrain often appears smooth and uniform at scales of ~1:25,000, yet at scales of ~1:5000 or less we were able to identify three principal textures: downslope lineated ([Fig. 5A](#)), smooth ([Fig. 5B](#)) and polygonised ([Fig. 5C](#)). Polygonal textures were more often most clearly expressed within the gully incisions, as previously noted in the literature ([Levy et al., 2009c](#); [Soare et al., 2014](#)) ([Fig. 5D](#)). As noted by [Conway and Balme \(2014\)](#), the lineations are cut by the gully incisions ([Fig. 5E](#)) and fresh incision walls have no polygonal textures and sharp breaks in slope, whereas incisions with polygonal textures are shallower and have a more subdued break in slope ([Fig. 5F](#)). We found that the pasted-on terrain is systematically associated with a change in the appearance of the crater rim compared to the opposite crater rim ([Fig. 6F vs. I](#)) and compared to crater rims of fresh equatorial craters ([Watters et al., 2015](#); [Tornabene et al., 2018](#)) ([Fig. 6F vs. D, G](#)). Bedrock is often exposed in the top few hundred metres of crater walls and is particularly evident in young impact craters ([Fig. 6D, G](#)). It usually appears as a series of sub parallel relatively

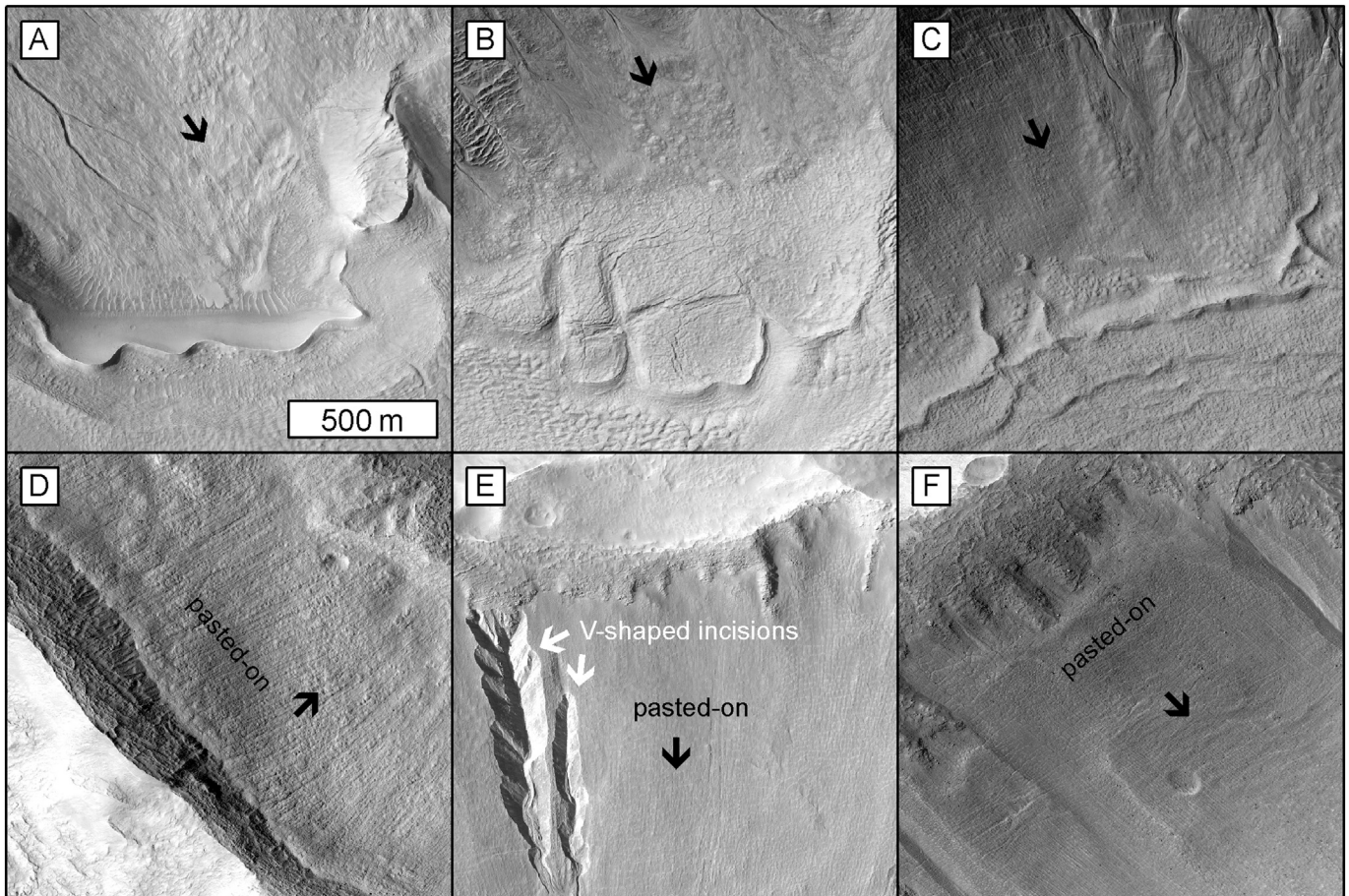


Fig. 4. Recognition of arcuate ridges and pasted-on terrain in HiRISE images at 1:25,000, north is up in all panels, the downslope-direction is indicated by the black arrows and the scale for all panels is as indicated in panel (A). (A–C) Arcuate ridges in HiRISE images: ESP_038236_1410, ESP_023809_1415 and ESP_020051_1420. (D–F) Pasted-on terrain in HiRISE images: ESP_027477_2170, ESP_038236_1410, and ESP_013858_1405. Note in panel (E) the sharply incised gullies with V-shaped incisions to the left of the panel, where the right-hand one of the pair is completely within the pasted-on terrain.

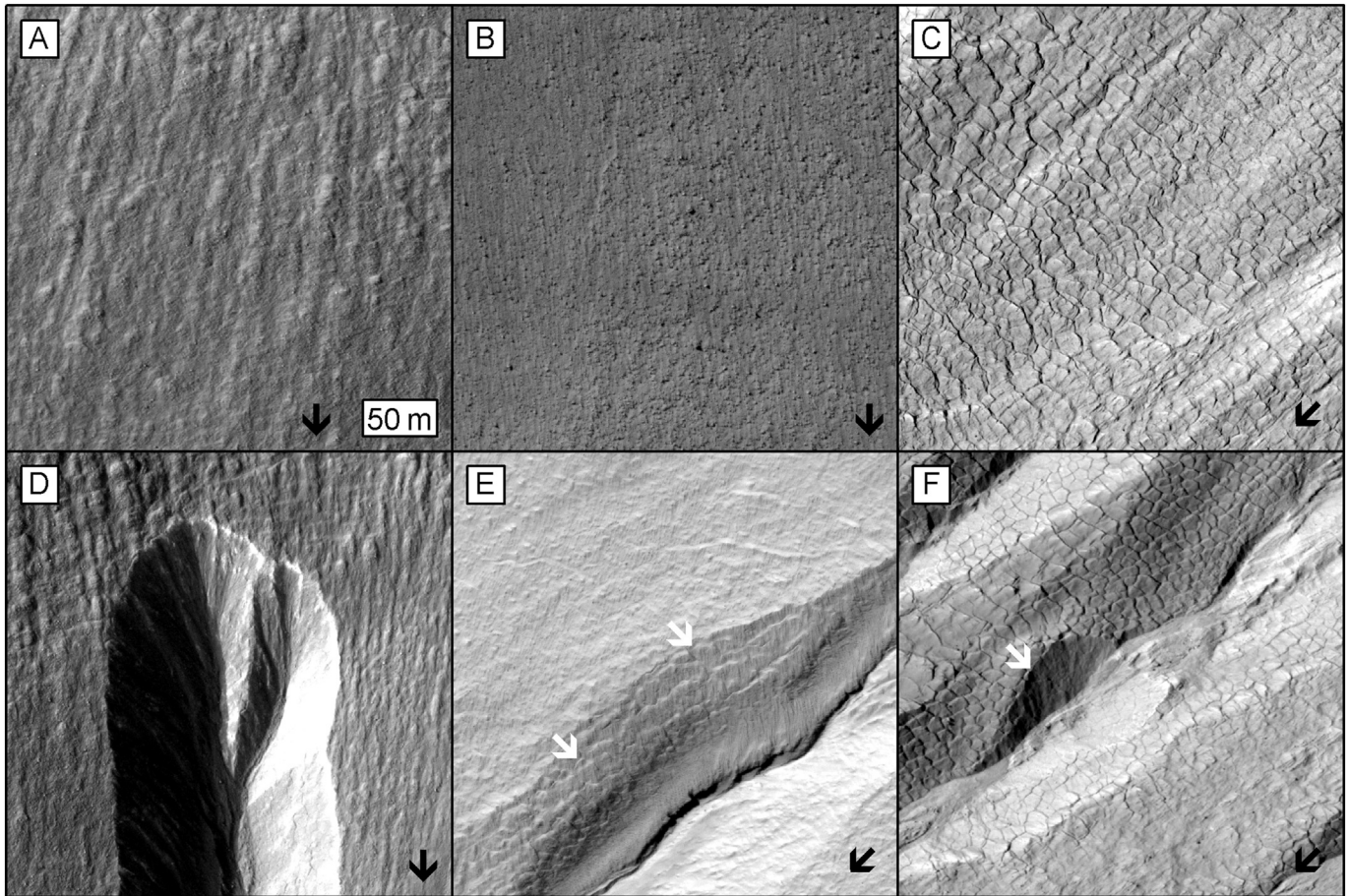


Fig. 5. Examples of pasted-on terrain textures, each image has the same scale as indicated in panel (A) at 1:5000. Black arrows indicate the downslope direction. (A) Lined texture of the pasted-on terrain on the south-facing wall of Bunnik Crater, HiRISE image PSP_002514_1420. (B) Smooth texture of the pasted-on terrain, with rocks visible at the surface in HiRISE image ESP_033173_1400. (C) Polygonised texture of the pasted-on terrain in HiRISE image ESP_011672_1395. (D) Lined texture of the pasted-on terrain cut by gully incision in Bunnik Crater, where polygons are weakly visible in the sun-facing wall of the incision, HiRISE image PSP_002514_1420. (E) Polygons visible inside the gully incision (white arrows) but not on the surrounding pasted-on terrain in HiRISE image ESP_033173_1400. (F) Sharp gully incision whose walls are not polygonised cutting through the polygonised pasted-on terrain (white arrow). Polygonal patterns are again present on more gently sloping incisions. HiRISE image ESP_011672_1395.

massive beds and, particularly in fresh equatorial impact craters, displays a *spur-and-gully* morphology with a series of regularly spaced shallow alcoves. The rim crest of these craters remains relatively linear despite the presence of these alcoves (Fig. 6D, G). In comparison, the crater wall immediately above the upslope boundary of pasted-on terrain does not have a spur-and-gully morphology but is rather planar with a distinctive *mottled* texture (we refer to this as *texturally altered bedrock* in the rest of this paper Fig. 6F). The rock exposure is rather patchy with no clear massive bedrock outcrop, and the surface is often dominated by loose-appearing metre- to decametre-scale boulders. Discontinuous rim-parallel lineations (Fig. 6F) are sometimes apparent with no clear relationship to the underlying bedrock structure. Where texturally altered bedrock is present, the crater rim has very little deviation from circular in planform (Fig. 6C), and sometimes the crest is sharp while it can also be rounded (Fig. 6J, K), particularly in older craters. This texture has been previously associated with erosion of crater walls (diameter <35 km) by lobate debris aprons in Alba Mons by Sinha and Vijayan (2017). This contrasts with the appearance of the rims of craters with gullies and no pasted-on terrain, which maintain the massive bedrock appearance, and have rim-traces that are crenulated with greatly accentuated spur-and-gully morphology compared to unmodified crater walls as noted in de Haas et al. (2015b, 2018) (Fig. 6B, E).

The pasted-on terrain can be found extending nearly all the way up to the top of the crater rim (Fig. 7A), or only on the lower half of the crater wall (Fig. 7B), or as remnants between extensive gully systems (Fig. 7C).

Pasted-on terrain can be found on the interior (Fig. 7A–C) and exterior crater walls (Fig. 7D) and is almost exclusively associated with an altered texture of the upslope bedrock. In two rare circumstances, texturally altered bedrock is found only on part of the wall with pasted-on terrain (illustrated in Fig. 7F–I). The first of these circumstances involves very young craters (as attested by few superposing impact craters <1 Ma, Table 1), where pasted-on terrain is found in the absence of any other evidence of glaciation (e.g., crater interior ice deposits, arcuate ridges, large lobate tongues, glacial textures) and also occurs without gullies. In the two cases that we found (one in the northern and one in the southern hemisphere; Fig. 7E, F) alcoves in texturally unaltered bedrock are present above some of the pasted-on terrain; but where the pasted-on terrain extends beyond the foot of the crater wall, the alcoves are reduced and textural alteration has occurred. In the second circumstance, pasted-on terrain can extend upward into wide (hundreds of metres) alcoves leaving texturally unaltered bedrock on the spurs separating the alcoves, yet texturally altered bedrock upslope (Fig. 7G). In other places where pasted-on terrain extends into alcoves, the bedrock on the alcove spurs and on the rim-crest are texturally altered as shown in Fig. 7H. In one example we found pasted-on terrain coexisting with terrain hosting textures normally associated with degrading latitude-dependent mantle, namely exposed layers and extensive pitting (e.g., Mustard et al., 2001; Schon et al., 2009a). As shown in Fig. 7I, the pasted-on terrain seems to be emerging from beneath this mantle.

Our global incision survey shows that the thickness of the pasted-on terrain tends to increase with increasing latitude in both hemispheres,

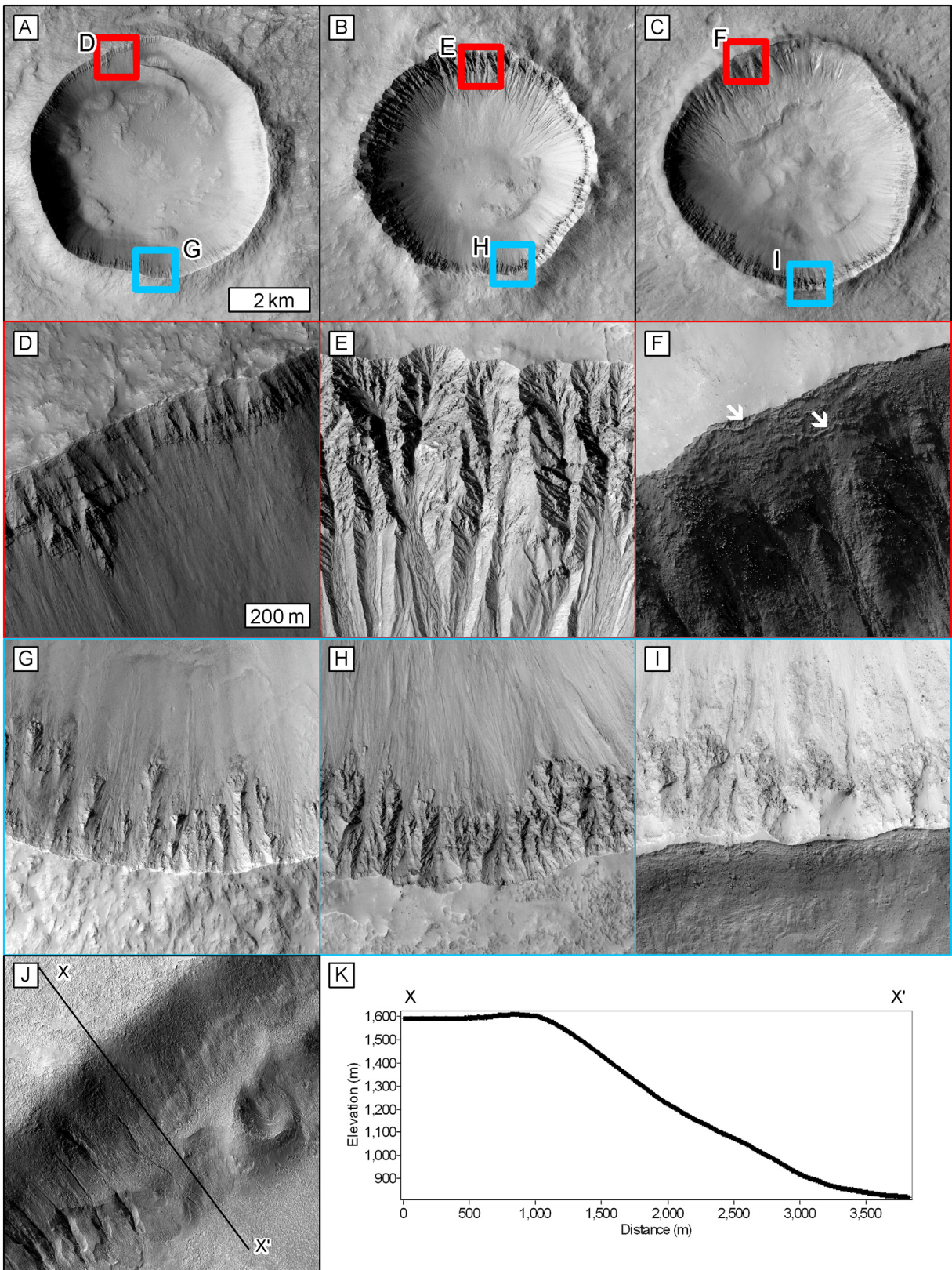


Fig. 6. Rock exposures in fresh equatorial impact craters (left panels), gullied impact craters (middle panels), and craters with pasted-on terrain (right panels). The scale in panels (A–C) is given in panel (A) and is 1:120,000 and the scale in panels (D–I) is given in panel (D) and is 1:15,000. North is up in all panels. All craters are in the southern hemisphere. Red panels show the pole-facing slopes and blue panels show the equator-facing slope. (A, D, G) Kenge Crater, a fresh equatorial crater from the database of Tornabene et al. (2018) in (A) CTX image B07_012315_1635 and (D, G) HiRISE image ESP_011893_1635. (B, E, H) Galap Crater with gullies eroded into the bedrock in (B) CTX image B09_012971_1421 and (E, H) HiRISE image PSP_003939_1420. (C, F, I) Nybyen Crater with pasted-on terrain and gullies in (C) CTX image G09_021563_1427 and (F, I) HiRISE image PSP_006663_1425. Discontinuous ridges are highlighted by white arrows. (J, K) A crater in the Newton Basin with a planed-off rim in (J) HiRISE image PSP_002620_1410 and (K) elevation profile taken from the publicly available DTM DTEEC_002620_1410_002686_1410_A01.

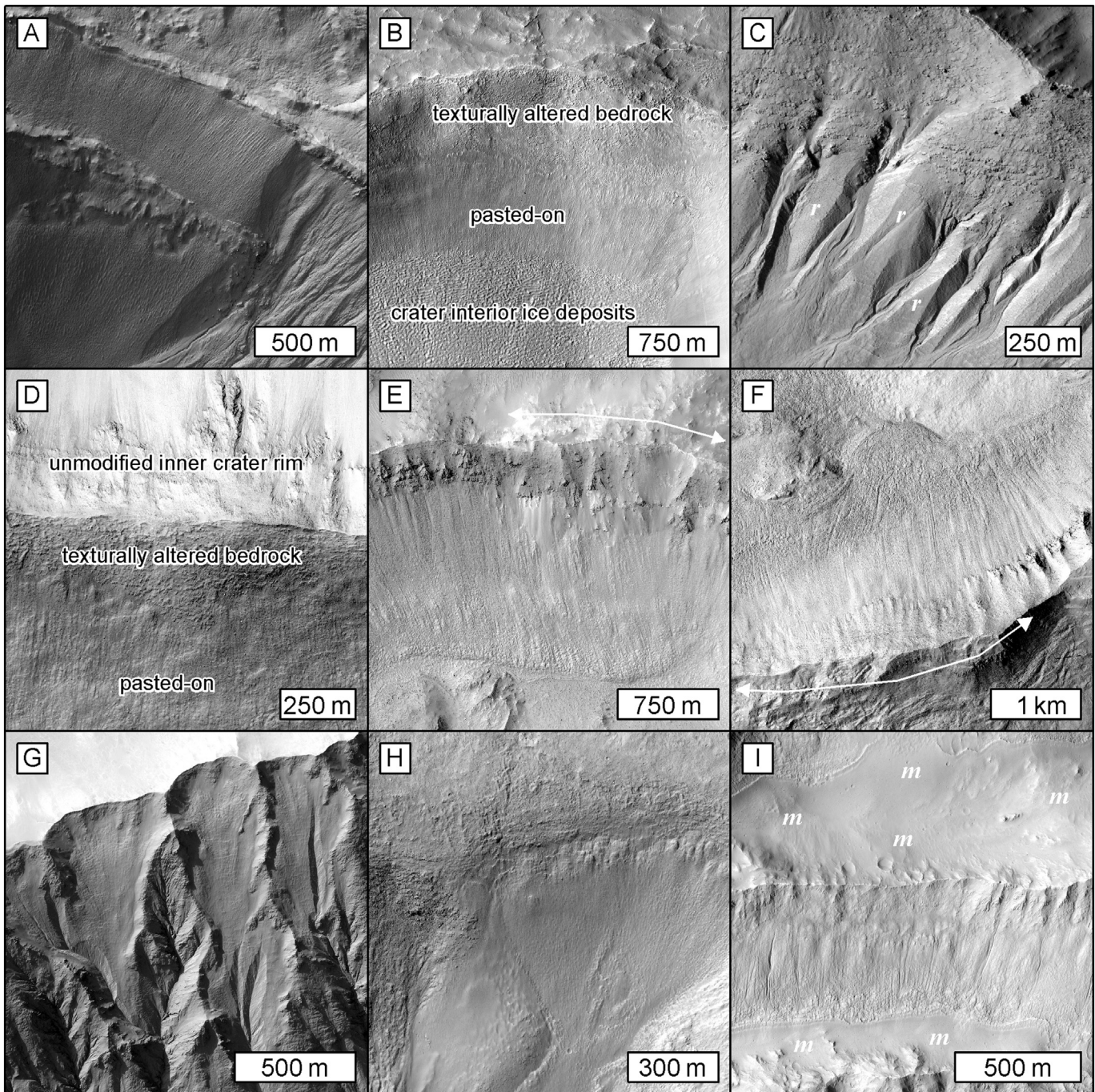


Fig. 7. Configuration of pasted-on terrain within craters on Mars. North is up in all panels. (A) Pasted-on terrain extending to within ~20–50 m of a crater rim in HiRISE image ESP_034363_1380. (B) Pasted-on terrain covering only the lower 1/2–1/3 of the inner crater wall in HiRISE image ESP_038157_1415. (C) Pasted-on terrain as remnants between gully systems (labelled by white 'r') in HiRISE image ESP_011672_1395. (D) Pasted-on terrain on the exterior wall of an impact crater in HiRISE image ESP_023809_1415. (E, F) Pasted-on terrain where only some of the bedrock has been texturally altered above it (extent indicated by arrowed line) and the rest still has alcoves. HiRISE images ESP_014400_1525 and PSP_009164_2140, respectively. (G, H) Pasted-on terrain extending upward into wide alcoves on crater walls and leaving spurs of bedrock with an unmodified texture in panel (G). HiRISE images PSP_006629_1425 and ESP_033398_1420 respectively. (I) Pasted-on terrain that appears to emerge from beneath mantle material (marked by 'm') with degradation textures as described by Mustard et al. (2001) and Schon et al. (2009a), HiRISE image ESP_011839_1460.

from a mean of ~10 m at 28–30° to 40 m at around 60°, with increasing scatter at higher latitudes (Fig. 8). The only difference between the hemispheres in Fig. 8 is that incisions are noted at lower latitudes in the southern hemisphere compared to the northern hemisphere (28°S vs. 32°N). Incision depths are greater in the Argyre Basin than elsewhere (Fig. 9A). Gullies with incisions follow the same spatial distribution as the gully population as a whole (Fig. 9) and form a larger percentage of the overall gully population in the northern hemisphere compared to the southern hemisphere (~100% compared to ~50% respectively; Fig. 9).

The pasted-on terrain, where present with other crater interior ice deposits, gradually transitions in texture and topography into these other bodies, not presenting a single clean delimitation between these units (Figs. 10, 4C, 7B).

2.3. Arcuate ridges and crater interior ice deposits

Fig. 9C shows the latitudinal distribution of the 148 arcuate ridges coexisting with incised gullies. Where ridges are associated with incised

Table 1
Summary of the craters included in this study, elevation data, and their ages.^a

Crater details						Digital terrain model (DTM) information								Dating	
Name	Latitude	Longitud	Diameter (km)	Features	Type	Method	Credit	Image1	Resolution (m)	Image2	Resolution (m)	Convergence (°)	Vertical error (m)	Source	Age
Zumba	28.65°S	226.90°E	3	Talus only	Unmodified	SS	OU	PSP_002118_1510	0.3	PSP_003608_1510	0.28	18.1	0.2	Hartmann et al. (2010), Schon et al. (2012)	(0.1–0.8) Ma
Corintho	16.95°N	141.70°E	14	Talus only	Unmodified	SS	UoA	PSP_003611_1970	0.3	PSP_004244_1970	0.3	18.1	0.2	Golombek et al. (2014b)	(0.1–3.0) Ma
Qara	16.41°N	209.7°E	3	Talus only	Unmodified	SS	UoA	PSP_005837_1965	0.3	PSP_005837_1965	0.32	20.1	0.2	de Haas et al. (2015b)	5.3 (4–8) Ma
Kenge	16.37°S	102.96°E	6	Talus only	Unmodified	SS	LPG	ESP_011893_1635	0.3	ESP_012315_1635	0.27	13.1	0.2	Fig. 12K	12.6 (5–30) Ma
Topola	15.82°N	267.8°E	8.0	Talus only	Unmodified	SS	LPG	ESP_023662_1960	0.6	ESP_023372_1960	0.55	25.5	0.3	Fig. 12J	15 (8–100) Ma
Yelwa	31.11°N	212.39°E	8	Talus only	Unmodified	ASP ²	LPG	ESP_020539_2115	0.6	ESP_020117_2115	0.58	16.7	0.4	Fig. 12D	20 (5–100) Ma
Kilmia	24.09°S	59.50°E	7	Talus only	Unmodified	SS	UoA	ESP_026861_1555	0.3	ESP_027349_1555	0.27	24.4	0.1	Fig. 12Q	1.1 (0.6–3) Ga
Crater A	50.19°N	175.51°E	2	Small bedrock gullies, facing slope	Gullied	SS	UoA	ESP_025366_2305	0.3	ESP_025498_2305	0.35	25.2	0.2	Fig. 12C	0.1 (0.01–0.7) Ma
Istok	45.11°S	274.2°E	5	Bedrock gullies	Gullied	SS	OU	PSP_006837_1345	0.3	PSP_007127_1345	0.26	20.1	0.1	Johnsson et al. (2014)	0.19 (0.1–1.0) Ma
Galap	37.66°S	192.93°E	6	Bedrock gullies	Gullied	SS	OU	PSP_003939_1420	0.3	PSP_003939_1420	0.29	21.7	0.2	de Haas et al. (2015b)	6.5 (5–9) Ma
Jaisalmer	33.47°N	84.15°E	14	Pasted on only, facing slope	Glaciated	SS	NHM	PSP_009098_2140	0.3	PSP_009164_2140	0.32	19	0.2	Fig. 12B	0.5 (0.4–50) Ma
Crater B	27.35°S	59.13°E	7	Pasted-on only, facing slope	Glaciated	SS	NHM	ESP_014400_1525	0.3	ESP_020703_1525	0.27	13.9	0.2	Fig. 12F	2.15 (0.5–15) Ma
Crater C	36.56°N	155.46°E	9	Pasted-on, arcuate ridges, facing slope	Glaciated	SS	NHM	PSP_010559_2170	0.6	ESP_016005_2170	0.6	15.8	0.4	Fig. 12I	2.43 (0.3–5) Ma
Talu	40.3°S	20.1°E	9	Gullies, pasted-on, arcuate ridges, facing slope	Glaciated	SS	OU	ESP_011672_1395	0.3	ESP_011817_1395	0.26	15.7	0.2	de Haas et al. (2018)	13 (10–22) Ma
Nybyen	37.03°S	343.36°E	6.0	Gullies, pasted-on, arcuate ridges, facing slope	Glaciated	SS	UoA	ESP_011436_1425	0.3	PSP_006663_1425	0.25	14.5	0.2	Fig. 12G	110 (5–300) Ma
Taltal	39.5°S	234.4°E	10	Gullies, pasted-on, arcuate ridges, facing slope	Glaciated	SS	LPG	ESP_031259_1400	0.5	ESP_037074_1400	0.5	5.9	1	de Haas et al. (2018)	220 (100–400) Ma
Taltal	39.51°S	234.17°E	10	Gullies, pasted-on, arcuate ridges, facing slope	Glaciated	ASP ¹	LPG	ESP_021989_1400	0.3	ESP_021712_1400	0.25	25.5	0.1	"	"
Dechu	42.24°S	202.19°E	0.0	Gullies, pasted-on, arcuate ridges, facing slope	Glaciated	SS	UoA	ESP_023546_1375	0.6	ESP_023612_1375	0.51	19.4	0.3	Fig. 12D	305 (80–600) Ma
Niquero	38.77°S	193.99°E	10.0	Gullies, pasted-on, arcuate ridges, facing slope	Glaciated	SS	NHM	ESP_030443_1410	0.5	ESP_030021_1410	0.51	23.5	0.3	Fig. 12H	1.3 (0.5–2.5) Ga
Corozal	38.7°S	159.4°E	8.0	Gullies, pasted-on, arcuate ridges, facing slope	Glaciated	SS	UoA	PSP_006261_1410	0.3	ESP_014093_1410	0.29	28.7	0.1	de Haas et al. (2018)	1.4 (0.8–2.5) Ga
Nqutu	37.9°S	169.6°E	20.0	Gullies, pasted-on, arcuate ridges	Glaciated	SS	Birk.	PSP_004085_1420	0.3	PSP_004019_1420	0.25	20.4	0.2	de Haas et al. (2018)	1.8 (1–3.5) Ga

^a Abbreviations: SS = SocetSet, ASP = Ames Stereo Pipeline, LPG = Laboratoire de Planétologie et Géodynamique, Birk. = Birkbeck University of London, NHM = Natural History Museum, London, UoA = University of Arizona, OU = Open University. In the method column 1 denotes that the ASP DTM was adjusted to HRSC H4234_0000 and 2 to H1525_0001.

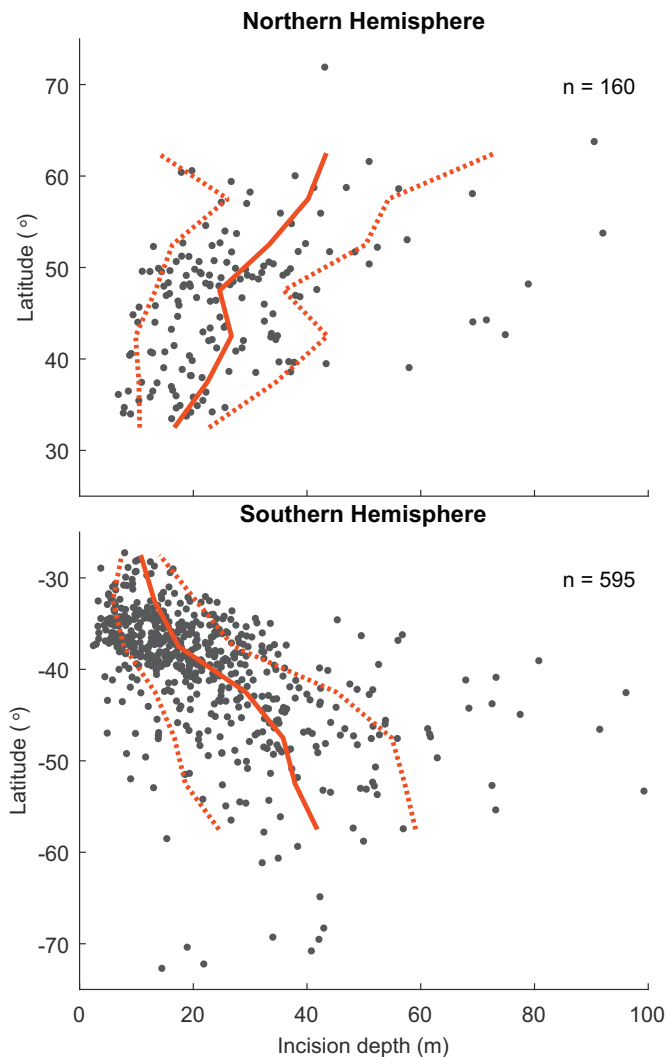


Fig. 8. Estimated gully incision depth against latitude, top: northern hemisphere and bottom: southern hemisphere. The solid lines represent mean values for each 5° of latitude. Dashed lines represent standard deviations for each 5° of latitude. The variable n is the number of data points within the graph.

gullies, they tend to occur at higher latitudes – a trend more obvious in the southern hemisphere. We find no difference between with thickness of pasted-on terrain in the systems with arcuate ridges and those without, even when considered by latitude (Fig. 9).

The arcuate ridges are often found in association with crater interior ice deposits (57% found within 5 km of the boundary of crater interior ice deposits mapped by Levy et al., 2014), which can form lobes of material that extend from the pole-facing crater wall beyond the ridges onto the crater floor (Figs. 3A, 10A–C, I). In both cases the arcuate ridges are commonly outlined by spatulate depressions that appear to push into the VFF. We found no evidence of arcuate ridges occurring without any kind of existing crater interior ice deposit. We find that pasted-on terrain always occurs upslope of the arcuate ridges and, by association, that arcuate ridges always coexist with texturally altered bedrock upslope (Fig. 10).

Although we did not survey for arcuate ridges that do not coexist with gullies (this is ongoing), Berman et al. (2005) systematically surveyed all the gullies and arcuate ridges in Newton Basin using Mars Orbiter Camera (MOC) narrow angle images at 1.5 m/pixel and THEMIS (Thermal Emission Imaging System) visible images. They found 188 craters with gullies, 118 craters with arcuate ridges, and 104 craters with both, consistent with our finding that up to ~55% of

incised gullies also have associated arcuate ridges (Fig. 9). Berman et al. (2009) found that for craters with diameters >20 km in Arabia terra, Newton Basin, and Eastern Hellas, arcuate ridges were almost exclusively associated with gullies. The arcuate ridges had an even stronger preference for pole-facing crater walls than gullies. Berman et al. (2005) and de Haas et al. (2018) noted a spatial correlation between gully alcoves and the position of the most arcuate sections of the ridges: inflections between successive arcuate segments have similar widths to the alcoves located topographically above them; our observations agree. Moreover, the arcuate ridges below the largest alcoves also protrude farthest onto the crater floor. The arcuate ridges mapped by Berman et al. (2005) systematically occurred with *patterned floors* interpreted as ice-rich crater fill (here termed *crater interior ice deposits*) and mantling materials. These crater interior ice deposits sloped away from the margins of the fill proximal to the arcuate ridges, the slope direction aligning with the lineations expressed within the surface of these fills, also noted by Head et al. (2008).

3. Erosion of crater walls

3.1. Approach

In order to assess the magnitude and rate of erosion associated with crater glaciation, we made a series of topographic measurements and dated host craters via measurement of crater size–frequency distributions.

The first criterion in our site selection was the existence of either a preexisting digital terrain model (DTM) or a suitable stereo pair of images for creating a DTM. From these we selected three classes of craters:

- Pristine impact craters in the databases of Watters et al. (2015) and Tornabene et al. (2018), preferably located in the equatorial latitudes, but otherwise without evidence for any of the following features: pasted-on terrain, other mantling deposits, arcuate ridges, or gullies.
- Craters with gullies, but no evidence of pasted-on terrain, other mantling deposits, or arcuate ridges; preferably possessing HiRISE elevation data spanning north- and south-facing walls.
- Craters with pasted-on terrain that have arcuate ridges and/or gullies, preferably having HiRISE elevation data spanning north- and south-facing walls.

In all cases we favoured craters with a simple rim morphology, lacking wall terraces and wall collapse features. This criteria and use of HiRISE images restricted our crater diameters to <20 km. We avoided craters located on antecedent relief (escarpments, faults, other crater rims, valleys).

Where existing HiRISE elevation data did not exist we used either the SocetSet ISIS3 workflow (Kirk et al., 2008) or the freely available Ames Stereo Pipeline (ASP) (Moratto et al., 2010; Shean et al., 2016) to produce additional elevation data. For both, we followed standard procedures in ISIS3 to produce single unprojected seamless images from the 9–10 individual HiRISE CCD images. These mosaicked images were map projected in ISIS3 to improve the point matching in ASP. We used standard settings to run ASP, with the Bayes EM subpixel mode with a 15 pixel subpixel kernel to improve results on steep terrain. We used ESA Mars Express High Resolution Stereo Camera elevation data to coregister and correct any tilting in the resulting point cloud with the routine ‘pc_align’. For the SocetSet workflow we followed the standard USGS procedure, but sometimes used the *low contrast* strategy at the DTM creation step, which can produce less noisy results.

In order to estimate the headwall retreat of the crater bedrock we measured the slope of the bedrock materials found just below the crest of the crater rim. We automatically extracted these data by taking 300-m-wide swath profiles perpendicular to the rim trace. We used swath profiles in order to generate data robust to noise in the elevation data and whose slopes would be independent of the presence or absence of alcoves. We mapped where the bedrock cropped out within each swath.

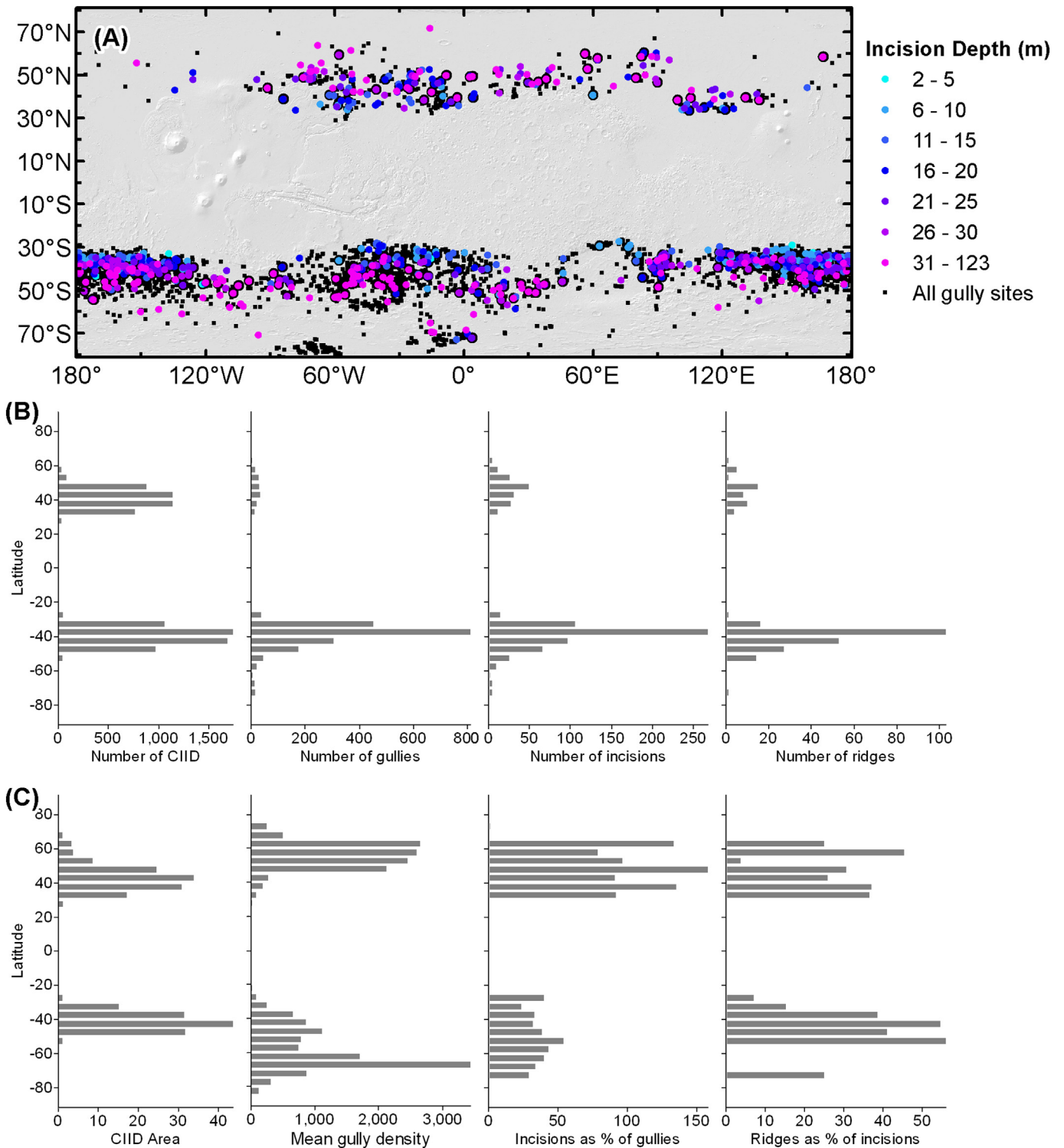


Fig. 9. Global and latitudinal distribution of gullies, gully incisions, crater interior ice deposits, and arcuate ridges. (A) Map of gullies (Harrison et al., 2015) and depth of incisions measured in this survey overlain on a relief-shaded rendering of the Mars Orbiter Laser Altimeter elevation data. (B) Bar charts giving the counts, from left to right, of crater interior ice deposits (CIID), gullies, incisions, and arcuate ridges per latitude band. Bar graphs were made from supplementary data of Levy et al. (2014) and Harrison et al. (2015). (C) From left to right: summed crater interior ice-deposit (CIID) area per 5° latitude bin in 10^3 km^2 , mean gully density per latitude from Conway et al. (2018a) that normalises gully density based on the frequency of steep slopes found at that location, number of incisions as a percentage of the number of gullies in the same latitude bin, and number of arcuate ridges as a percent of the number of incisions per latitude bin. Note that the percent of incisions exceeds 100% because of the nature of the two surveys: Harrison et al. (2015) counted sites (in which many gullies could be present), and our incision survey counted individual gullies; hence there are latitude bins where the number of incisions exceeds the number of sites.

For each swath profile we created an average profile, by binning the data by distance every metre from the crater rim and taking the mean of the points within each bin. We performed a linear fit of the elevation data within bedrock outcrops between 20 and 400 m from the crater rim as

an estimation of the upper bedrock slope of the inner crater wall and between 20 and 100 m on the exterior crater wall. This procedure is illustrated in Fig. 11. We did not measure any cases where pasted-on terrain extended up to the crater rim because no bedrock is exposed.

We classified the swath profiles into four types depending on their association with identified landforms within each crater: i) unmodified, ii) gullies present, but no evidence of glacial modification, iii) gullies present with evidence of glacial modification; and iv) evidence of glacial modification, but no gullies.

In order to convert the reduction in slope to a headwall retreat rate, we first need to estimate the amount (length l , Fig. 11) of crater wall that has experienced this reduction in slope and then combine this recession length with the crater age to obtain a minimum headwall retreat rate for our studied craters. We measured the mean distance from the crater rim over which bedrock was exposed to provide a minimum estimate of the horizontal length (l in Fig. 11) of the crater wall that had undergone slope reduction. We calculated two slope-reduction quantities:

- (i) the slope reduction with respect to the opposing (unmodified) wall in the same crater (if available) to give an estimate of the acceleration in erosion over the background rate; and
- (ii) the slope reduction with respect to the maximum average wall slope value of pristine equatorial craters to give the cumulative erosion over the lifetime of the crater.

To estimate the headwall retreat rate under the more likely scenario that periods of enhanced erosion punctuated the background headwall retreat rate, we followed Levy et al. (2016) and calculated the retreat rate over a time period of 0.5 Ma based on the slope-reduction given by (i). Levy et al. (2016) used a time interval of 0.5 Ma based on previous estimates for the duration of the last glacial epoch by Fassett et al. (2014) and the amount of time required, according to glacial flow modelling, for a typical LDA to form (Fastook et al., 2014). For these relatively small systems this duration is probably too long, but it provides a conservative estimate of erosion rate.

We used Crater Tools and CraterStats extensions for ArcGIS (Michael and Neukum, 2010; Kneissl et al., 2011) to estimate the ages of those ejecta blankets of our study craters, which did not already have published ages. In brief: we outlined the continuous impact ejecta on CTX images, which was then used as our crater count area. We counted all impact craters that had raised rims and were not covered/infilled by the ejecta. We fitted the Hartmann and Neukum (2001) isochrons to the resulting cumulative size-frequency distributions to obtain an estimated age and error (Fig. 12). These ages are taken as maximum values for the age of the features found within the craters because the features formed after the impact. We were conservative in determining the potential uncertainties on the crater counting: we manually placed isochrons that bracketed our fitted ages and touched the error bars and/or points at the oldest and youngest end of the data. In one case no identifiable primary craters were visible on the ejecta surface at CTX resolution so we calculated a maximum age by placing one *false* impact crater in the count area of 55 m diameter – the smallest diameter that we judged to be identifiable in the CTX image.

3.2. Headwall retreat rate of glaciers and gullies

We used a data set comprising three gullied craters, nine craters with arcuate ridges, two craters with pasted-on terrain yet no arcuate ridges, six fresh craters, and one degraded-looking equatorial

crater with no gullies, pasted-on terrain, or arcuate ridges (Table 1, Fig. 13). These craters have diameters ranging between 1.7 and 20 km.

We found that the upper wall slopes are $\sim 39^\circ$ for the two youngest equatorial craters (≤ 5 Ma, Zumba and Corinto), and in our oldest equatorial example (Kilmia, 1.1 Ga) the upper wall slope has reduced to 27° (Table 2 and Figs. 14, 15). In the terrestrial literature we found that a peak in slope exists at a similar value of $\sim 39^\circ$ in mountain ranges, which is thought to represent the strength of the bedrock (e.g., Burbank et al., 1996; Katsube and Oguchi, 1999; Korup, 2008; Lin et al., 2009). Similarly for the youngest craters in our modified sample (0.5–6.5 Ma craters A, B, C, Istok, Jaisalmer, Galap) the slopes of the walls unmodified by either gullies or glacial processes have high slope values with a range of $34\text{--}41^\circ$ (Figs. 14, 15). The unmodified walls of older craters (1.3–1.4 Ga, Niquero, Corozal,) have lower slopes in the range of $32\text{--}34^\circ$.

The reduction in interior crater wall bedrock slope in the three gullied yet unglaciated craters is $4\text{--}5^\circ$ compared to their unmodified crater walls and $6\text{--}9^\circ$ compared to slopes in fresh equatorial craters (Figs. 14, 15; Table 2). The interior walls of craters that have evidence of glaciation are further reduced: up to 8° (on average 4°) lower compared to conjugate unmodified walls and up to 15° (on average 11°) compared to fresh equatorial craters. We also found that when pasted-on terrain was present on exterior crater walls, these bedrock slopes were reduced compared to unmodified exterior crater walls (Figs. 14, 15; Table 2), although the signal is not as strong as for the inner walls. This is probably because of a larger initial variation in the slope of exterior crater walls, as shown by their variability in fresh equatorial craters (a range of 8° to 21° with standard deviations of $3\text{--}10^\circ$, Table 2). Finally, for Jaisalmer Crater and Crater B (the youngest glaciated craters) we noted that wall sectors with pasted-on terrain and texturally altered bedrock had lower slopes than rim portions with only pasted-on terrain and both were lower than the unmodified portions of the crater wall (Fig. 14C).

For the gullied craters the bedrock extends on average 120–520 m down the crater wall (Table 2); therefore, the crater wall has receded by 1–70 m at the top. For Galap this results in an estimated headwall retreat rate of 92 m My^{-1} and for Istok 10 m My^{-1} , compared to 4.5 and 75 m My^{-1} backweathering rates estimated by de Haas et al. (2015b) using an independent method.

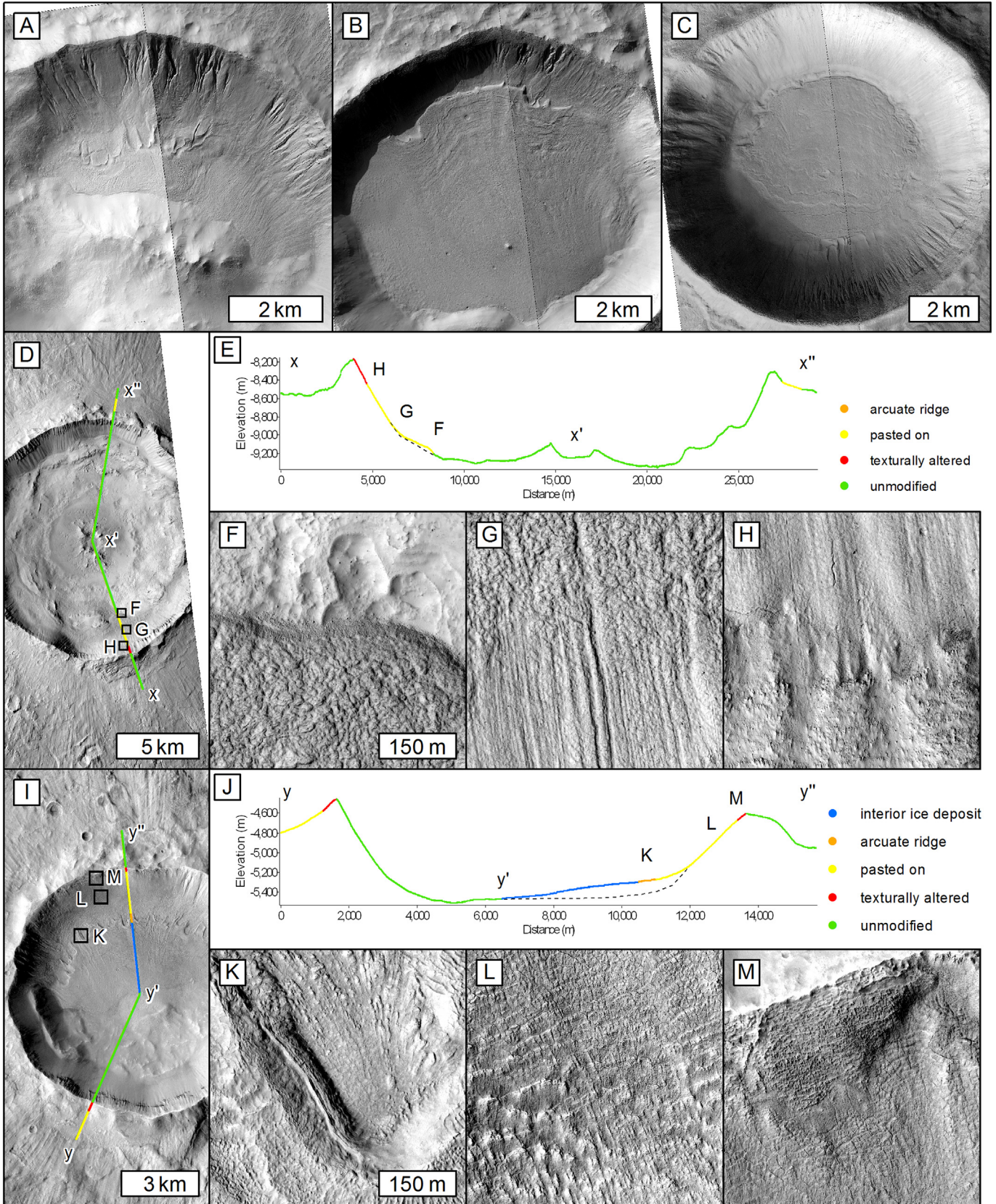
The slopes within glaciated craters are partially covered by pasted-on terrain, hence as a conservative estimate we can assume that only the bedrock that is exposed has been affected by the slope reduction. The pasted-on terrain is found between 121 and 714 m and on average 368 m distance from the rim in our studied craters (Table 2). We find that headwall retreat rates range between 0.04 and 132 m My^{-1} for unmodified walls of glaciated and gullied craters and overlap with the values of 0.22 to 7.6 m My^{-1} for completely unmodified craters. We further find that the headwall retreat rates of glaciated walls fall between 0.08 and 181 m My^{-1} . When these headwall retreat rates are plotted against crater age (Fig. 15E), a decreasing trend in headwall retreat rate against age is observed. Similarly for the glaciated crater walls, the calculated headwall retreat rate has a similar decrease with crater age but transposed to higher headwall retreat rates than the unmodified walls. Calculating the headwall retreat rate for the glaciated crater walls over a fixed time interval of 0.5 Ma (as detailed in Section 3.1) and using the slope reduction compared to the unmodified

Fig. 10. Relationship between pasted-on terrain, arcuate ridges, and lobate or crater interior ice deposits. North is up in all panels. (A) Arcuate ridges within a lobe of crater interior ice deposits where the lobate margin appears to curve around obstacles. HiRISE images ESP_023809_1415 and ESP_024943_1415. (B) Arcuate ridges into crater interior ice deposits that extend across the whole crater floor with flowlines extending toward the south in the southern hemisphere. HiRISE images ESP_016227_1405 and ESP_016438_1405. (C) Arcuate ridges into crater interior ice deposits that extend across the whole crater floor with no flowlines, yet pitted surface texture similar to other VFF, in the northern hemisphere. HiRISE images ESP_013277_2155 and ESP_022059_2150. (D) Crater E overview in CTX image P19_008307_2138 showing the position of the cross-profile in (E). (F–H) Panels using HiRISE image PSP_009164_2140 at 1:10,000 showing (F) the boundary between the pasted-on terrain and the crater floor, (G) the transition from the lineated pasted-on terrain texture to glacial texture midway down the crater wall, and (H) the boundary between the lineated pasted-on terrain and the texturally altered bedrock. (I) Taltal Crater overview in CTX image G09_021712_1402, showing the location of the cross-profile in panel (J). (K–M) Panels using HiRISE image ESP_21712_1400 at 1:10,000 showing (K) the boundary between the pasted-on terrain and the arcuate ridges, (L) the transition between the polygonised pasted-on texture and VFF surface textures midway down the crater wall, and (M) the boundary between the polygonised pasted-on terrain and the texturally altered bedrock.

wall of the same crater (rather than compared to a fresh equatorial crater wall), we find that headwall retreat rate no longer has a substantial trend with age (Fig. 15F).

We briefly note here that our data do not show that glaciated inner crater walls have significantly and/or systematically lower elevation

than unmodified inner walls in the same crater as observed previously by Berman et al. (2005) and Head et al. (2008). We posit that this could be because of the fact that we find erosion on the inner and outer crater walls, hence north- and south-facing walls are being lowered by the action of glaciation.



4. Glacial erosion

4.1. Mechanisms of glacier erosion on earth

Mechanical erosion by glaciers is dominated by abrasion, quarrying, plucking, and glaciotectionism (see [Benn and Evans, 2010](#), for an extensive review). Abrasion is the process by which the glacier bed and entrained clasts are scoured either by debris entrained within basal glacier ice or, less commonly, by the basal ice itself (e.g., [Hallet, 1979](#)). Quarrying is the process by which bed-clast contact, or overriding of bedrock cavities, generates foci of pressure at the ice-bed interface and liberates fragments from the bed (e.g., [Iverson, 1991](#); [Hallet, 1996](#); [Cohen et al., 2006](#)). Plucking involves freezing of meltwater within, or deformation of basal ice into, bedrock fractures and prizing-off of fragments under subsequent glacier motion (e.g., [Boulton, 1979](#); [Röthlisberger and Iken, 1981](#)). Finally, glaciotectionism is the process by which subglacial, submarginal, and/or proglacial materials deform under stresses induced by glacial ice (e.g., [Hart and Boulton, 1991](#)).

Glacier thermal regime exerts a fundamental control upon the efficacy of glacial erosion on Earth. This arises from its influence on the generation of meltwater, entrainment of erosional tools (i.e. debris), and dynamics of ice-bed interactions (e.g., [Hallet et al., 1996](#); [Hambrey and Glasser, 2012](#)). The thermal regimes of glaciers are categorised according to their temperature relative to the pressure melting point of ice and are controlled by complex interactions between climatic, environmental, and glaciological parameters ([Benn and Evans, 2010](#)). Temperate (warm-based) glaciers (e.g., Haut Glacier d'Arolla, Swiss Alps; [Goodsell et al., 2005](#)) are at the pressure melting point of ice throughout, whereas cold-based glaciers (e.g., Meserve Glacier, Antarctic Dry Valleys; [Holdsworth and Bull, 1970](#)) are entirely below the pressure melting point. Polythermal glaciers (e.g., Midre Lovénbreen, Svalbard; [Björnsson et al., 1996](#)), where warm ice at the pressure melting point coexists with cold ice below the pressure melting point, represent an intermediate condition between temperate and cold-based glaciers.

The efficiency of mechanical erosion by glaciers is greatly enhanced in the presence of meltwater. Under a wet-based thermal regime, significant basal sliding can occur at an unfrozen ice-bed interface, promoting efficient abrasion of the bed (e.g., [Hallet, 1979](#)) and liberation of rock fragments via plucking. Sliding over obstacles at the bed also opens lee-side cavities, promoting quarrying (e.g., [Iverson, 1991](#); [Hallet, 1996](#)). Quarrying is particularly effective under wet-based regimes because meltwater, which is dynamic on shorter timescales than glacial ice, can greatly enhance pressure fluctuations at the bed ([Iverson, 1991](#); [Cohen et al., 2006](#)). Liquid water is thought to play an important, possibly essential, role in promoting glaciotectionic deformation. Pore water reduces the yield stress of glacial sediments, making them more susceptible to deformation under stresses induced by glacial ice (e.g., [Bennett, 2001](#)). Despite generally lower meltwater volumes associated with glaciers in cold-climate or permafrost regions, ground ice and/or frozen glacier margins may encourage glaciotectionic processes by preventing efficient drainage of meltwater from aquifers that they confine (e.g., [Moran et al., 1979](#); [Fitzsimons, 1996](#); [Boulton et al., 1999](#); [Benn and Evans, 2010](#)).

The frozen ice-bed interface and absence of meltwater in cold-based glacial systems leads to the assumption that cold-based glaciers flow entirely by internal deformation, do not erode their beds, and exert little or no detectable geomorphic influence upon the underlying landscape. Indeed, coverage by cold-based ice is frequently invoked as a protective mechanism to explain the preservation of features generated by previous wet-based glaciations (e.g., [Dyke, 1993](#); [Smith et al., 2009](#)). However, theoretical ([Shreve, 1984](#)) and field-based ([Echelmeyer and Wang, 1987](#)) studies have noted that sliding rates of cold-based glaciers are, in fact, non-zero when integrated over long timescales ([Cuffey et al., 2000](#); [Waller, 2001](#)). Field observations have also identified evidence for reworking of cold glacier beds ([Cuffey et al., 2000](#); [Atkins et al.,](#)

[2002](#); [Lloyd Davies et al., 2009](#)), such that it is becoming increasingly evident that cold-based glaciers can exert significant geomorphic influence over timescales of glacial advance, although still substantially less than warm-based glaciers.

In examining isotopic composition of dirty basal ice layers derived from marginal apron overriding at Meserve glacier in the Antarctic Dry Valleys, [Cuffey et al. \(2000\)](#) suggested that interstitial water films between ice and immersed solids within dirty basal ice layers of cold-based glaciers may permit sliding and abrasion down to temperatures of $-30\text{ }^{\circ}\text{C}$, an effect that could be particularly important in the presence of a highly saline substrate. Additionally, [Lloyd Davies et al. \(2009\)](#) proposed a mechanical model by which abrasion and quarrying can operate beneath cold-based glaciers in the absence of liquid water, based on field observations in the Allan Hills region of Antarctica. Ice-marginal aprons comprising collapsed ice blocks commonly accumulate at the foot of steep terminal ice cliffs of cold-based glaciers. These aprons can be incorporated into basal ice as they are overridden during glacier advance ([Cuffey et al., 2000](#); [Atkins et al., 2002](#); [Lloyd Davies et al., 2009](#)). [Lloyd Davies et al. \(2009\)](#) suggested that this incorporates a weak, low-density layer into the submarginal basal ice that focusses stress onto up-glacier bedrock contacts and promotes fracturing and quarrying of bedrock protuberances. Entrained rocks are then available as tools for abrasion during subsequent glacier motion ([Lloyd Davies et al., 2009](#)).

4.2. Landscapes of glacial erosion and application to Mars

We now consider the potential contributions of these erosional processes to the following geomorphic features that we observe on Mars: texturally altered bedrock of upper walls of impact craters, lowering of slopes on texturally altered crater walls compared to fresh crater walls, instances of sharp crater rim crests despite lowered wall slopes, and associated slope-side pasted-on terrain and arcuate ridges that are commonly but not ubiquitously associated with spatulate depressions within crater interior ice deposits.

Many geomorphic features that are indicative of past glacial erosion, including striae, gouges, fractures, scrapes, and chattermarks ([Atkins et al., 2002](#); [Lloyd Davies et al., 2009](#); [Benn and Evans, 2010](#)), are undetectable at the decametre- to metre-scale resolutions of existing orbital remote sensing data sets for either Earth or Mars. However, the integrated effect of these processes operating over large areas typically manifests as smoothed, rounded, planed-off, or a *really-scoured* surfaces ([Benn and Evans, 2010](#)). Such landscapes bear similarities to the smoothed morphologies of the walls of the glaciated craters in our survey, within which the upper bedrock protuberances (*spur and gully* forms) have been planed-off and possibly old gully alcoves strongly modified ([de Haas et al., 2018](#)). If the textural disruption of these slopes is a primary morphology inherited directly from glacial erosion, it seems more consistent with erosion via quarrying and plucking, which can generate rough, *craggy* surfaces (e.g., [Roberts and Long, 2005](#)), than by abrasion, which tends to smooth and polish bedrock surfaces ([Fig. 16](#)). Highly brecciated and fractured bedrock associated with impact crater walls ([de Haas et al., 2015a](#)) may make these bedrock surfaces particularly susceptible to erosion by quarrying and plucking, as in tectonically active glaciated regions on Earth (e.g., [Hallet et al., 1996](#)). Further, the amount of slope lowering we observe is independent of the estimated initial slope. This is consistent with glacial erosion, which is more strongly influenced by the ice-surface slope (which controls basal shear stress) than the bed-slope ([Oerlemans, 1984](#)).

Another possible contributor to the textural alteration of the bedrock is enhanced weathering under the ice or snowpack at the top of the slope ([Fig. 16E](#)). In a terrestrial setting, rock weathering in cold regions is controlled by moisture availability (e.g., [Sass, 2005](#)) and by the existence of the thermal conditions required for ice segregation. These conditions are enhanced by the presence of snowpatches or snowfields (e.g., [Thorn and Hall, 1980](#)), as ice lens growth during ice segregation is

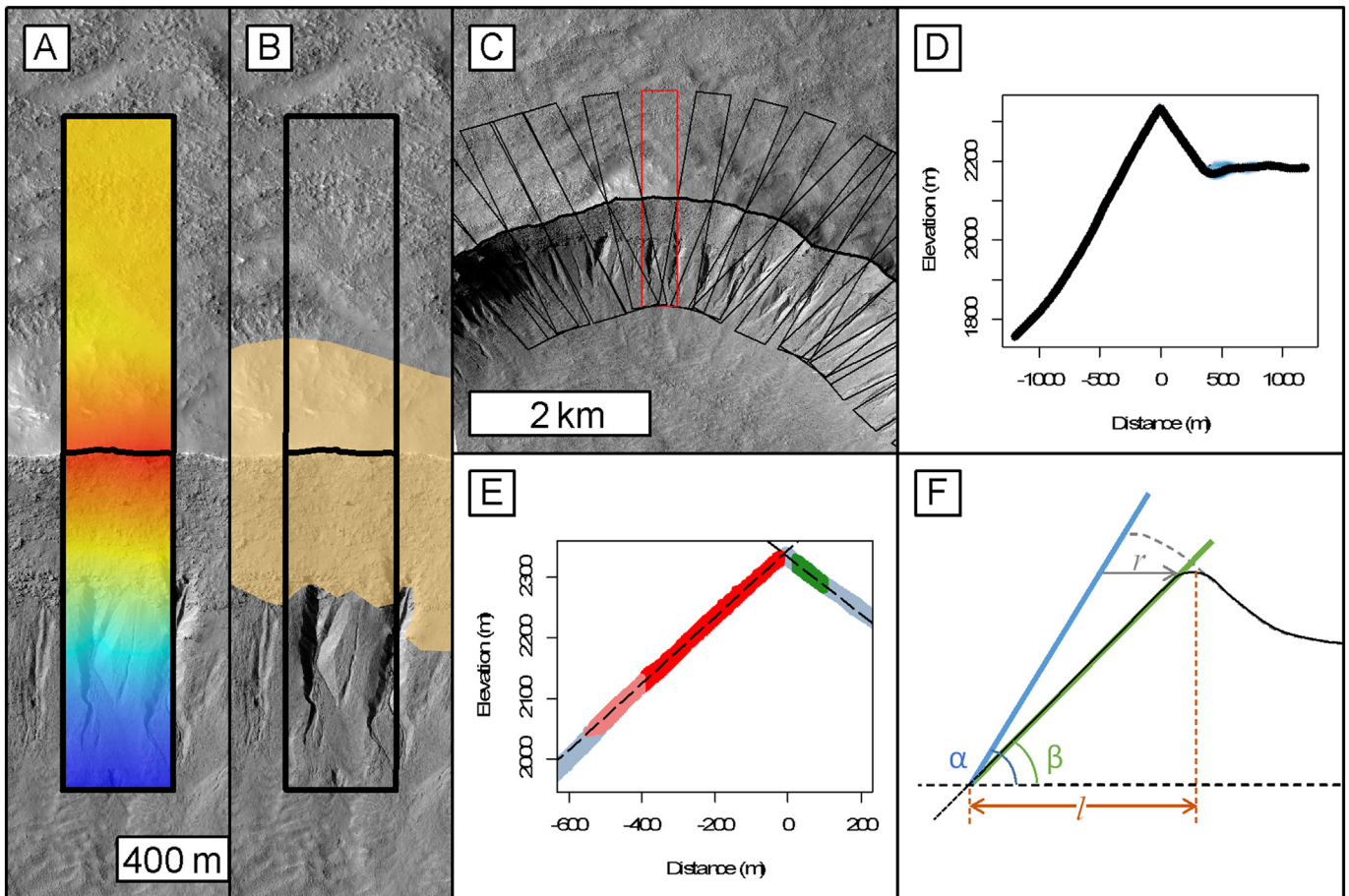


Fig. 11. Overview of approach for measuring recession rates of crater walls. (A) Talu Crater with elevation swath overlain on HiRISE image ESP_011672_1395 (red colours are high elevations, blue colours low). (B) The swath profile from panel (A) with the mapped bedrock shown in orange. (C) Overview of the swath profiles measured on the northern rim of Talu Crater with the one in panel (A) highlighted in red. (D) Elevation data against distance from the rim-crest extracted from the swath shown in panel (A) with blue shades representing the raw data and black points showing the mean elevation every 1 m. (E) The same profile as in panel (D) but showing only the crater rim. Grey points are all the profile datapoints, superposed by red points that are used to perform a linear fit to obtain the bedrock slope on the inner wall (points 20–400 m from the rim with bedrock outcrop), pink points are bedrock outcrop lying farther than 400 m from the rim, and green points are those used to perform a linear fit to obtain the slope of the bedrock on the exterior wall (points 20–100 m from the rim with bedrock outcrop). Linear fits are shown as black dashed lines. (F) Diagram illustrating the method by which we calculated the headwall retreat. The black line represents the crater wall for which we want to estimate the retreat with the green line representing the linear fit to obtain the slope β . The dotted grey line is either a pristine crater wall or an unmodified wall in the same crater with the blue line representing the linear fit to obtain its slope α . The orange distance l is the exposed length of bedrock as observed from the orthorectified images. The recession r is calculated as $l - l (\tan \beta / \tan \alpha)$.

favoured by slow freezing rates and sustained below-freezing temperatures (Matsuoka and Murton, 2008). Ice lens formation is the primary cause of physical rock breakdown or frost-shattering (Murton et al., 2006; Hales and Roering, 2007; Matsuoka and Murton, 2008). These physical weathering mechanisms require the presence of thin films of liquid water, yet ice segregation on Mars has been hypothesised to occur without need for the liquid phase (e.g., Lacelle et al., 2013; Sizemore et al., 2015).

The observed lowering of crater wall slopes presents a more complex challenge for the glacial hypothesis. Glaciers tend to steepen upper valley slopes, in longitudinal (e.g., MacGregor et al., 2000) and cross-sectional (Hirano and Aniya, 1988; Harbor, 1992) profiles, giving rise to classic U-shaped valley and cirque landscapes. Conversely, our observations show shallower crater wall slopes, and an absence of pronounced U-shaped undulations or bedrock-confined overdeepenings. However, Hirano and Aniya (1988) and Harbor (1992) found topographic steepening to be an outcome of enhancement of vertical erosion by topographic confinement of glaciers and its effect on ice flow. Glaciers that are not topographically confined can preferentially widen rather than deepen their host valleys, resulting in broad-scale lowering of slopes (Hirano and Aniya, 1988). We therefore suggest that valley and cirque-style glacial configurations are inconsistent with our

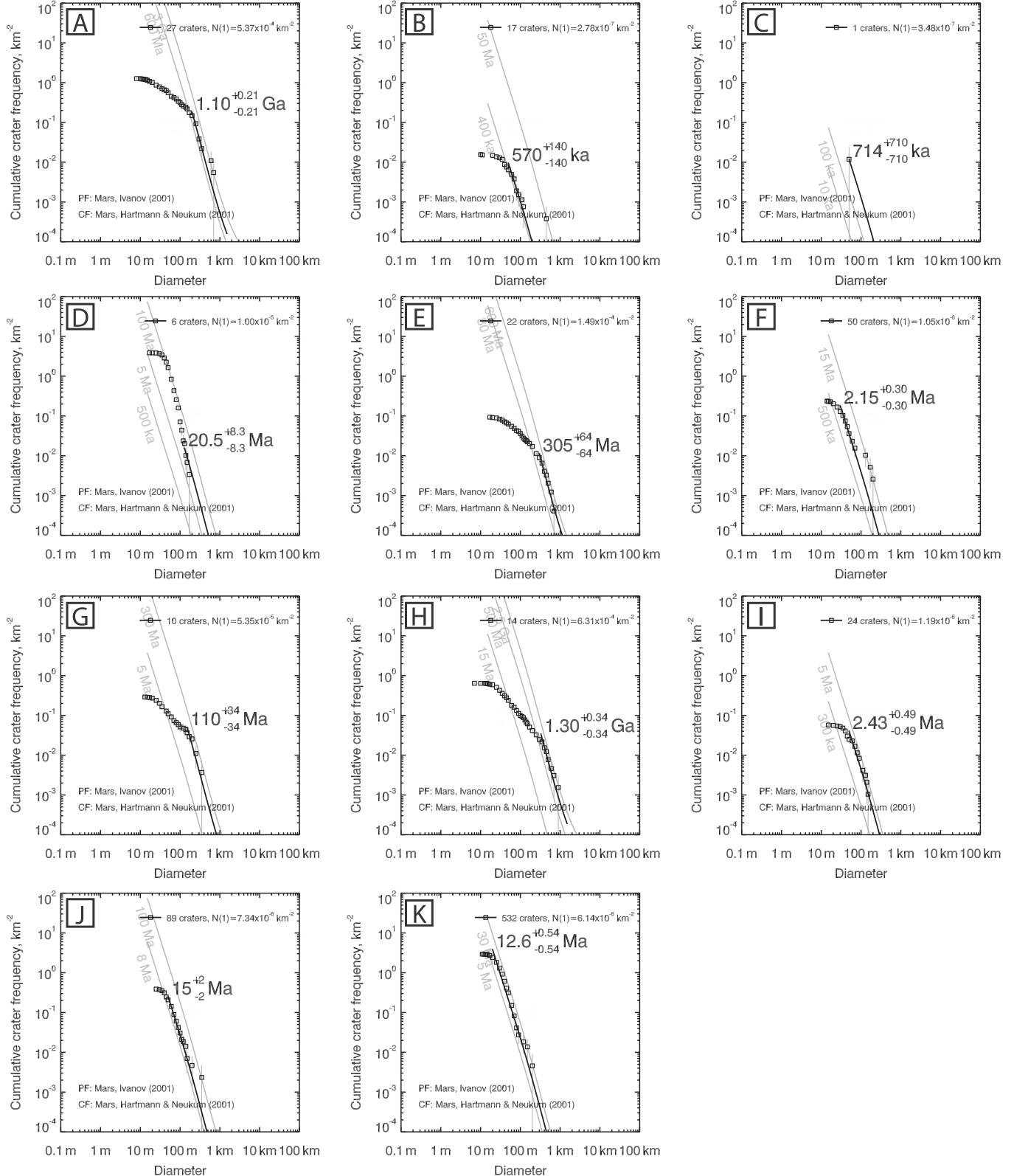
observations and that unconfined, piedmont-style (LDA-like) glaciers may provide the optimum explanation for the observed morphologies. The location of pasted-on terrain in wide alcoves (which could be interpreted to resemble cirques) does not necessarily imply that the ice was limited to those alcoves. Weak vertical erosion could explain the presence of distinct rim and interalcove crests in some instances, despite clear evidence that these same rim segments have undergone significant lowering of slope.

However, the present understanding of glacial slope modification on Earth is largely based on assumptions that glaciers inherit preexisting fluvial valleys with gentle slopes and have a ready supply of meltwater to their beds (e.g., Hirano and Aniya, 1988; Harbor, 1992; MacGregor et al., 2000). These assumptions conflict significantly with the present understanding of recent glacier thermal regimes on Mars (largely cold-based) and the impact crater wall landscapes explored here, which have steep initial slopes and lack mature fluvial valleys. Therefore, we emphasise that constraining the configuration of glacial ice at small spatial scales would be highly speculative given existing data and the distinctly atypical initial topography compared to terrestrial case studies upon which glacial theory is based.

The magnitude of lowering of crater wall slopes, demonstrates that significant volumes of material have been mobilised by crater wall

erosion. Within the surveyed craters, pasted-on terrain is invariably located downslope of texturally-altered bedrock. Accordingly, we propose that upper crater walls and rims may have provided a viable source of debris for this pasted-on terrain and that glaciers could have acted as important erosional and depositional agents in its formation. In this context, the origin for the downslope lineations within pasted-on

terrain could be streamlined glacial bedforms such as flutes or megascale glacial lineations. However, the pasted-on terrain is significantly more extensive and voluminous (Christensen, 2003; Conway and Balme, 2014; Section 2.2) than rare, patchy, and thin (<2 m thick) till deposits identified in association with cold-based glaciers on Earth (Atkins et al., 2002; Lloyd Davies et al., 2009). If the pasted-on terrain



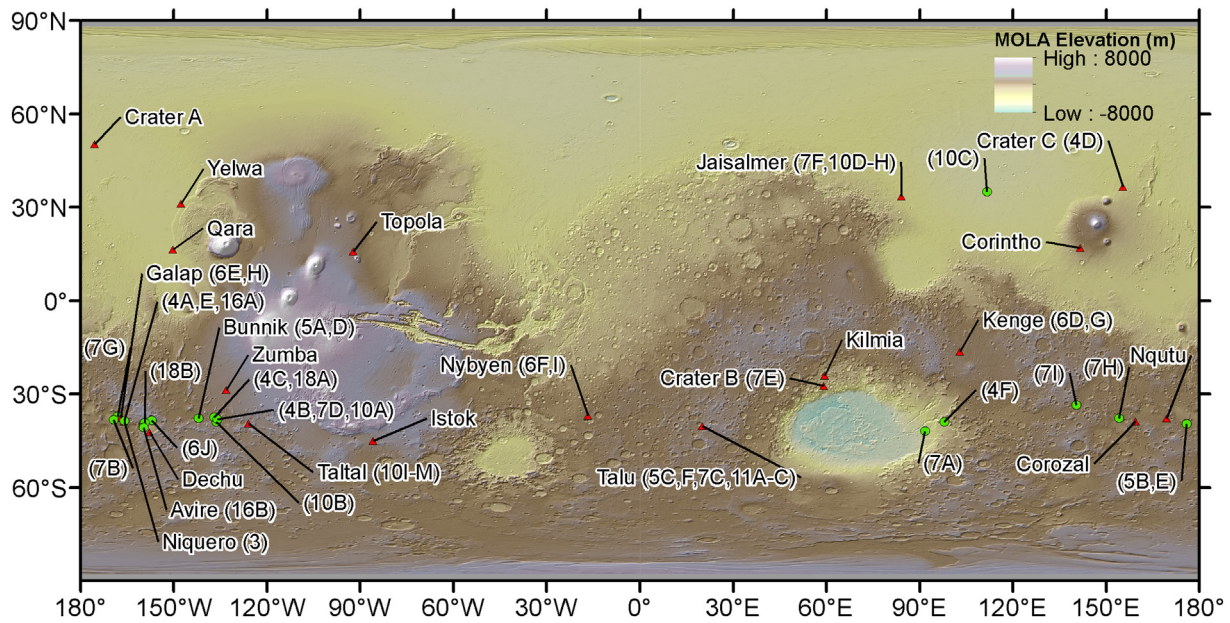


Fig. 13. Location map of the DTMs used in this study (triangles) and locations of the additional sites used in the figures (circles) on a MOLA elevation shaded relief base map. The numbers/letters in brackets identify the relevant figure(s).

on formerly glaciated crater walls is indeed glacial till, some degree of meltwater activity seems necessary, contrary to the idea that Amazonian glaciation was almost entirely cold-based (with a few localised and transient exceptions, e.g., Fassett et al., 2010; Hobley et al., 2014; Scanlon et al., 2014, 2015; Gallagher and Balme, 2015; Butcher et al., 2017). We therefore emphasise that the origin of the pasted-on terrain should be investigated further.

Given that aeolian processes are widespread and active geomorphic agents on Mars in the present day and have been shown to modify gullied slopes (de Haas et al., 2013, 2015c), an aeolian origin for the down-slope lineations within pasted-on terrain might be just as likely as an origin as streamlined glacial bedforms such as flutes or megascale glacial lineations. Therefore, convergence of form between morphologies generated by glacial and aeolian streamlining prevents conclusive distinction between these formation mechanisms given the resolution of HiRISE images. Thus, their potential origin as streamlined glacial bedforms should not be excluded considering the apparent close association between pasted-on terrain and glaciated slopes.

Prominent arcuate ridges provide particularly convincing evidence for past glaciation of crater walls. Although hypotheses that such arcuate ridges represent protalus ramparts have been proposed (Whalley and Azizi, 2003), they are widely interpreted as end moraines based on their similarity to moraine ridges on Earth and to arcuate ridges bounding other ice-rich glacier-like forms on Mars (e.g., Milliken et al., 2003; Arfstrom and Hartmann, 2005; Hubbard et al., 2014; Brough et al., 2016a). Typically, multiple arcuate ridges coexist, forming laterally extensive moraine complexes. Although some arcuate ridge complexes can clearly be associated with bedrock alcoves in the crater

walls above (Fig. 17A) (Arfstrom and Hartmann, 2005), many arcuate ridges lack distinct association to discrete undulations in the crater walls (Fig. 17B). Thus, we consider the ridges to be more consistent with unconfined piedmont-style glaciation, as proposed above, than with the formation of each arcuate section at the terminus of a discrete glacier tongue. The highly curvilinear morphologies of the ridge complexes are not inconsistent with such an origin, as differential flow within broad ice lobes on Earth commonly forms highly curvilinear moraine complexes (Fig. 18B) (Bennett, 2001; Arfstrom and Hartmann, 2005).

The common association between arcuate ridges and spatulate depressions within crater interior ice deposits (Head et al., 2008) indicates that ice-contact bulldozing contributes to the formation (e.g., Arfstrom and Hartmann, 2005). However, several features lead us to support that glaciotectionic processes also provided a significant contribution to their formation, as was considered by Arfstrom and Hartmann (2005). The distinction between bulldozing and glaciotectionic processes is in the nature of ice contact; while bulldozing relates to movement of material in contact with glacial ice, glaciotectionism can influence materials tens to hundreds of metres below glacier beds and into the proglacial zone (Benn and Evans, 2010). Compressive stresses induced by convergence of crater wall glaciers with preexisting crater floor ice bodies, such as crater interior ice deposits (e.g., Fig. 10), would enhance the likelihood that glaciotectionism supplemented bulldozing in moraine construction where these preexisting ice bodies are present. Furthermore, bulldozing of crater floor materials alone cannot necessarily provide adequate explanation for apparent disruption within crater interior ice deposit surfaces beyond the arcuate ridges (Fig. 17). Thus, complex

Fig. 12. Crater size-frequency distribution for the eleven previously undated craters in our study (Table 1). Binning is performed via the pseudo-log method of Neukum (1983) and Hartmann and Neukum (2001). (A) Kilmia Crater where CTX image G22_026861_1557 was used to count the craters. Fitting was performed between diameters of 200 m and 1.5 km. (B) Jaisalmer Crater where CTX images P21_009164_2137, P15_006949_2150, P19_008307_2138, and P21_009098_2138 were used to count the craters. Fitting was performed between diameters of 50 m and 1 km. (C) Unnamed crater 'Crater A' where CTX image G19_025498_2305 was used to count the craters. For this crater no primary craters could be found, so one crater measuring 55 m in diameter was placed in the count area to obtain a maximum age. (D) Yelwa Crater where CTX image G06_020539_2114 was used to count the craters. Fitting was performed between diameters of 130 m and 1 km. (E) Dechu Crater where CTX images P12_005798_1396, P07_003675_1391, G14_023612_1375, and D10_031102_1378 were used to count the craters. Fitting was performed between diameters of 300 m and 1.5 km. (F) Unnamed crater 'Crater B' where CTX image G06_020703_1524 was used to count the craters. Fitting was performed between diameters of 30 m and 1 km. (G) Nybyen Crater where CTX image B05_011436_1427 was used to count the craters. Fitting was performed between diameters of 150 m and 1.5 km. (H) Niquero Crater where CTX images F01_036258_1410, P03_002383_1417, and P11_005284_1419 were used to count the craters. Fitting was performed between diameters of 330 m and 1.5 km. (I) Unnamed crater 'Crater C' where CTX images B02_010559_2168 and G22_026910_2168 were used to count the craters. Fitting was performed between diameters of 50 m and 1 km. (J) Topola crater where CTX image G14_023662_1960 was used to count the craters. Fitting was performed between diameters of 50 m and 1 km. (K) Kenge Crater where CTX image F23_044780_1635 was used to count the craters. Fitting was performed between diameters of 20 m and 1 km.

Table 2
Summary of results for each site, including number of classes, slopes, exposed bedrock length, retreat distance, and retreat rate^a.

Crater name	Number of profiles in each class		Mean inner wall slope (°)				Mean outer wall slope (°)	
	Inner wall	Outer wall	Gullied	Glaciated + gullied/glaciated	Pasted-on	Unmodified	Glaciated	Unmodified
Zumba	gu(0),gg(0),gl(0),po(30),un(0)	un(30),gl(0)				39.25 ± 1.09		9.43 ± 4.19
Corintho	gu(0),gg(0),gl(0),po(23),un(0)	un(23),gl(0)				40.66 ± 5.59		21.54 ± 9.96
Qara	gu(0),gg(0),gl(0),po(26),un(0)	un(26),gl(0)				35.89 ± 2.04		7.92 ± 2.97
Kenge	gu(0),gg(0),gl(0),po(32),un(0)	un(32),gl(0)				37.47 ± 0.65		14.17 ± 5.48
Topola	gu(0),gg(0),gl(0),po(33),un(0)	un(33),gl(0)				38.45 ± 1.15		19.38 ± 3.30
Yelwa	gu(0),gg(0),gl(0),po(34),un(0)	un(34),gl(0)				39.01 ± 1.14		19.11 ± 4.00
Kilmia	gu(0),gg(0),gl(0),po(36),un(0)	un(36),gl(0)				26.53 ± 2.15		10.64 ± 5.18
Crater A	gu(9),gg(0),gl(0),po(10),un(0)	un(19),gl(0)	39.68 ± 1.29			37.06 ± 2.54		26.70 ± 3.97
Istok	gu(20),gg(0),gl(0),po(22),un(0)	un(42),gl(0)	36.39 ± 1.97			41.60 ± 5.41		13.44 ± 4.89
Galap	gu(22),gg(0),gl(0),po(22),un(0)	un(44),gl(0)	33.35 ± 1.48			37.25 ± 1.94		16.18 ± 7.16
Jaisalmer	gu(0),gg(0),gl(10),po(16),un(13)	un(23),gl(16)		33.61 ± 1.55	32.88 ± 2.63	34.37 ± 1.70	1.55 ± 6.61	19.96 ± 9.09
Crater B	gu(0),gg(0),gl(5),po(28),un(10)	un(28),gl(15)		32.59 ± 1.06	36.47 ± 2.64	34.04 ± 3.08	1.06 ± 4.46	16.76 ± 6.23
Crater C	gu(0),gg(0),gl(0),po(12),un(16)	un(2),gl(26)		30.28 ± 3.32		34.35 ± 1.03	3.32 ± 7.47	23.02 ± 11.57
Talu	gu(0),gg(21),gl(0),po(12),un(0)	un(21),gl(12)		30.16 ± 1.34		34.71 ± 1.74	1.34 ± 4.12	20.50 ± 7.41
Nybyen	gu(6),gg(15),gl(0),po(17),un(0)	un(20),gl(18)	37.61 ± 2.21	32.34 ± 1.36		36.88 ± 2.12	1.36 ± 4.62	20.72 ± 5.85
Taltal E	gu(0),gg(14),gl(0),po(16),un(0)	un(17),gl(13)		28.77 ± 2.86		31.93 ± 2.02	2.86 ± 4.11	18.24 ± 4.06
Taltal W	gu(0),gg(0),gl(0),po(10),un(12)	un(12),gl(10)		24.75 ± 2.14		33.06 ± 1.79	2.14 ± 5.79	17.80 ± 5.99
Dechu	gu(18),gg(45),gl(0),po(9),un(0)	un(22),gl(50)	32.18 ± 3.14	27.83 ± 2.87		29.93 ± 1.79	2.87 ± 5.64	4.04 ± 3.15
Niquero	gu(0),gg(13),gl(0),po(15),un(4)	un(17),gl(15)		27.79 ± 2.88		34.48 ± 1.47	2.88 ± 2.58	17.44 ± 11.21
Corozal	gu(0),gg(19),gl(0),po(23),un(0)	un(17),gl(25)		26.68 ± 2.11		31.04 ± 2.11	2.11 ± 3.09	16.12 ± 6.37
Nqutu	gu(0),gg(18),gl(0),po(0),un(0)	un(18),gl(0)		24.14 ± 2.84				12.85 ± 6.95

Crater name	Exposed rock length (m)			
	Gullied	Glaciated + gullied/glaciated	Pasted-on	Unmodified
Zumba				138(+186/−37)
Corintho				245(+304/−132)
Qara				227(+97/−68)
Kenge				202(+215/−108)
Topola				212(+206/−68)
Yelwa				401(+376/−136)
Kilmia				610(+362/−512)
Crater A	118(+52/−15)			134(+47/−36)
Istok	338(+146/−185)			146(+123/−41)
Galap	508(+207/−113)			316(+203/−133)
Jaisalmer		438(+217/−254)	356(+335/−147)	264(+278/−67)
Crater B		453(+215/−161)	277(+108/−64)	361(+285/−173)
Crater C		192(+223/−73)		238(+257/−71)
Talu		431(+260/−188)		423(+157/−131)
Nybyen	283(+151/−108)	333(+450/−179)		306(+188/−92)
Taltal E		253(+351/−187)		439(+350/−182)
Taltal W		121(+187/−29)		384(+245/−199)
Dechu	522(+213/−170)	454(+393/−329)		512(+156/−158)
Niquero		290(+604/−271)		297(+208/−179)
Corozal		714(+386/−270)		593(+406/−320)
Nqutu		583(+173/−291)		

Crater name	Retreat distance (m)				
	Unmodified compared to equatorial	Glacial compared to equatorial	Gullied compared to equatorial	Glacial compared to same crater	Gullied compared to same crater
Zumba	3.42(+4.6/−0.91)				
Corintho	0				
Qara	30.94(+13.17/−9.22)				
Kenge	17.18(+18.27/−9.14)				
Topola	11.05(+10.72/−3.52)				
Yelwa	12.03(+11.28/−4.07)				
Kilmia	246.5(+146.08/−207.02)				
Crater A	13.21(+4.61/−3.54)		1.27(+0.44/−0.34)		0
Istok	0		17.57(+14.75/−4.92)		24.86(+20.87/−15.38)
Galap	29.16(+18.7/−12.24)		67.78(+43.46/−28.45)		42.55(+27.28/21.66)
Jaisalmer	48.57(+51.01/−12.39)	90.39(+44.87/−52.45)		12.24(+6.08/−7.1)	
Crater B	69.96(+55.23/−33.44)	107.34(+51.06/−38.12)		24.36(+11.59/−8.65)	
Crater C	43.85(+47.3/−13)	58.11(+67.56/−21.99)		27.96(+32.5/−10.58)	
Talu	73.28(+27.19/−22.73)	132.01(+79.56/−57.48)		69.42(+41.84/−30.23)	
Nybyen	31.91(+19.57/−9.6)	81.42(+109.9/−43.72)		52.1(+70.32/−27.97)	
Taltal E	112.45(+89.54/−46.49)	87.05(+120.85/−64.58)		30.1(+41.79/−22.33)	
Taltal W	85.67(+54.68/−44.28)	54.38(+84.14/−12.89)		35.28(+54.58/−8.36)	
Dechu	160.07(+48.84/−49.51)	167.97(+145.28/−121.54)		37.69(+32.6/−27.27)	
Niquero	53.51(+37.46/−32.28)	107.41(+224.08/−100.41)		67.38(+140.58/−62.99)	
Corozal	166.82(+114.31/−90.02)	285.58(+154.34/−108.21)		117.85(+63.69/−44.65)	
Nqutu		271.06(+80.59/−135.17)			

Table 2 (continued)

Crater name	Retreat rate (m/My)				
	Unmodified compared to equatorial	Glacial compared to equatorial	Gullied compared to equatorial	Glacial compared to same crater	Gullied compared to same crater
Zumba	7.6(+10.22/±2.01)				
Corintho	0				
Qara	5.84(+2.48/−1.74)				
Kenge	1.36(+1.45/−0.73)				
Topola	0.74(+0.71/−0.23)				
Yelwa	0.6(+0.56/−0.2)				
Kilmia	0.22(+0.13/−0.19)				
Crater A	132.14(+46.09/−35.43)		12.71(+4.43/−3.41)		0
Istok	0		92.46(+77.62/−25.91)		35.78(+13.93/−41.74)
Galap	4.49(+2.88/−1.88)		10.43(+6.69/−4.38)		49.37(+35.72/−54.57)
Jaisalmer	97.14(+102.03/−24.78)	180.77(+89.74/−104.89)		24.49(+12.16/−14.21)	
Crater B	32.54(+25.69/−15.56)	49.92(+23.75/−17.73)		48.73(+23.18/−17.31)	
Crater C	18.04(+19.47/−5.35)	23.91(+27.8/−9.05)		55.92(+65.01/−21.16)	
Talu	5.64(+2.09/−1.75)	10.15(+6.12/−4.42)		138.84(+83.68/−60.46)	
Nybyen	0.29(+0.18/−0.09)	0.74(+1/−0.4)		104.2(+140.64/−55.95)	
Taltal E	0.51(+0.41/−0.21)	0.4(+0.55/−0.29)		60.2(+83.57/−44.66)	
Taltal W	0.39(+0.25/−0.2)	0.25(+0.38/−0.06)		70.56(+109.16/−16.72)	
Dechu	0.52(+0.16/−0.16)	0.55(+0.48/−0.4)		75.38(+65.2/−54.55)	
Niquero	0.04(+0.03/−0.02)	0.08(+0.17/−0.08)		134.77(+281.16/−125.98)	
Corozal	0.12(+0.08/−0.06)	0.2(+0.11/−0.08)		235.7(+127.38/−89.31)	
Nqutu		0.15(+0.04/−0.08)			

^a Abbreviations: gu = gullied, gl = glaciated, gg = gullies and glaciated, po = pasted-on only, un = un modified. For slopes standard deviations are provided as the uncertainty values and for bedrock length the variance is given. This variance is propagated into the retreat distance and retreat rate calculations. Zero retreat rates are given where the mean slope of the bedrock is greater than or equal to the comparison slope (opposite wall, or equatorial slope).

stress regimes influencing submarginal and proglacial materials may also be required to explain the full suite of arcuate ridge and modification features in crater interior ice deposits that we observe.

Landforms associated with glaciotectionic deformation of material at or below glacier margins on Earth include thrust block moraine ridges (Fig. 18A and C; e.g., Bennett, 2001), hill-hole pairs (Fig. 18D; e.g., Rise et al., 2016), and rafted megablocks (e.g., Bennett et al., 1999). We have identified in our study possible examples of all three landform types, shown in Fig. 19. Longitudinal ridges within crater interior ice-deposit surfaces (Fig. 19), proximal to the spatulate depressions, could represent faulting of proglacial materials under stresses induced by crater wall glaciation (Figs. 18A, 19A).

Cold-based glaciers on Earth are rarely associated with prominent moraine ridges at their margins. However, despite subfreezing temperatures and deep, continuous permafrost in the Antarctic Dry Valleys, Fitzsimons (1996) described several arcuate, sharp-crested, ice-cored moraine ridges at the entry points of glaciers into saline proglacial lakes (Fig. 18C). Salinity of pore water exerts a critical control upon the deformability of sediments and glaciotectionic moraine formation at the cold margins of glaciers in permafrost environments on Earth (Etzelmüller et al., 1996). Thus, while we do not invoke saline proglacial lakes such as those in the Antarctic Dry Valleys (Fitzsimons, 1996) to explain the origin of the arcuate ridges on Mars, we do suggest that salinity of the martian substrate may play an essential role in generating deformable glacier beds despite subfreezing temperatures. Salts, such as perchlorates and sulphates capable of freezing-point depression, are known to be abundant on the martian surface from in situ investigations (e.g., Hecht et al., 2009) and orbital spectral observations (e.g., Langevin et al., 2005; Massé et al., 2010) as well as from theoretical considerations of surface geochemistry (e.g., Chevrier and Altheide, 2008; Chevrier et al., 2009; Toner et al., 2014). Generation of small interstitial meltwater films at the interfaces between impurities and ice crystals within the basal ice of cold-based glaciers in the Antarctic Dry Valleys has been posited as a mechanism for permitting basal sliding at rates that, while negligible on small timescales, can be significant over very long timescales (see Section 4.1 above; Cuffey et al., 2000). Abundant salts detected on Mars' surface could therefore provide a ready supply of impurities to glacier beds and permit generation of interstitial meltwater films and basal sliding at subfreezing temperatures. It has been

suggested that this mechanism could be effective at temperatures down to $-30\text{ }^{\circ}\text{C}$ on Earth (Cuffey et al., 2000).

Our results only provide evidence for meltwater generation in the latest phase of glaciation ($\sim 5\text{--}10\text{ Ma}$) and only for small, thin glaciers rather than the more ancient VFF. Although recent studies have identified compelling evidence for rare, localised occurrences of past basal melting of glaciers on Mars, in relation to existing VFF (e.g., Hubbard et al., 2011; Gallagher and Balme, 2015; Butcher et al., 2017) and to past late Amazonian-epoch glaciation (e.g., Scanlon et al., 2014, 2015), a majority of Amazonian-aged glacial assemblages on Mars provide little apparent evidence for the role of meltwater (e.g., Head and Marchant, 2003; Marchant and Head, 2007). Fassett et al. (2010) attributed rare valleys on VFF surfaces to localised melting from the reflection of solar insolation by adjacent topography, rather than melting induced by bulk VFF thermal regime or climate. Hence, Amazonian glaciation on Mars was likely predominantly cold-based and the closest terrestrial analogues to existing VFF are thought to be cold-based debris-covered glaciers in the Antarctic Dry Valleys (e.g., Head and Marchant, 2003; Hambrey and Fitzsimons, 2010).

In summary, the landscape assemblage described here provides the first evidence that liquid water could indeed have played a role in late Amazonian glaciation. Although the quantities were likely relatively limited, the geographical distribution was widespread: pasted-on terrain and texturally altered bedrock are found on almost every sloping surface in the mid-latitudes. We do not support the production of large quantities of meltwater as this would have obliterated the arcuate ridges and even the pasted-on terrain and would have produced a suite of landforms akin to wet-based glaciers on Earth (e.g., eskers, meltwater channels, hummocky moraines).

4.3. Glaciation and erosion rates

Comparisons of sediment fluxes from glaciated and nonglaciated basins by Hallet et al. (1996) found that, on Earth, glaciation is *unsurpassed* in its ability to erode and mobilise sediment compared to other erosional mechanisms operating over similar timescales. They attribute comparable sediment yields from lowland rivers draining marine clays in nonglaciated basins to high susceptibility of these clays to mass wasting and, in particular, gullying (Hallet et al., 1996). The discussion

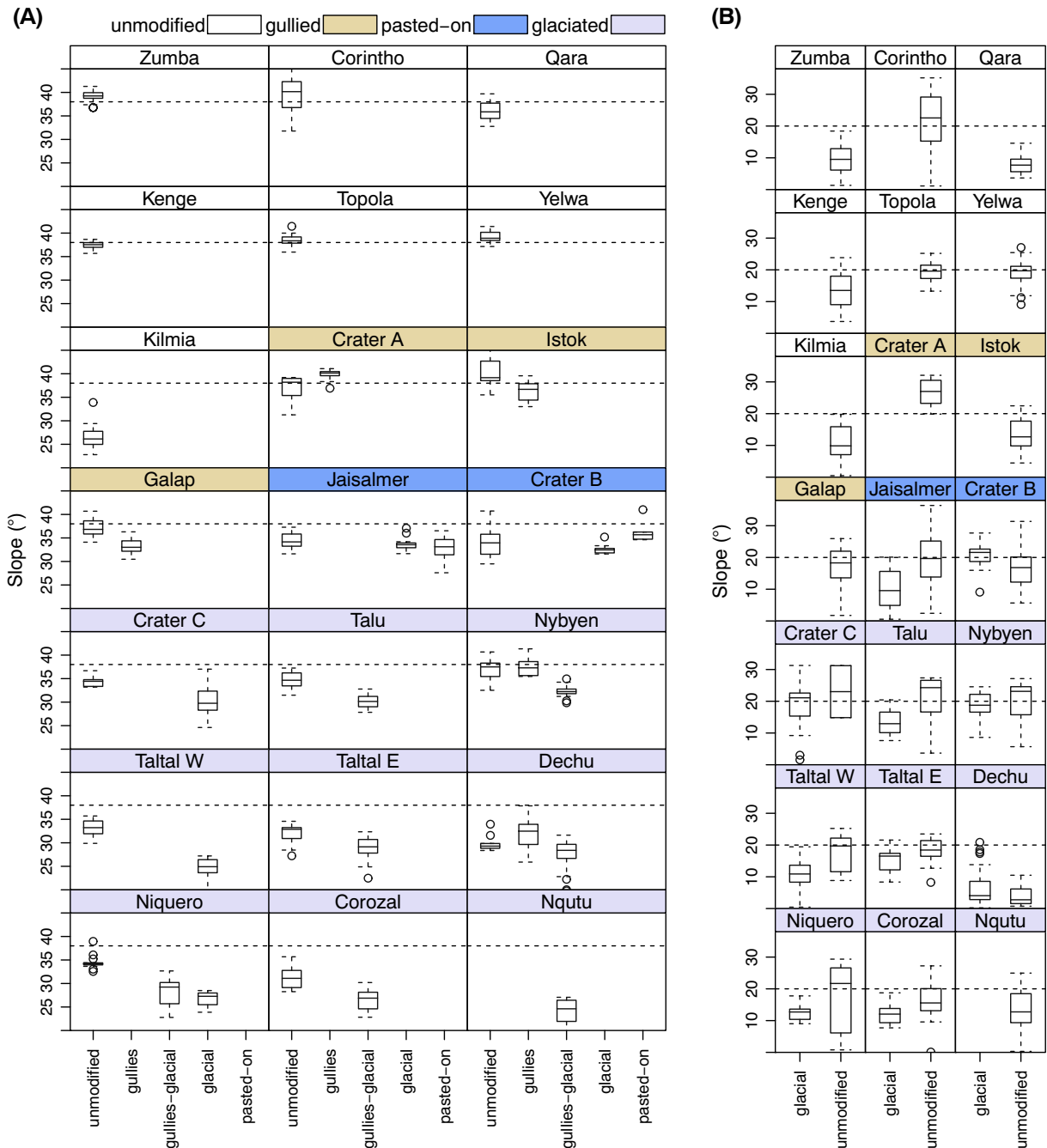


Fig. 14. Box plots displaying results from our crater wall slope-analysis. Black boxes indicate the interquartile range, whiskers the maximum and minimum values, horizontal black line the median value, and black dots outliers (classed as those values farther than 1.5 interquartile-ranges from the median). (A) Box plots of slope data gathered for the inner crater wall of our studied craters. Dotted line is arbitrarily located at 38° for reference. (B) Box plots of slope data gathered for the exterior crater wall of our studied craters. Dotted line is arbitrarily located at 20° for reference. Note: pasted-on refers to parts of the crater wall with pasted-on terrain yet little textural alteration of the bedrock, whereas glacial refers to areas with pasted-on terrain and textural alteration of the bedrock (Fig. 7F). In the items in the legend refer to different classes of crater: unmodified = unmodified equatorial craters, gullied = gullied and unglaciated craters, pasted-on = craters with pasted-on terrain but no arcuate ridges or interior ice deposit, and glaciated = glaciated craters.

above demonstrates that even cold-based glaciers can erode their beds but at rates that are orders of magnitude lower than erosion by wet-based glaciation. Cold-based polar glaciers typically erode their beds at rates of $\sim 10^1 \text{ m My}^{-1}$ (Hallet et al., 1996; Cuffey et al., 2000), compared to rates of $\sim 10^3 \text{ m My}^{-1}$ for small temperate valley glaciers in the Swiss Alps and $10^4\text{--}10^5 \text{ m My}^{-1}$ beneath large, fast-flowing temperate glaciers in southeast Alaska (Hallet et al., 1996). However, when integrated over long timescales, the cumulative geomorphic influence of cold-based glaciation may be detectable; Cuffey et al. (2000) estimated that 10 to 30 m of erosion may have occurred in the U-shaped valley occupied by Meserve glacier on Earth, over a period of $\sim 10 \text{ My}$

of cold-based glaciation. Rates of glacial erosion are greatly enhanced in the presence of weak (e.g., sedimentary or highly fractured) bedrock, particularly in tectonically active regions such as southeast Alaska and the Himalaya (Hallet et al., 1996).

The fastest retreat rates found in this study of $\sim 10^2 \text{ m My}^{-1}$ (Table 2; Fig. 15) exceed the expected erosion rate on Earth for cold-based glaciers and are instead equivalent to erosion rates for temperate valley glaciers where melt is abundant. Similar erosion rates for icecaps and glaciers are predicted over 0.1 Ma timescales on Earth for newly constructed volcanic provinces (e.g., Iceland, Geirsdóttir et al., 2007) or actively uplifting areas (e.g., New Zealand, Egholm et al., 2012). Our highest erosion rates

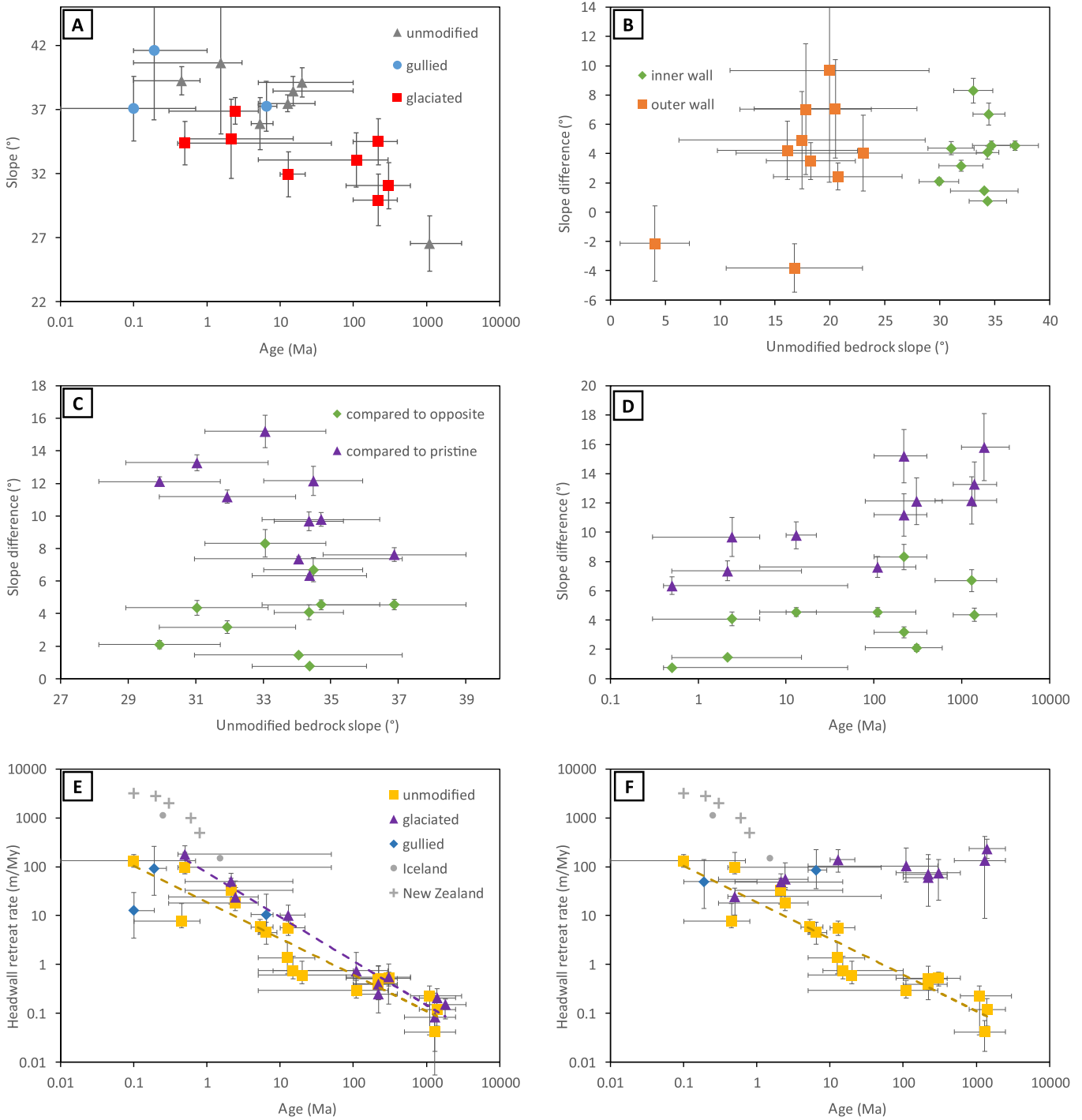


Fig. 15. Wall slopes, reduction in wall slope, and headwall retreat rate for our studied craters. (A) The slope of exposed bedrock in the unmodified walls of craters in this study, including craters with neither glacial nor gully features (unmodified), craters with gullies but no glacial features (gullied), and craters with glacial features (glaciated). (B) The slope difference between glaciated walls and unmodified walls from the same crater versus the unmodified wall slopes for outer and inner crater walls. (C–D) The slope difference against unmodified wall slope and age respectively. The legend for both plots is in panel (C). (E) Estimated headwall retreat rate against age for our craters separated into unmodified crater walls and those affected by glacial erosion and gully erosion. Plotted for comparison are erosion rates from modelled glacial landscapes in New Zealand (Egholm et al., 2012) and measured glacial erosion from Iceland (Geirsdóttir et al., 2007). Trendlines are added only to guide the eye. (F) The same plot as in panel (E), but the headwall retreat rate is calculated over a fixed 500 ky interval and uses the slope difference compared to the unmodified wall in the same crater (rather than comparison to an equatorial crater wall slope). NB: The error bars for slope represent the standard deviation of the slope measurements and age error bars the potential age range for the host craters (Table 1). The uncertainty in slope difference is calculated by propagation of errors and the uncertainty in retreat rate is dominated by the length of exposed bedrock, hence uncertainties are calculated by recalculating the retreat rate using the minimum and maximum length of the exposed bedrock for that crater.

are above those estimated by Levy et al. (2016) for VFF: namely 10^{-2} – 10^1 m My⁻¹ of erosion. In our study headwall retreat rates <math>10^1 m My⁻¹ are only found for craters with ages >5 Ma, and these craters have similar headwall retreat rates to those estimated by Levy et al. (2016). For comparison, crater erosion rates by aeolian processes in

equatorial regions of Mars are estimated to be on the order of 10^0 – 10^1 m My⁻¹ over 0.5–2 Ma timescales (Golombek et al., 2014a), decreasing with increasing temporal baseline. The decrease in erosion rate over time reflects the diffusive nature of the dry denudation processes, and the diffusivity is 10^2 – 10^3 times lower than terrestrial values and similar

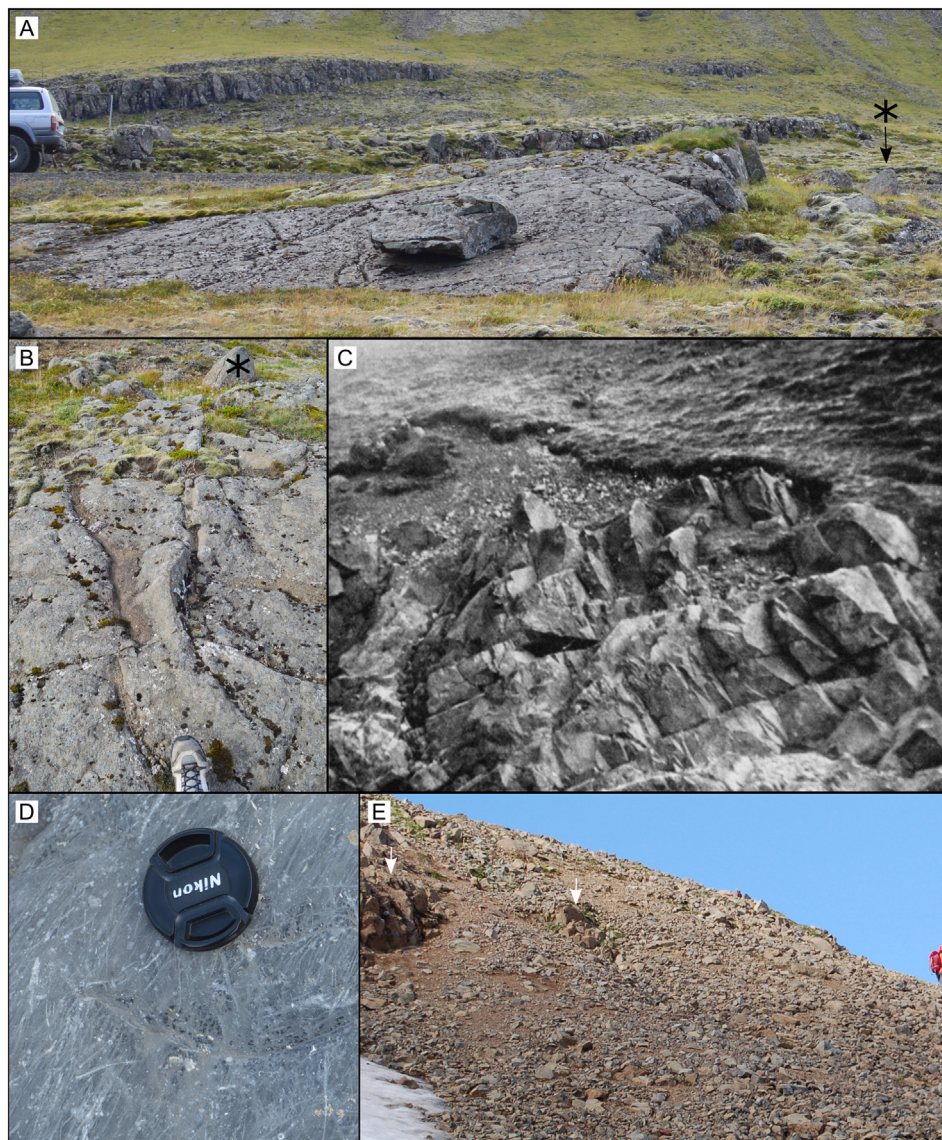


Fig. 16. Examples of differences in macroscale morphology between surfaces influenced by glacier abrasion or plucking on Earth and a comparison to slopes affected by periglacial erosion. (A) A small *rôche moutonnée* (image credit Frances Butcher) at the eastern end of Hvalfjörður (west Iceland), looking toward the southern side of Botnsdalur showing the difference in macroscale surface texture generated by abrasion on the stoss slope and plucking on the lee slope. Ice flow was from left to right. The star indicates the same boulder that is visible in panel (B), looking along the same landform close to its crest, showing the transition from smoothed to craggy surface form (image credit Frances Butcher). (C) A craggy surface in Glenridding Beck (The Lake District, UK) generated by plucking by glacial ice. Reproduced from Hay (1934). (D) Small-scale forms generated by abrasion and quarrying on the glacially smoothed surface of a transported boulder in Long Hill esker pit, County Westmeath, Ireland. Striae formed by abrasion are oriented in the former direction of ice flow (either bottom left to top right, or vice versa). A crescentic or lunate gouge (dependent on ice flow direction) formed by glacial quarrying of the boulder surface crosses the centre of the image (image credit Frances Butcher). (E) Periglacially modified slopes on the eastern flank of Lambahnjúkur in northern Iceland with two bedrock outcrops (white arrows), illustrating the similarity between macro-scale morphology of surfaces affected by plucking (e.g., panel C) and periglacial processes. (Source: image credit Costanza Morino).

to that on the Moon (Golombek et al., 2006; Fassett and Thomson, 2014; Golombek et al., 2014a).

A single (recent) event of intense glacial erosion related to the presence of the pasted-on terrain, is one way in which to explain the parallel trends on Fig. 15E. This does not preclude the possibility that previous erosion events have occurred and are either too ancient to be distinguishable from the diffusive decline in crater bedrock outcrop slopes or occurred earlier than our studied timeframe and been overprinted by this later event – a notion supported by the slightly elevated erosion rates expressed by craters older than 1 Ga in Fig. 15F. As shown in Fig. 15B, the erosion intensity seems independent of slope – which is not the case for diffusion-like processes that tend to diminish in intensity with decreasing slope – hence that the glaciated craters would follow this trend seems improbable unless it was imposed by the ongoing background crater degradation. If punctuated

accelerated erosion by glaciers was happening throughout a crater's history, we would expect the glaciated crater walls and unmodified glacier walls to diverge with crater age on Fig. 15E and the glaciated crater walls to have increasing erosion rates with time in Fig. 15F, which is not the case. If we assume a single 500-ky event of glaciation we see that the headwall retreat rates become independent of age with values of $\sim 10^2$ m My⁻¹ (Fig. 15F). This single event is supported by the morphology of the arcuate ridges – they are never found as multiple superposed sets. Because our youngest crater with pasted-on terrain dates to 0.5 (0.4–50) Ma, this one event is likely to be shorter; hence, the retreat rates are probably an order of magnitude higher. Further it is likely that the bedrock slope lowering extends underneath the pasted-on terrain that we see today, another factor leading to a potential underestimation of the headwall retreat rate. Given the large uncertainty on the age of the youngest crater and that our other craters with

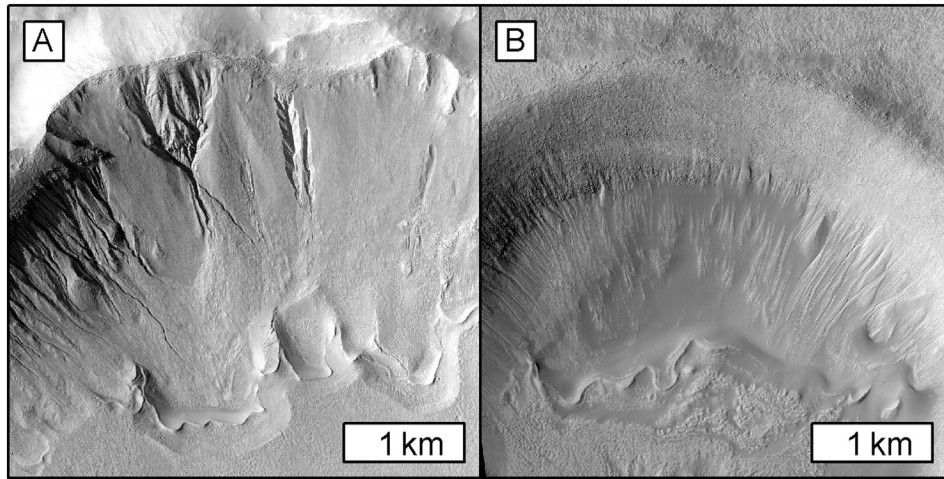


Fig. 17. Examples of sinuous arcuate ridges with and without associated upslope alcoves. (A) HiRISE image ESP_038236_1410 where loops in the arcuate ridges appear to be associated with upslope alcoves of a similar width. (B) Avire Crater in HiRISE image ESP_029467_1390 with a similarly sinuous arcuate ridge to panel (A) but without any obvious upslope alcoves.

past-on terrain date to >10 Ma (consistent also with dating presented in de Haas et al., 2018), these dates point to the “glacial event” having occurred between 5 and 10 Ma. It seems logical to link it to the shift in mean obliquity that happened ~5 Ma, but further dating on young craters with pasted-on terrain and texturally altered bedrock would be

needed to substantiate this claim. Previous work has linked this decrease in mean obliquity as the transition point between *glacial* and *interglacial* Mars with recent high obliquity excursions representing mini-ice-ages (Head et al., 2003; Madeleine et al., 2014). This shift marks a transition from a period with lower average surface

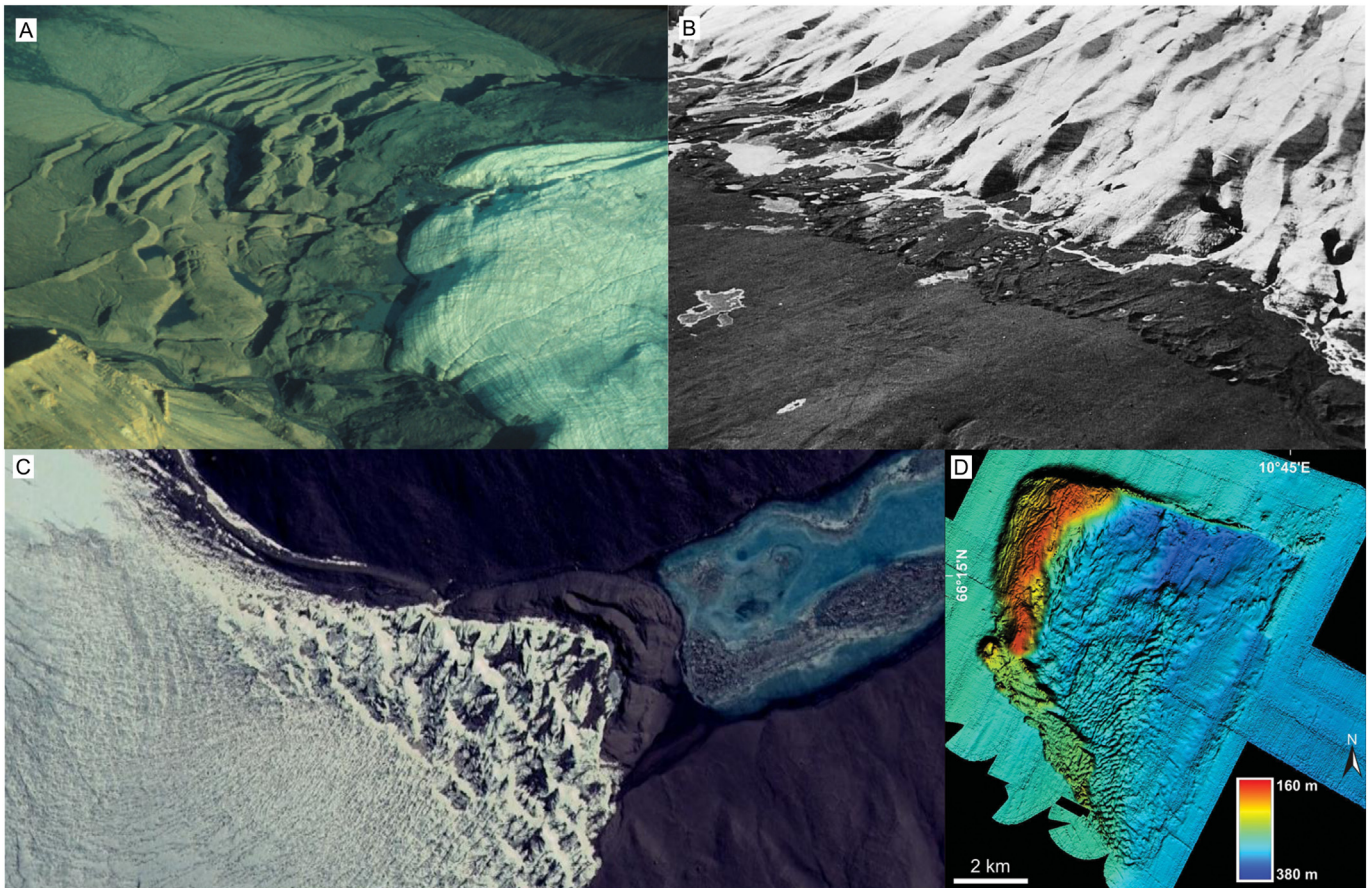


Fig. 18. Examples of arcuate glaciotectionic landforms on Earth. (A) Oblique view of active thrusts within proglacial sediments of a piedmont glacier, Canada (taken from Evans, 2007). No scale was provided in the original publication, but we estimate the valley floor to be 1.5 km wide. (B) Oblique view of small seasonal glaciotectionic moraines at Briðamerkurjökull, Iceland illustrating the highly arcuate nature of some moraine complexes in front of a broad glacier terminus (taken from Bennett, 2001). No scale was provided in the original publication, but such seasonal ridges are typically metres in width. (C) A thrust-block moraine comprising lacustrine sediments (Fitzsimons, 1996) at the terminus of Wright Lower Glacier, Antarctic Dry Valleys. The ridge is ~80 m wide at its widest point and north is toward the top (Digital Earth image from Google Earth). (D) Marine bathymetry showing an arcuate hill-hole pair on the Norwegian continental shelf (taken from Rise et al., 2016).

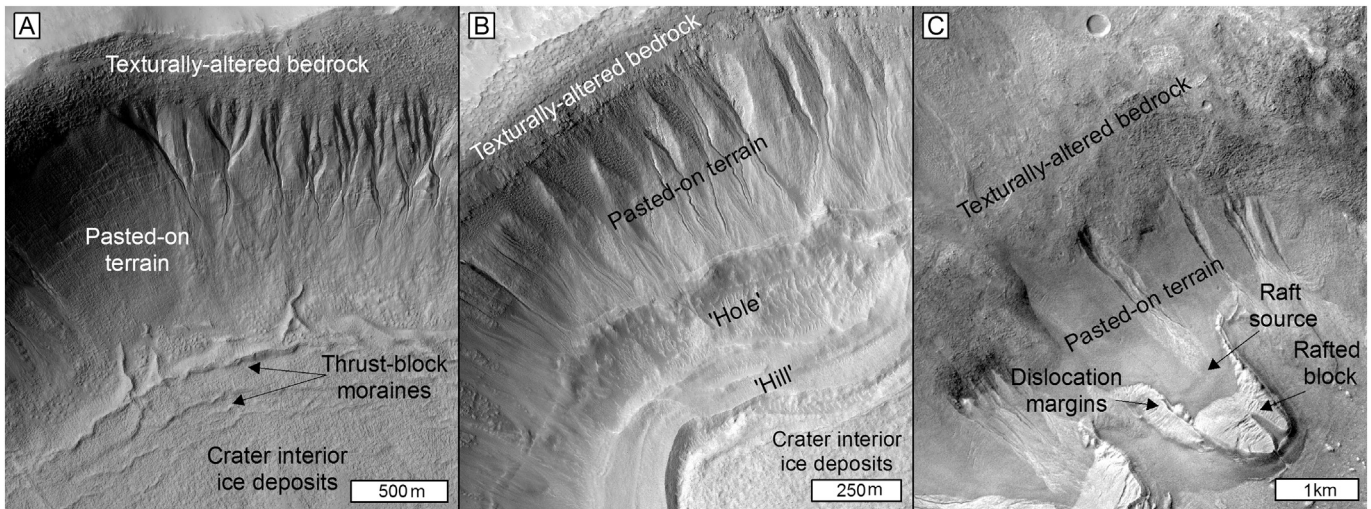


Fig. 19. Possible glaciectonic landforms on Mars. (A) Possible examples of glaciectonic landforms beyond the foot of the glaciated crater wall, possibly analogous to the proglacial thrust block moraines in Fig. 18A. HiRISE image ESP_020051_1420. (B) Example of lower crater wall hole which truncates gully fans upslope of arcuate ridge (hill) at CCF margins. This may be analogous to hill-hole pairs on Earth (e.g., Fig. 18D). HiRISE image PSP_003253_1405. (C) Possible example of a rafted megablock at the foot of a slope within the rim of the Argyre impact basin. Note that this feature is not within an impact crater included in our slope measurement survey. However, it provides the best type example of similar features observed within impact craters and illustrates the same relationships between texturally altered bedrock, pasted-on terrain, and arcuate ridges. The bright lobate plateau appears to have been mobilised downslope along shear planes that are visible within upslope lateral extensions of the block. Its plateau morphology, gently sloping upslope margin, steep downslope margin, and clear source region leads us to propose that it represents a rafted megablock mobilised by stresses induced below the margin of a glacier. It does not appear to have been distorted or reworked. Hence we favour a raft origin over a hill-hole origin. An alternate interpretation is that it represents an extant lobe of glacier ice. CTX image G11_022685_1402.

temperatures to higher average surface temperatures, particularly in the mid-latitudes (e.g., Kreslavsky et al., 2008).

This general shift in climate conditions is supported by observational evidence as follows. Berman et al. (2009) reported that GLFs (termed lobate forms by these authors) tend to be found in smaller craters (<70 km in diameter) with no particular trend observed for other crater interior ice deposits. This crater diameter dependency was further explored in Fassett et al. (2014) who found that synglacial craters tend to be of smaller diameter than preglacial craters. They concluded that this observation is a function of the age and duration of the *glacial* epoch superposed on the crater production function. In agreement, recent work by Hepburn et al. (2018) reported that smaller glacial forms

are significantly younger than LDA, LVF, or crater interior ice deposits (including CCF), as detailed in Section 1.1. That the present epoch is one of glacial retreat is broadly acknowledged (Brough et al., 2016a). Our results agree with the broad overall picture from this previous work; that a long glacial epoch that comprised several phases of glacial growth was followed by glacial retreat, dominating present conditions. Our results also show that crater interior ice deposits predate the pasted-on terrain (as noted by Levy et al., 2009b) and that the presence or absence of the crater interior ice deposits do not seem to have any relation to the amount of erosion recorded by these craters (Fig. 20).

However, the question still remains as to how the terminal stages of an ice age under cold and dry Amazonian conditions could generate the

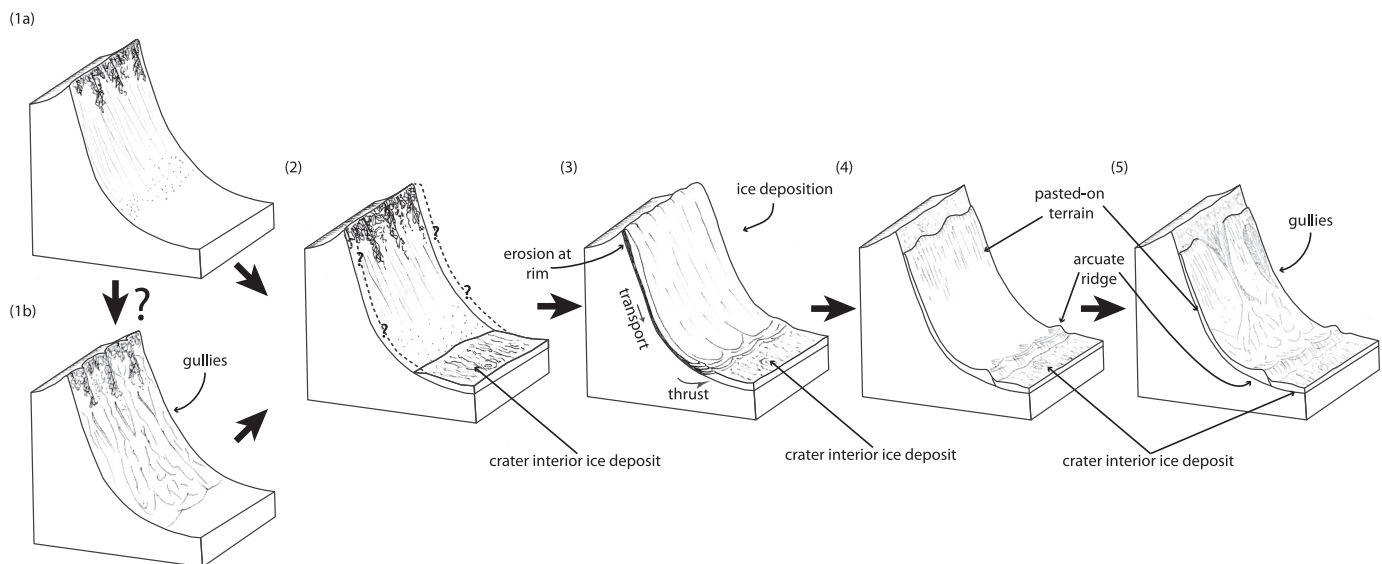


Fig. 20. Schematic diagram illustrating the development of pasted-on terrain, arcuate ridges, and gullies on crater walls on Mars. Step 1a is a pristine crater wall with exposed bedrock, and step 1b shows the development of gullies. Steps 1a and 1b could lead to step 2 onward, but evidence of the starting configuration is erased at step 3. At step 2 crater floor ice deposits are laid down by some process that does not significantly erode the crater wall. At step 3 glacial erosion occurs, scouring rock from the crater rim and transporting the debris downslope, depositing it as till (pasted-on terrain). On interaction with the preexisting ice deposit, the moist till is thrust-up forming moraines (arcuate ridges). After the glacier has sublimated away at step 4 onward, the crater wall hosts pasted-on terrain (till) and arcuate ridges (moraines), and later (step 5) gullies can be formed into these easily erodible deposits.

conditions for production of meltwater, even if only in small amounts. Other authors examining glacial melt on Mars (e.g., Fasset et al., 2010; Hobley et al., 2014; Scanlon et al., 2015; Butcher et al., 2017) have reviewed and proposed the following scenarios: (i) orbital-driven increases in surface temperature with current atmospheric composition/pressure, (ii) increased surface snow/ice thickness reducing heat loss to the atmosphere, (iii) geothermal heat increase, (iv) atmospheric change inducing heating caused by impact or volcanic events (greenhouse effect), and (v) direct heating caused by impact events.

We can immediately rule out direct heating caused by impact events and geothermal heat increase because both of these would be expected to be expressed locally rather than at a global scale as our results indicate. Insulation by thick snow and ice are unlikely because the ice thicknesses in our proposed glaciers is almost certainly less than the >1-km thickness estimated for this effect to become important (e.g., Carr and Head, 2003) – because their moraines are <100 m in height. Atmospheric changes caused by impacts require a large enough impact to substantially change the atmosphere and such impacts are estimated to produce craters hundreds of kilometres in size (Segura et al., 2008). According to the Hartmann and Neukum (2001) production function, this should happen on Mars every ~1 Ga and Lyot Crater at 215 km in diameter is generally thought to be the youngest example, whose age is generally agreed to be older than 1 Ga (Harrison et al., 2010). This leaves the two remaining scenarios of atmospheric heating through secular changes in orbital parameters and/or injection of greenhouse gases from volcanic events. Alone, changes in orbital parameters are not anticipated to cause substantial surface warming with the current atmospheric density and composition (e.g., Kreslavsky et al., 2008; Mansfield et al., 2018). Volcanism is thought to have continued into the Amazonian (Neukum et al., 2004; Werner, 2009) with estimates as recent as the last few Ma for Elysium Mons (Vaucher et al., 2009) and low shields in Tharsis (Hauber et al., 2011b), which could tie with the timing of the glacial erosion event. However, further work would be needed on the dating and duration of the glacial erosion event to assess if recent volcanic activity would be of sufficient intensity and duration to cause the required temperature increase. As noted in Section 4.3, another factor likely to be playing a role is the abundant presence of salts on Mars, which would diminish the perturbation required by either climate or volcanic-induced atmospheric change to generate subglacial meltwater. We suggest these possibilities as fruitful avenues to direct future studies.

5. Gully-glacier interactions on Mars

Our headwall retreat rate calculations reveal that, unlike on Earth, glacial and gully headwall retreat rates appear to be broadly equivalent on Mars. This means that even if gullies were present on the crater walls prior to the glacial erosion event, then that much evidence remains is unlikely (Fig. 20). Hence, we hypothesise that all gullies that are visible today were created after this glacial erosion event (~5 Ma), consistent with other dating studies. Craters that postdate the glacial erosion event possess gullies that solely erode bedrock, and craters that predate the glacial erosion event possess gullies that primarily erode into pasted-on terrain (Fig. 20). Gullies in both contexts have similar-sized alcoves (de Haas et al., 2018). Our estimates of headwall retreat by gullies are similar to those calculated by de Haas et al. (2015b) using a different method. These estimates of martian gully retreat align with estimates of terrestrial rockwall retreat rates in Arctic, Nordic, and Alpine environments of 10^1 – 10^4 m My⁻¹ (see summary in Fig. 12 of de Haas et al., 2015b), strengthening the case made by these authors for water as a catalyst for backweathering in these craters.

We suggest that pasted-on terrain on formerly glaciated crater walls could partly represent subglacial deposits, which would explain the frequent observation of downslope lineations present on the surface of this unit. We also note that the pasted-on terrain also often expresses a polygonised surface texture and that it blends gradually into more

glacier-like textures lower on the crater wall (topographically and morphologically), suggesting that it could also represent part of a glacier-like body in and of itself. This is supported by measurements made by Conway and Balme (2014) who found that the pasted-on terrain contains between 46% and 95% ice by volume. Also Dickson et al. (2015) found that the pasted-on terrain often expressed contouring fractures, which cross-cut and are superposed by gully-fans (located mid- to lower-crater wall) hinting that this unit could still be in motion. The topographic relaxation of gully incisions as they become polygonised (Conway and Balme, 2014) supports this notion. The fact that our work shows that gully incisions tend to deepen toward higher latitudes in both hemispheres could therefore be interpreted as evidence that the pasted-on terrain thickens and has higher ice content at higher latitudes (Fig. 9), a concept supported by the recent finding of near-pure surface ice deposits by Dundas et al. (2018) at latitudes of 55°. Our work reveals that glacial erosion must have liberated a substantial quantity of rock debris, and logically this should be found downslope within the pasted-on terrain. Further, the surface textures expressed by the pasted-on terrain do not support debris covered ice, as suggested for the martian VFF (lack of pitting, expanded craters, holds cracks, and polygons) (Soare et al., 2017). Hence, we suggest that these are ice-rich sediments rather than sediments covering ice. De Haas et al. (2015c) found that incisions into gully-fans downslope of pasted-on terrain were much less likely to expose metre-scale boulders than incisions whose catchments included exposed bedrock, implying that the sediments within the pasted-on terrain tend to be finer grained than those liberated directly from rockwalls.

Our hypothesis for a single glacial event at around 5–10 Ma fits with the interpretation made by Dickson et al. (2015) of one episode of pasted-on terrain emplacement based on the stratigraphic relationships between gullies and pasted-on terrain (they call it 'LDM'). Conway and Balme (2014) also found no evidence for layering within the incisions into the pasted-on terrain. Dickson et al. (2015) noted that inverted gully channels and that fans mainly occur on equator-facing slopes between 40°S and 50°S, where our study shows that the pasted-on terrain is at its thickest. We hypothesise that these inverted topographies are produced by the loss of ice: gullies could have deposited debris on top of glacial ice and when the surrounding ice has been lost, the gully deposits (channels and fans) preserve some of the ice and protrude from the surrounding surface. These inverted gullies appear beheaded, not because their upper half has been buried (as suggested by Dickson et al., 2015), but because it has been eroded away. If too much ice is removed then the inverted gullies disappear (explaining their paucity where the pasted-on terrain is thin).

The observation by Dickson et al. (2015) that some gullies appear to be buried by the pasted-on terrain seems to contradict our hypothesis that this unit represents a glacial till under which a significant erosive event has occurred – such deposits should have been removed. However, Dickson et al. (2015) only presented two examples of gully deposits being revealed from under the pasted-on terrain, and both of these could be interpreted as being degraded gully deposits atop pasted-on terrain. Another possibility to explain these observations is that another mantling deposit superposes the pasted-on terrain, a possibility supported by occasional observations of pasted-on terrain emerging from under a light-toned mantle (e.g., Fig. 71): a phenomenon also observed by Soare et al. (2017). Many authors have noticed that alcoves appear from under the pasted-on terrain (e.g., Christensen, 2003; Dickson et al., 2015; de Haas et al., 2018), yet the link between these alcoves and preexisting gullies is uncertain and only circumstantial. Hence, we believe that the population of gullies we see today postdates the glacial event that laid down the pasted-on terrain (Fig. 20).

Our hypothesis that the pasted-on terrain is predominantly an ice-rich glacial till is supported by the way in which gullies erode into it. Gullies always have a V-shaped incision, or chute, whenever they encounter the pasted-on terrain. Such incisions are also common in similar-scaled systems on Earth when the sediment they incise into is

granular and loose (Fig. 21). The examples we present here are from glacial and volcanoclastic terrains where the loose surface deposits are quickly stripped by flowing liquid water, often involving debris flows,

producing sharp V-shaped incisions whose floors are located upon more resistant materials (Ballantyne and Benn, 1994; Ferrucci et al., 2005). V-shaped incisions into glacial moraines on Earth occur during

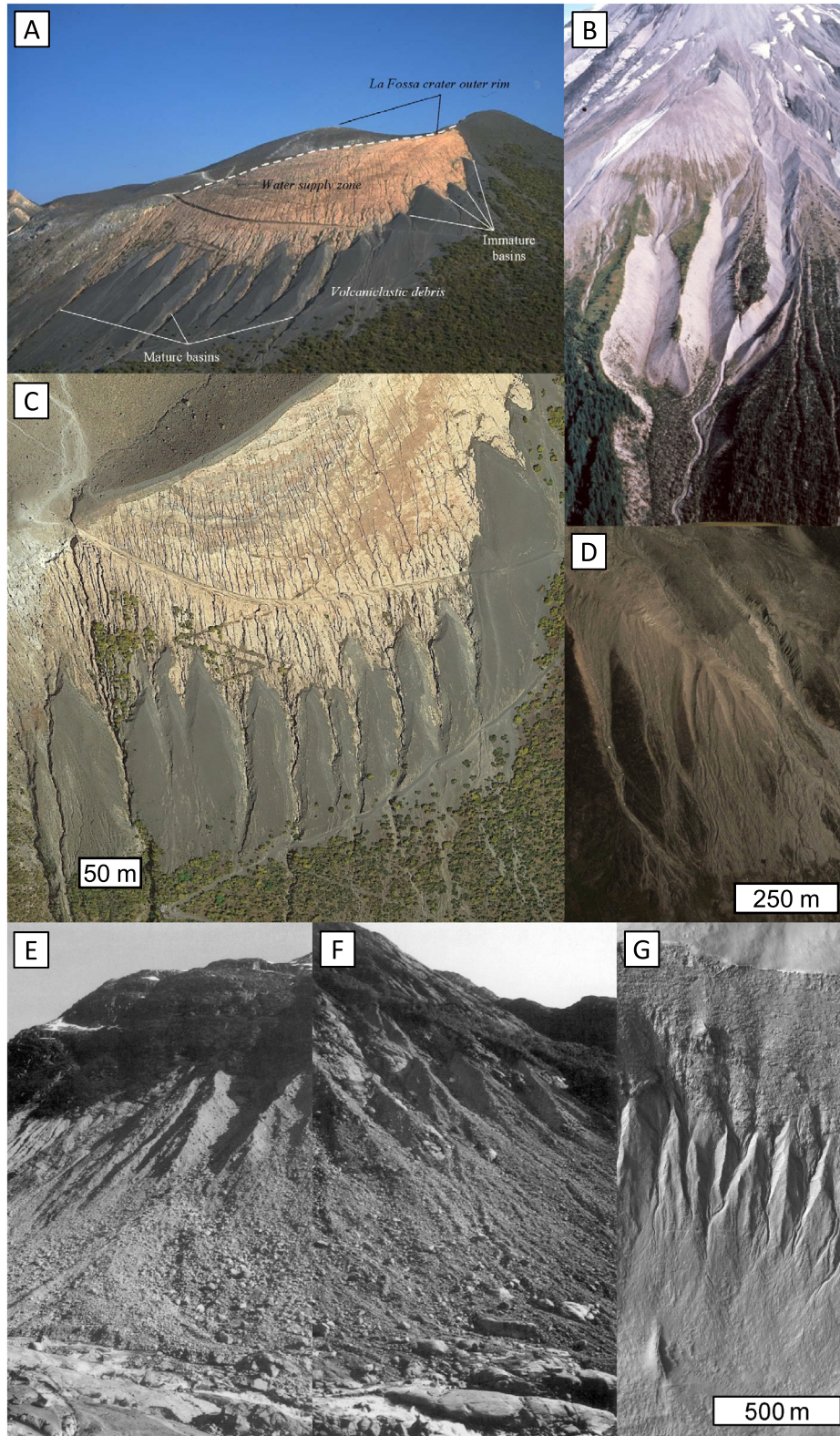


Fig. 21. Gullies incising into unconsolidated glacial and volcanic sediments on Earth. (A) Debris flows dissecting the unconsolidated volcanoclastic deposits on the side of La Fossa Cone on Vulcano Island, Italy. Image from Ferrucci et al. (2005). (B) Photo from 1979 of gullies incised into the west side of Mt. St Helens from the USGS photo library, id: mhob0056. (C) Google Earth image of the same suite of gullies as shown in (A). (D) Google Earth image of gullies cut into moraine from glaciers in west Greenland (70.381N, 52.255W). (E–F) Slopes in Fåbergstølsdalen where gullies cut into the drift deposits and where debris flow deposits are seen in the fans in the foreground. Images from Ballantyne and Benn (1994), Figs. 4 and 5. (G) Gullies stripping pasted-on terrain on Mars, HiRISE image PSP_002066_1425.

the paraglacial phase of glacial retreat and can penetrate through ice-rich moraine deposits (e.g., Bennett et al., 2000; Ewertowski and Tomczyk, 2015). Where stripping of the pasted-on terrain is advanced, rills can be seen converging over the bedrock to meet at the incisions on Mars (Figs. 6F, 7C, 21G), and a similar phenomenon happens on Earth (Fig. 21C). Isolated gullies within the pasted-on terrain could originate by flow of water at the lower boundary of the pasted-on terrain, initiating collapse and upslope propagation of the incision (see Fig. 21B for a terrestrial example and Figs. 5D and 7G for martian ones). Our work shows that gullies can substantially erode the rims of impact craters without pasted-on terrain. However, substantial incision into the bedrock by gullies is rare in the presence of pasted-on terrain (e.g., Dickson et al., 2015). One of the reasons could be that gully-forming processes are enhanced on steep slopes, hence the lowering of the crater wall slope associated with the pasted-on terrain reduces the erosive capacity of the gullies. Second, much of the erosional potential of the gullies could be taken up in stripping the pasted-on terrain. Third, the pasted-on terrain could be forming a protective layer and inhibiting the continuous weathering of the bedrock needed to initiate and grow the alcoves.

Our previous work has shown that dense concentrations of extant VFF are anticorrelated with dense gully populations (Conway et al., 2017), yet gullies are intimately associated with pasted-on terrain and arcuate ridges (Christensen, 2003; e.g., Berman et al., 2005; Head et al., 2008; Dickson et al., 2015). In this work we have presented evidence in favour of small quantities of meltwater being involved in lowering crater wall slopes where texturally altered bedrock and pasted-on terrain are present. Does this suggest a role of water in the formation of martian gullies? Unfortunately, the findings reported in this paper do not provide any resolution to the ongoing debate between CO₂ sublimation (e.g., Dundas et al., 2017, and references therein) and meltwater generation (e.g., Conway et al., 2018a, 2018b, and references therein) for forming martian gullies. A meltwater hypothesis for this recent glacial erosion event on Mars leads to the reasonable assumption that gullies can be produced via a similar yet less widespread mechanism, which has been occurring periodically since this glacial erosion event. However, CO₂ and H₂O ices are often found together (Vincendon et al., 2010; e.g., Vincendon, 2015), and without more detailed knowledge on how CO₂ sublimation might engender sediment transport assessing whether the morphological evidence fits with this transport mechanism remains difficult (Conway et al., 2018b).

Finally, texturally altered bedrock and pasted-on terrain are more spatially widespread than gullies and occur at low slope angles where gullies are not found. Hence, even if gullies do not represent episodes of flowing liquid water at the surface of Mars, the wet-based glacial erosion event that we report on here does present evidence for a significant occurrence of widespread, recent melt on Mars.

6. Conclusions

We have found evidence for extensive crater wall erosion by very recent (~5–10 Ma) small-scale glaciers on Mars that we estimate achieved headwall retreat rates up to ~10² m My⁻¹. This erosion rate is of the same order of magnitude as the landscape change brought about by the youngest gullies (<1 Ma) incised into bedrock on Mars.

We posit that the erosion of these crater walls is driven by small amounts of subglacial melt, possibly favoured by brines, using the following lines of evidence based on Earth analogy:

- Recent headwall retreat rates are equivalent to wet-based rather than cold-based glaciers on Earth.
- Formation of arcuate ridges and associated deformational features at the base of crater walls involved a component of glacial tectonism, which requires pore water.
- The presence of texturally altered bedrock, which is consistent with ice-segregation and frost-shattering on Earth.

- Pasted-on terrain, found topographically below the texturally altered bedrock represents glacial till deposits. We suggest the downslope lineations often found on this deposit could be glacial in origin. The till interpretation is supported by the nature of the gully erosion. This provides an alternate explanation to that the pasted-on terrain is simply a thicker version of the latitude-dependant mantle — an airfall deposit of ice nucleated on dust (e.g., Mustard et al., 2001; Kreslavsky and Head, 2002).

Our results suggest that the accelerated crater wall slope reduction was brought about in a pulse of erosion, which may have occurred sometime 5–10 Ma coincident with a significant climate shift brought about by a change in Mars' mean orbital obliquity. This shift alone probably cannot explain the generation of basal pore water, and we suggest that the influence of volcanic greenhouse gases and/or the influence of salts as additional potential contributing factors. Gullies seem to postdate this event and have caused significant reworking of the pasted-on terrain on the steepest slopes. The magnitude of the glacial erosion is the same as that brought about by the youngest modern gullies, and hence evidence of gullies predating the glacial erosion is likely difficult to find. Although our results cannot directly advocate that gullies are produced by meltwater runoff, the nature of this wet glacial event does provide strong evidence for meltwater generation in Mars' recent history.

Acknowledgements

We thank the three reviewers (Goro Komatsu, Daniel Berman and Vic Baker) for their thoughtful comments and whose suggested modifications greatly improved the manuscript. SJC is supported for her HiRISE work by the French Space Agency, CNES. FEGB is supported by STFC grant ST/N50421X/1. TdH is funded by the Netherlands Organization for Scientific Research (NWO) via Rubicon grant 019.153LW.002. JMD gratefully acknowledges UK Space Agency (UK SA) funding (ST/R002355/1). PMG acknowledges support from the UK Space Agency (grants ST/L00254X/1, ST/R002355/1).

References

- Arfstrom, J., Hartmann, W.K., 2005. Martian flow features, moraine-like ridges, and gullies: terrestrial analogs and interrelationships. *Icarus* 174:321–335. <https://doi.org/10.1016/j.icarus.2004.05.026>.
- Aston, A.H., Conway, S.J., Balme, M.R., 2011. Identifying Martian gully evolution. *Geol. Soc. Lond. Spec. Publ.* 356:151–169. <https://doi.org/10.1144/SP356.9>.
- Atkins, C.B., Barrett, P.J., Hicock, S.R., 2002. Cold glaciers erode and deposit: evidence from Allan Hills, Antarctica. *Geology* 30:659–662. [https://doi.org/10.1130/0091-7613\(2002\)030<0659:CGEAE>2.0.CO;2](https://doi.org/10.1130/0091-7613(2002)030<0659:CGEAE>2.0.CO;2).
- Baker, V.R., 2014. Terrestrial analogs, planetary geology, and the nature of geological reasoning. *Planet. Geol. Field Symp. Kitakyushu Jpn. 2011 Planet. Geol. Terr. Analogs.* 95: pp. 5–10. <https://doi.org/10.1016/j.pss.2012.10.008>.
- Baker, V.R., 2017. Debates-hypothesis testing in hydrology: pursuing certainty versus pursuing uberty. *Water Resour. Res.* 53:1770–1778. <https://doi.org/10.1002/2016WR020078>.
- Baker, D.M.H., Head, J.W., 2015. Extensive Middle Amazonian mantling of debris aprons and plains in Deuteronilus Mensae, Mars: implications for the record of mid-latitude glaciation. *Icarus* 260:269–288. <https://doi.org/10.1016/j.icarus.2015.06.036>.
- Baker, D.M.H., Head, J.W., Marchant, D.R., 2010. Flow patterns of lobate debris aprons and linedated valley fill north of Ismeniae Fossae, Mars: evidence for extensive mid-latitude glaciation in the Late Amazonian. *Icarus* 207:186–209. <https://doi.org/10.1016/j.icarus.2009.11.017>.
- Ballantyne, C.K., Benn, D.I., 1994. Paraglacial slope adjustment and resedimentation following recent glacier retreat, Fobergstadalen, Norway. *Arct. Alp. Res.* 26:255–269. <https://doi.org/10.2307/1551938>.
- Bamber, J.L., Griggs, J.A., Hurkmans, R.T.W.L., Dowdeswell, J.A., Gogineni, S.P., Howat, I., Mouginot, J., Paden, J., Palmer, S., Rignot, E., Steinhage, D., 2013. A new bed elevation dataset for Greenland. *Cryosphere* 7:499–510. <https://doi.org/10.5194/tc-7-499-2013>.
- Benn, D.I., Evans, D.J.A., 2010. *Glaciers & Glaciation. Second Edition.* Hodder Education, London.
- Bennett, M.R., 2001. The morphology, structural evolution and significance of push moraines. *Earth-Sci. Rev.* 53:197–236. [https://doi.org/10.1016/S0012-8252\(00\)00039-8](https://doi.org/10.1016/S0012-8252(00)00039-8).
- Bennett, M.R., Huddart, D., Glasser, N.F., 1999. Large-scale bedrock displacement by cirque glaciers. *Arct. Antarct. Alp. Res.* 31:99–107. <https://doi.org/10.2307/1552627>.
- Bennett, M.R., Huddart, D., Glasser, N.F., Hambrey, M.J., 2000. Resedimentation of debris on an ice-cored lateral moraine in the high-Arctic (Kongsvegen, Svalbard). *Geomorphology* 35:21–40. [https://doi.org/10.1016/S0169-555X\(00\)00017-9](https://doi.org/10.1016/S0169-555X(00)00017-9).

- Berman, D.C., Hartmann, W.K., Crown, D.A., Baker, V.R., 2005. The role of arcuate ridges and gullies in the degradation of craters in the Newton Basin region of Mars. *Icarus* 178:465–486. <https://doi.org/10.1016/j.icarus.2005.05.011>.
- Berman, D.C., Crown, D.A., Bleamaster III, L.F., 2009. Degradation of mid-latitude craters on Mars. *Icarus* 200:77–95. <https://doi.org/10.1016/j.icarus.2008.10.026>.
- Berman, D.C., Crown, D.A., Joseph, E.C.S., 2015. Formation and mantling ages of lobate debris aprons on Mars: insights from categorized crater counts. *Planet. Space Sci.* 111: 83–99. <https://doi.org/10.1016/j.pss.2015.03.013>.
- Björnsson, H., Gjessing, Y., Hamran, S.-E., Hagen, J.O., Liestøl, O., Pálsson, F., Erlingsson, B., 1996. The thermal regime of sub-polar glaciers mapped by multi-frequency radio-echo sounding. *J. Glaciol.* 42:23–32. <https://doi.org/10.3189/S0022143000030495>.
- Boulton, G.S., 1979. Processes of glacier erosion on different substrata. *J. Glaciol.* 23:15–38. <https://doi.org/10.1017/S0022143000029713>.
- Boulton, G.S., van der Meer, J.J.M., Beets, D.J., Hart, J.K., Ruegg, G.H.J., 1999. The sedimentary and structural evolution of a recent push moraine complex: Holmstrømbreen, Spitsbergen. *Quat. Sci. Rev.* 18:339–371. [https://doi.org/10.1016/S0277-3791\(98\)00068-7](https://doi.org/10.1016/S0277-3791(98)00068-7).
- Boynton, W.V., Feldman, W.C., Squyres, S.W., Prettyman, T.H., Brückner, J., Evans, L.G., Reedy, R.C., Starr, R., Arnold, J.R., Drake, D.M., Englert, P.A.J., Metzger, A.E., Mitrofanov, I., Trombka, J.I., d'Uston, C., Wänke, H., Gasnault, O., Hamara, D.K., Janes, D.M., Marcialis, R.L., Maurice, S., Mikheeva, I., Taylor, G.J., Tokar, R., Shinohara, C., 2002. Distribution of hydrogen in the near surface of Mars: evidence for subsurface ice deposits. *Science* 297:81–85. <https://doi.org/10.1126/science.1073722>.
- Brough, S., Hubbard, B., Hubbard, A., 2016a. Former extent of glacier-like forms on Mars. *Icarus* 274:37–49. <https://doi.org/10.1016/j.icarus.2016.03.006>.
- Brough, S., Hubbard, B., Souness, C., Grindrod, P.M., Davis, J., 2016b. Landscapes of poly-phase glaciation: eastern Hellas Planitia, Mars. *J. Maps* 12:530–542. <https://doi.org/10.1080/17445647.2015.1047907>.
- Burbank, D.W., Leland, J., Fielding, E., Anderson, R.S., Brozovic, N., Reid, M.R., Duncan, C., 1996. Bedrock incision, rock uplift and threshold hillslopes in the northwestern Himalayas. *Nature* 379:505. <https://doi.org/10.1038/379505a0>.
- Butcher, F.E.G., Balme, M.R., Gallagher, C., Arnold, N.S., Conway, S.J., Hagermann, A., Lewis, S.R., 2017. Recent basal melting of a mid-latitude glacier on Mars. *J. Geophys. Res. Planets*. <https://doi.org/10.1002/2017JE005434>.
- Byrne, S., Dundas, C.M., Kennedy, M.R., Mellon, M.T., McEwen, A.S., Cull, S.C., Daubar, I.J., Shean, D.E., Seelos, K.D., Murchie, S.L., Cantor, B.A., Arvidson, R.E., Edgett, K.S., Reufer, A., Thomas, N., Harrison, T.N., Posiolova, L.V., Seelos, F.P., 2009. Distribution of mid-latitude ground ice on Mars from new impact craters. *Science* 325: 1674–1676. <https://doi.org/10.1126/science.1175307>.
- Carr, M.H., 2001. Mars global surveyor observations of Martian fretted terrain. *J. Geophys. Res. Planets* 106:23571–23593. <https://doi.org/10.1029/2000JE001316>.
- Carr, M.H., Head, J.W., 2003. Basal melting of snow on early Mars: a possible origin of some valley networks: basal melting of snow on early Mars. *Geophys. Res. Lett.* 30. <https://doi.org/10.1029/2003GL018575>.
- Chevrier, V., Altheide, T.S., 2008. Low temperature aqueous ferric sulfate solutions on the surface of Mars. *Geophys. Res. Lett.* 35, L22101. <https://doi.org/10.1029/2008GL035489>.
- Chevrier, V.F., Hanley, J., Altheide, T.S., 2009. Stability of perchlorate hydrates and their liquid solutions at the Phoenix landing site, Mars. *Geophys. Res. Lett.* 36, 10202.
- Christensen, P.R., 2003. Formation of recent martian gullies through melting of extensive water-rich snow deposits. *Nature* 422:45–48. <https://doi.org/10.1038/nature01436>.
- Cohen, D., Hooyer, T.S., Iverson, N.R., Thomason, J.F., Jackson, M., 2006. Role of transient water pressure in quarrying: a subglacial experiment using acoustic emissions. *J. Geophys. Res. Earth Surf.* 111, F03006. <https://doi.org/10.1029/2005JF000439>.
- Conway, S.J., Balme, M.R., 2014. Decametre-thick remnant glacial ice deposits on Mars. *Geophys. Res. Lett.* 41:5402–5409. <https://doi.org/10.1002/2014GL060314>.
- Conway, S.J., Balme, M.R., 2016. A novel topographic parameterization scheme indicates that martian gullies display the signature of liquid water. *Earth Planet. Sci. Lett.* 454:36–45. <https://doi.org/10.1016/j.epsl.2016.08.031>.
- Conway, S.J., Balme, M.R., Soare, R.J., 2015. Using gullies to estimate the thickness of the latitude dependent mantle on Mars. *Lunar and Planetary Science Conference*, p. 2964 *Lunar and Planetary Science Conference*.
- Conway, S.J., Harrison, T.N., Soare, R.J., Britton, A., Steele, L., 2017. New slope-normalised global gully density and orientation maps for Mars. *Geol. Soc. Lond. Spec. Publ.* 467 in press. <https://doi.org/10.1144/SP467.3>.
- Conway, S.J., Harrison, T.N., Lewis, S.R., 2018a. Chapter 3: Martian gullies and their connection with the martian climate. In: Soare, R.J., Conway, S.J., Clifford, S.M. (Eds.), *Dynamic Mars: Recent and Current Landscape Evolution of the Red Planet*. Elsevier.
- Conway, S.J., de Haas, T., Harrison, T.N., 2018b. Martian gullies: a comprehensive review of observations, mechanisms and the insights from Earth analogues. *Geol. Soc. Lond. Spec. Publ.* 467 (under revision).
- Costard, F., Forget, F., Mangold, N., Peulvast, J.P., 2002. Formation of recent Martian debris flows by melting of near-surface ground ice at high obliquity. *Science* 295:110–113. <https://doi.org/10.1126/science.106698>.
- Cuffey, K.M., Conway, H., Gades, A.M., Hallet, B., Lorrain, R., Severinghaus, J.P., Steig, E.J., Vaughn, B., White, J.W.C., 2000. Entrainment at cold glacier beds. *Geology* 28: 351–354. [https://doi.org/10.1130/0091-7613\(2000\)28<351:EACGB>2.0.CO;2](https://doi.org/10.1130/0091-7613(2000)28<351:EACGB>2.0.CO;2).
- Dickson, J.L., Head, J.W., Fassett, C.I., 2012. Patterns of accumulation and flow of ice in the mid-latitudes of Mars during the Amazonian. *Icarus* 219:723–732. <https://doi.org/10.1016/j.icarus.2012.03.010>.
- Dickson, J.L., Head, J.W., Goudge, T.A., Barbieri, L., 2015. Recent climate cycles on Mars: stratigraphic relationships between multiple generations of gullies and the latitude dependent mantle. *Icarus* 252:83–94. <https://doi.org/10.1016/j.icarus.2014.12.035>.
- Diniega, S., Byrne, S., Bridges, N.T., Dundas, C.M., McEwen, A.S., 2010. Seasonality of present-day Martian dune-gully activity. *Geology* 38:1047–1050. <https://doi.org/10.1130/G31287.1>.
- Dundas, C.M., McEwen, A.S., Diniega, S., Byrne, S., Martinez-Alonso, S., 2010. New and recent gully activity on Mars as seen by HiRISE. *Geophys. Res. Lett.* 37. <https://doi.org/10.1029/2009GL013151>.
- Dundas, C.M., Diniega, S., Hansen, C.J., Byrne, S., McEwen, A.S., 2012. Seasonal activity and morphological changes in martian gullies. *Icarus* 220:124–143. <https://doi.org/10.1016/j.icarus.2012.04.005>.
- Dundas, C.M., Byrne, S., McEwen, A.S., Mellon, M.T., Kennedy, M.R., Daubar, I.J., Saper, L., 2014. HiRISE observations of new impact craters exposing Martian ground ice. *J. Geophys. Res. Planets* 119, 2013JE004482. <https://doi.org/10.1002/2013JE004482>.
- Dundas, C.M., Diniega, S., McEwen, A.S., 2015. Long-term monitoring of Martian gully formation and evolution with MRO/HiRISE. *Icarus* 251:244–263. <https://doi.org/10.1016/j.icarus.2014.05.013>.
- Dundas, C.M., McEwen, A.S., Diniega, S., Hansen, C.J., Byrne, S., McElwaine, J.N., 2017. The formation of gullies on Mars today. *Geol. Soc. Lond. Spec. Publ. Martian Gullies and Their Earth Analogues* <https://doi.org/10.1144/SP467.5>.
- Dundas, C.M., Bramson, A.M., Ojha, L., Wray, J.J., Mellon, M.T., Byrne, S., McEwen, A.S., Putzig, N.E., Viola, D., Sutton, S., Clark, E., Holt, J.W., 2018. Exposed subsurface ice sheets in the Martian mid-latitudes. *Science* 359:199–201. <https://doi.org/10.1126/science.aao1619>.
- Dyke, A.S., 1993. Landscapes of cold-centred Late Wisconsinan ice caps, Arctic Canada. *Prog. Phys. Geogr.* 17:223–247. <https://doi.org/10.1177/030913399301700208>.
- Echelmeyer, K., Wang, Z., 1987. Direct observation of basal sliding and deformation of basal drift at sub-freezing temperatures. *J. Glaciol.* 33:83–98. <https://doi.org/10.3189/S0022143000005396>.
- Egholm, D.L., Pedersen, V.K., Knudsen, M.F., Larsen, N.K., 2012. Coupling the flow of ice, water, and sediment in a glacial landscape evolution model. *Geomorphology* 141–142:47–66. <https://doi.org/10.1016/j.geomorph.2011.12.019>.
- Etzelmüller, B., Hagen, J.O., Vatne, G., Ødegård, R.S., Sollid, J.L., 1996. Glacier debris accumulation and sediment deformation influenced by permafrost: examples from Svalbard. *Ann. Glaciol.* 22:53–62. <https://doi.org/10.3189/1996AoG22-1-53-62>.
- Evans, D.J.A., 2007. GLACIAL LANDFORMS|glacitectonic structures and landforms. In: Elias, S.A. (Ed.), *Encyclopedia of Quaternary Science*. Elsevier, Oxford:pp. 831–838. <https://doi.org/10.1016/B0-44-452747-8/00084-3>.
- Ewertowski, M.W., Tomczyk, A.M., 2015. Quantification of the ice-cored moraines' short-term dynamics in the high-Arctic glaciers Ebbabreen and Ragnarbreen, Petuniabukta, Svalbard. *Geomorphology* 234:211–227. <https://doi.org/10.1016/j.geomorph.2015.01.023>.
- Fassett, C.I., Thomson, B.J., 2014. Crater degradation on the lunar maria: Topographic diffusion and the rate of erosion on the Moon. *J. Geophys. Res. Planets* 119. <https://doi.org/10.1002/2014JE004698> (2014)E004698).
- Fassett, C.I., Dickson, J.L., Head, J.W., Levy, J.S., Marchant, D.R., 2010. Supraglacial and proglacial valleys on Amazonian Mars. *Icarus* 208:86–100. <https://doi.org/10.1016/j.icarus.2010.02.021>.
- Fassett, C.I., Levy, J.S., Dickson, J.L., Head, J.W., 2014. An extended period of episodic northern mid-latitude glaciation on Mars during the Middle to Late Amazonian: implications for long-term obliquity history. *Geology* 42:763–766. <https://doi.org/10.1130/G35798.1>.
- Fastook, J.L., Head, J.W., Marchant, D.R., 2014. Formation of lobate debris aprons on Mars: assessment of regional ice sheet collapse and debris-cover armorings. *Icarus* 228: 54–63. <https://doi.org/10.1016/j.icarus.2013.09.025>.
- Feldman, W.C., Prettyman, T.H., Maurice, S., Plaut, J.J., Bish, D.L., Vaniman, D.T., Mellon, M.T., Metzger, A.E., Squyres, S.W., Karunatillake, S., Boynton, W.V., Elphic, R.C., Funsten, H.O., Lawrence, D.J., Tokar, R.L., 2004. Global distribution of near-surface hydrogen on Mars. *J. Geophys. Res.* 109. <https://doi.org/10.1029/2003JE002160>.
- Ferrucci, M., Pertusati, S., Sulpizio, R., Zanchetta, G., Pareschi, M.T., Santacroce, R., 2005. Volcaniclastic debris flows at La Fossa Volcano (Vulcano Island, southern Italy): insights for erosion behaviour of loose pyroclastic material on steep slopes. *J. Volcanol. Geotherm. Res.* 145:173–191. <https://doi.org/10.1016/j.jvolgeores.2005.01.013>.
- Fisher, D.A., 2005. A process to make massive ice in the martian regolith using long-term diffusion and thermal cracking. *Icarus* 179:387–397. <https://doi.org/10.1016/j.icarus.2005.07.024>.
- Fitzsimons, S.J., 1996. Formation of thrust-block moraines at the margins of dry-based glaciers, south Victoria Land, Antarctica. *Ann. Glaciol.* 22:68–74. <https://doi.org/10.3189/1996AoG22-1-68-74>.
- Gallagher, C., Balme, M., 2015. Eskers in a complete, wet-based glacial system in the Phlegra Montes region, Mars. *Earth Planet. Sci. Lett.* 431:96–109. <https://doi.org/10.1016/j.epsl.2015.09.023>.
- Geirsdóttir, Á., Miller, G.H., Andrews, J.T., 2007. Glaciation, erosion, and landscape evolution of Iceland. *J. Geodyn.* 43:170–186. <https://doi.org/10.1016/j.jog.2006.09.017>.
- Golombek, M.P., Grant, J.A., Crumpler, L.S., Greeley, R., Arvidson, R.E., Bell, J.F., Weitz, C.M., Sullivan, R., Christensen, P.R., Soderblom, L.A., Squyres, S.W., 2006. Erosion rates at the Mars Exploration Rover landing sites and long-term climate change on Mars. *J. Geophys. Res. Planets* 111. <https://doi.org/10.1029/2006JE002754>.
- Golombek, M.P., Warner, N.H., Ganti, V., Lamb, M.P., Parker, T.J., Fergason, R.L., Sullivan, R., 2014a. Small crater modification on Meridiani Planum and implications for erosion rates and climate change on Mars. *J. Geophys. Res. Planets* 119. <https://doi.org/10.1002/2014JE004658> (2014)E004658).
- Golombek, M.P., Bloom, C., Wigton, N., Warner, N., 2014b. Constraints on the age of Corinto Crater from mapping secondaries in Elysium Planitia on Mars. *Lunar and Planetary Science Conference*, p. 1470.
- Goodsell, B., Hambrey, M.J., Glasser, N.F., 2005. Debris transport in a temperate valley glacier: Haut Glacier d'Arolla, Valais, Switzerland. *J. Glaciol.* 51:139–146. <https://doi.org/10.3189/172756505781829647>.
- de Haas, T., Hauber, E., Kleinhans, M.G., 2013. Local late Amazonian boulder breakdown and denudation rate on Mars. *Geophys. Res. Lett.* <https://doi.org/10.1002/grl.50726>.

- de Haas, T., Hauber, E., Conway, S.J., van Steijn, H., Johnsson, A., Kleinhans, M.G., 2015a. Earth-like aqueous debris-flow activity on Mars at high orbital obliquity in the last million years. *Nat. Commun.* 6. <https://doi.org/10.1038/ncomms8543>.
- de Haas, T., Conway, S.J., Krautblatter, M., 2015b. Recent (Late Amazonian) enhanced backweathering rates on Mars: paracrater evidence from gully-alcoves? *J. Geophys. Res. Planets* 120:2169–2189. <https://doi.org/10.1002/2015JE004915>.
- de Haas, T., Ventra, D., Hauber, E., Conway, S.J., Kleinhans, M.G., 2015c. Sedimentological analyses of martian gullies: the subsurface as the key to the surface. *Icarus* 258: 92–108. <https://doi.org/10.1016/j.icarus.2015.06.017>.
- de Haas, T., Conway, S.J., Butcher, F.E.G., Levy, J.S., Grindrod, P.M., Balme, M.R., Goudge, T.A., 2018. Time will tell: temporal evolution of Martian gullies and paleoclimatic implications. *Geol. Soc. Lond. Spec. Publ.* 467 in press. <https://doi.org/10.1144/SP467.1>.
- Hales, T.C., Roering, J.J., 2007. Climatic controls on frost cracking and implications for the evolution of bedrock landscapes. *J. Geophys. Res.* 112. <https://doi.org/10.1029/2006JF000616>.
- Hallet, B., 1979. A theoretical model of glacial abrasion. *J. Glaciol.* 23:39–50. <https://doi.org/10.1017/S0022143000029725>.
- Hallet, B., 1996. Glacial quarrying: a simple theoretical model. *Ann. Glaciol.* 22:1–8. <https://doi.org/10.3189/1996AOG22-1-1-8>.
- Hallet, B., Hunter, L., Bogen, J., 1996. Rates of erosion and sediment evacuation by glaciers: a review of field data and their implications. *Glob. Planet. Chang.* 12:213–235. [https://doi.org/10.1016/0921-8181\(95\)00021-6](https://doi.org/10.1016/0921-8181(95)00021-6).
- Hambrey, M.J., Fitzsimons, S.J., 2010. Development of sediment–landform associations at cold glacier margins, Dry Valleys, Antarctica. *Sedimentology* 57:857–882. <https://doi.org/10.1111/j.1365-3091.2009.0123.x>.
- Hambrey, M.J., Glasser, N.F., 2012. Discriminating glacier thermal and dynamic regimes in the sedimentary record. *Sediment. Geol.* 251–252:1–33. <https://doi.org/10.1016/j.sedgeo.2012.01.008>.
- Harbor, J.M., 1992. Numerical modeling of the development of U-shaped valleys by glacial erosion. *GSA Bull.* 104:1364–1375. [https://doi.org/10.1130/0016-7606\(1992\)104<1364:NMOTDO>2.3.CO;2](https://doi.org/10.1130/0016-7606(1992)104<1364:NMOTDO>2.3.CO;2).
- Harrison, T.N., Malin, M.C., Edgett, K.S., Shean, D.E., Kennedy, M.R., Lipkaman, L.J., Cantor, B.A., Posiolova, L.V., 2010. Impact-induced overland fluid flow and channelized erosion at Lyot Crater, Mars. *Geophys. Res. Lett.* 37. <https://doi.org/10.1029/2010GL045074>.
- Harrison, T.N., Osinski, G.R., Tornabene, L.L., Jones, E., 2015. Global documentation of gullies with the Mars reconnaissance orbiter context camera and implications for their formation. *Icarus* 252:236–254. <https://doi.org/10.1016/j.icarus.2015.01.022>.
- Hart, J.K., Boulton, G.S., 1991. The interrelation of glaciotectonic and glaciodepositional processes within the glacial environment. *Quat. Sci. Rev.* 10:335–350. [https://doi.org/10.1016/0277-3791\(91\)90035-S](https://doi.org/10.1016/0277-3791(91)90035-S).
- Hartmann, W.K., Neukum, G., 2001. Cratering chronology and the evolution of Mars. *Space Sci. Rev.* 96:165–194. <https://doi.org/10.1023/A:1011945222010>.
- Hartmann, W.K., Quantin, C., Werner, S.C., Popova, O., 2010. Do young martian ray craters have ages consistent with the crater count system? *Icarus* 208:621–635. <https://doi.org/10.1016/j.icarus.2010.03.030>.
- Hartmann, W.K., Ansan, V., Bertram, D.C., Mangold, N., Forget, F., 2014. Comprehensive analysis of glaciated martian crater Greg. *Icarus* 228:96–120. <https://doi.org/10.1016/j.icarus.2013.09.016>.
- Hauber, E., Reiss, D., Ulrich, M., Preusker, F., Trauthan, F., Zanetti, M., Hiesinger, H., Jaumann, R., Johnsson, L., Johnsson, A., Van Gassel, S., Olymo, M., 2011a. Landscape evolution in Martian mid-latitude regions: insights from analogous periglacial landforms in Svalbard. *Geol. Soc. Lond. Spec. Publ.* 356:111–131. <https://doi.org/10.1144/SP356.7>.
- Hauber, E., Brož, P., Jagert, F., Jodłowski, P., Platz, T., 2011b. Very recent and wide-spread basaltic volcanism on Mars: recent wide-spread volcanism on Mars. *Geophys. Res. Lett.* 38. <https://doi.org/10.1029/2011GL047310>.
- Hay, T., 1934. The glaciology of the Ullswater area. *Geogr. J.* 136–148. <https://doi.org/10.2307/1786895>.
- Head, J.W., Marchant, D.R., 2003. Cold-based mountain glaciers on Mars: Western Arsia Mons. *Geology* 31:641–644. [https://doi.org/10.1130/0091-7613\(2003\)031<0641:CMGOMW>2.0.CO;2](https://doi.org/10.1130/0091-7613(2003)031<0641:CMGOMW>2.0.CO;2).
- Head, J.W., Mustard, J.F., Kreslavsky, M.A., Milliken, R.E., Marchant, D.R., 2003. Recent ice ages on Mars. *Nature* 426:797–802. <https://doi.org/10.1038/nature02114>.
- Head, J.W., Marchant, D.R., Kreslavsky, M.A., 2008. Formation of gullies on Mars: link to recent climate history and insolation microenvironments implicate surface water flow origin. *Proc. Natl. Acad. Sci. U. S. A.* 105:13258–13263. <https://doi.org/10.1073/pnas.0803760105>.
- Head, J.W., Marchant, D.R., Dickson, J.L., Kress, A.M., Baker, D.M., 2010. Northern mid-latitude glaciation in the Late Amazonian period of Mars: criteria for the recognition of debris-covered glacier and valley glacier landsystem deposits. *Earth Planet. Sci. Lett.* 294:306–320. <https://doi.org/10.1016/j.epsl.2009.06.041>.
- Hecht, M.H., Kounaves, S.P., Quinn, R.C., West, J.J., Young, S.M.M., Ming, D.W., Catling, D.C., Clark, B.C., Boynton, W.V., Hoffman, J., Deflores, L.P., Gospodinova, K., Kapit, J., Smith, P.H., 2009. Detection of perchlorate and the soluble chemistry of martian soil at the Phoenix lander site. *Science* 325:64. <https://doi.org/10.1126/science.1172466>.
- Hepburn, A., Ng, F., Livingstone, S.J., Hubbard, B., 2018. Polyphase Mid-Latitude Glaciation on Mars Evidenced By Dating of Superimposed Lobate Debris Aprons. Presented at the European Geosciences Union General Assembly, Vienna, Austria, pp. EGU2018–1087.
- Hirano, M., Aniya, M., 1988. A rational explanation of cross-profile morphology for glacial valleys and of glacial valley development. *Earth Surf. Process. Landf.* 13:707–716. <https://doi.org/10.1002/esp.3290130805>.
- Hobley, D.E.J., Howard, A.D., Moore, J.M., 2014. Fresh shallow valleys in the Martian mid-latitudes as features formed by meltwater flow beneath ice. *J. Geophys. Res. Planets* 119. <https://doi.org/10.1002/2013JE004396> (2013JE004396).
- Holdsworth, G., Bull, C., 1970. The flow law of cold ice: investigations on Meserve Glacier, Antarctica. *Int. Assoc. Hydrol. Sci. Publ.* 86, 204–216.
- Holt, J.W., Safaenili, A., Plaut, J.J., Head, J.W., Phillips, R.J., Seu, R., Kempf, S.D., Choudhary, P., Young, D.A., Putzig, N.E., Biccari, D., Gim, Y., 2008. Radar sounding evidence for buried glaciers in the southern mid-latitudes of Mars. *Science* 322:1235–1238. <https://doi.org/10.1126/science.1164246>.
- Hubbard, B., Milliken, R.E., Kargel, J.S., Limaye, A., Souness, C., 2011. Geomorphological characterisation and interpretation of a mid-latitude glacier-like form: Hellas Planitia, Mars. *Icarus* 211:330–346. <https://doi.org/10.1016/j.icarus.2010.10.021>.
- Hubbard, B., Souness, C., Brough, S., 2014. Glacier-like forms on Mars. *Cryosphere* 8: 2047–2061. <https://doi.org/10.5194/tc-8-2047-2014>.
- Iverson, N.R., 1991. Potential effects of subglacial water-pressure fluctuations on quarrying. *J. Glaciol.* 37:27–36. <https://doi.org/10.3189/S0022143000042763>.
- Jakosky, B.M., Mellon, M.T., Varnes, E.S., Feldman, W.C., Boynton, W.V., Haberle, R.M., 2005. Mars low-latitude neutron distribution: possible remnant near-surface water ice and a mechanism for its recent emplacement. *Icarus* 175:58–67. <https://doi.org/10.1016/j.icarus.2004.11.014>.
- Jawin, E.R., Head, J.W., Marchant, D.R., 2018. Transient post-glacial processes on Mars: geomorphologic evidence for a paraglacial period. *Icarus* 309:187–206. <https://doi.org/10.1016/j.icarus.2018.01.026>.
- Johnsson, A., Reiss, D., Hauber, E., Hiesinger, H., Zanetti, M., 2014. Evidence for very recent melt-water and debris flow activity in gullies in a young mid-latitude crater on Mars. *Icarus* 235:37–54. <https://doi.org/10.1016/j.icarus.2014.03.005>.
- Karlsson, N.B., Schmidt, L.S., Hvidberg, C.S., 2015. Volume of Martian midlatitude glaciers from radar observations and ice flow modeling. *Geophys. Res. Lett.* 42:2627–2633. <https://doi.org/10.1002/2015GL063219>.
- Katsube, K., Oguchi, T., 1999. Altitudinal changes in slope angle and profile curvature in the Japan alps: a hypothesis regarding a characteristic slope angle. *Geogr. Rev. Jpn. Ser. B* 72:63–72. <https://doi.org/10.4157/grj1984b.72.63>.
- Kirk, R.L., Howington-Kraus, E., Rosiek, M.R., Anderson, J.A., Archinal, B.A., Becker, K.J., Cook, D.A., Galuszka, D.M., Geissler, P.E., Hare, T.M., Holmberg, I.M., Keszthelyi, L.P., Redding, B.L., Delamere, W.A., Gallagher, D., Chapel, J.D., Eliason, E.M., King, R., McEwen, A.S., 2008. Ultrahigh resolution topographic mapping of Mars with MRO HiRISE stereo images: meter-scale slopes of candidate Phoenix landing sites. *J. Geophys. Res. Planets* 113. <https://doi.org/10.1029/2007JE003000>.
- Kneissl, T., van Gassel, S., Neukum, G., 2011. Map-projection-independent crater size-frequency determination in GIS environments—new software tool for ArcGIS. *Planet. Space Sci.* 59:1243–1254. <https://doi.org/10.1016/j.pss.2010.03.015>.
- Korup, O., 2008. Rock type leaves topographic signature in landslide-dominated mountain ranges. *Geophys. Res. Lett.* 35. <https://doi.org/10.1029/2008GL034157>.
- Kostama, V.-P., Kreslavsky, M.A., Head, J.W., 2006. Recent high-latitude icy mantle in the northern plains of Mars: characteristics and ages of emplacement. *Geophys. Res. Lett.* 33, L11201. <https://doi.org/10.1029/2006GL025946>.
- Kreslavsky, M.A., Head, J.W., 2000. Kilometer-scale roughness of Mars: results from MOLA data analysis. *J. Geophys. Res.* 105:26695–26712. <https://doi.org/10.1029/2000JE001259>.
- Kreslavsky, M.A., Head, J.W., 2002. Mars: nature and evolution of young latitude-dependent water-ice-rich mantle. *Geophys. Res. Lett.* 29. <https://doi.org/10.1029/2002GL015392> (14–1).
- Kreslavsky, M.A., Head, J.W., Marchant, D.R., 2008. Periods of active permafrost layer formation during the geological history of Mars: implications for circum-polar and mid-latitude surface processes. *Planet. Space Sci.* 56:289–302. <https://doi.org/10.1016/j.pss.2006.02.010>.
- Kress, A.M., Head, J.W., 2008. Ring-mold craters in lineated valley fill and lobate debris aprons on Mars: evidence for subsurface glacial ice. *Geophys. Res. Lett.* 35:23206. <https://doi.org/10.1029/2008GL035501>.
- Lacelle, D., Davila, A.F., Fisher, D., Pollard, W.H., DeWitt, R., Heldmann, J., Marinova, M.M., McKay, C.P., 2013. Excess ground ice of condensation–diffusion origin in University Valley, Dry Valleys of Antarctica: evidence from isotope geochemistry and numerical modeling. *Geochim. Cosmochim. Acta* 120:280–297. <https://doi.org/10.1016/j.gca.2013.06.032>.
- Langevin, Y., Poulet, F., Bibring, J.P., Gondet, B., 2005. Sulfates in the north polar region of Mars detected by OMEGA/Mars express. *Science* 307:1584–1586. <https://doi.org/10.1126/science.1109091>.
- Laskar, J., Robutel, P., 1993. The chaotic obliquity of the planets. *Nature* 361:608–612. <https://doi.org/10.1038/361608a0>.
- Laskar, J., Correia, A.C.M., Gastineau, M., Joutel, F., Levrard, B., Robutel, P., 2004. Long term evolution and chaotic diffusion of the insolation quantities of Mars. *Icarus* 170: 343–364. <https://doi.org/10.1016/j.icarus.2004.04.005>.
- Levrard, B., Forget, F., Montmessin, F., Laskar, J., 2004. Recent ice-rich deposits formed at high latitudes on Mars by sublimation of unstable equatorial ice during low obliquity. *Nature* 431:1072–1075. <https://doi.org/10.1038/nature03055>.
- Levrard, B., Forget, F., Montmessin, F., Laskar, J., 2007. Recent formation and evolution of northern Martian polar layered deposits as inferred from a Global Climate Model. *J. Geophys. Res. Planets* 112. <https://doi.org/10.1029/2006JE002772>.
- Levy, J.S., Head, J.W., Marchant, D.R., 2007. Lineated valley fill and lobate debris apron stratigraphy in Nilosyrtris Mensae, Mars: evidence for phases of glacial modification of the dichotomy boundary. *J. Geophys. Res.* 112. <https://doi.org/10.1029/2006JE002852>.
- Levy, J.S., Head, J.W., Marchant, D., 2009a. Thermal contraction crack polygons on Mars: classification, distribution, and climate implications from HiRISE observations. *J. Geophys. Res. Planets* 114, 01007.
- Levy, J.S., Head, J.W., Marchant, D.R., 2009b. Concentric crater fill in Utopia Planitia: history and interaction between glacial “brain terrain” and periglacial mantle processes. *Icarus* 202:462–476. <https://doi.org/10.1016/j.icarus.2009.02.018>.
- Levy, J.S., Head, J.W., Marchant, D.R., Dickson, J.L., Morgan, G.A., 2009c. Geologically recent gully-polygon relationships on Mars: insights from the Antarctic dry valleys on the roles of permafrost, microclimates, and water sources for surface flow. *Icarus* 201: 113–126. <https://doi.org/10.1016/j.icarus.2008.12.043>.

- Levy, J., Head, J.W., Marchant, D.R., 2010. Concentric crater fill in the northern mid-latitudes of Mars: formation processes and relationships to similar landforms of glacial origin. *Icarus* 209:390–404. <https://doi.org/10.1016/j.icarus.2010.03.036>.
- Levy, J.S., Head, J.W., Marchant, D.R., 2011. Gullies, polygons and mantles in Martian permafrost environments: cold desert landforms and sedimentary processes during recent Martian geological history. *Geol. Soc. Lond. Spec. Publ.* 354:167–182. <https://doi.org/10.1144/SP354.10>.
- Levy, J.S., Fassett, C.I., Head, J.W., Schwartz, C., Watters, J.L., 2014. Sequestered glacial ice contribution to the global Martian water budget: Geometric constraints on the volume of remnant, midlatitude debris-covered glaciers. *J. Geophys. Res. Planets* 119. <https://doi.org/10.1002/2014JE004685> (2014JE004685).
- Levy, J.S., Fassett, C.I., Head, J.W., 2016. Enhanced erosion rates on Mars during Amazonian glaciation. *Icarus* 264:213–219. <https://doi.org/10.1016/j.icarus.2015.09.037>.
- Li, H., Robinson, M.S., Jurdy, D.M., 2005. Origin of martian northern hemisphere mid-latitude lobate debris aprons. *Icarus* 176:382–394. <https://doi.org/10.1016/j.icarus.2005.02.011>.
- Lin, Z., Oguchi, T., Chen, Y.-G., Saito, K., 2009. Constant-slope alluvial fans and source basins in Taiwan. *Geology* 37:787–790. <https://doi.org/10.1130/G25675A.1>.
- Lloyd Davies, M.T., Atkins, C.B., van der Meer, J.J.M., Barrett, P.J., Hicock, S.R., 2009. Evidence for cold-based glacial activity in the Allan Hills, Antarctica. *Quat. Sci. Rev.* 28:3124–3137. <https://doi.org/10.1016/j.quascirev.2009.08.002>.
- MacGregor, K.R., Anderson, R.S., Anderson, S.P., Waddington, E.D., 2000. Numerical simulations of glacial-valley longitudinal profile evolution. *Geology* 28:1031–1034. [https://doi.org/10.1130/0091-7613\(2000\)28<1031:NSOGLP>2.0.CO;2](https://doi.org/10.1130/0091-7613(2000)28<1031:NSOGLP>2.0.CO;2).
- Madeleine, J.B., Forget, F., Head, J.W., Levrard, B., Montmessin, F., Millour, E., 2009. Amazonian northern mid-latitude glaciation on Mars: a proposed climate scenario. *Icarus* 203:390–405. <https://doi.org/10.1016/j.icarus.2009.04.037>.
- Madeleine, J.-B., Head, J.W., Forget, F., Navarro, T., Millour, E., Spiga, A., Colaitis, A., Määttä, A., Montmessin, F., Dickson, J.L., 2014. Recent Ice Ages on Mars: the role of radiatively active clouds and cloud microphysics. *Geophys. Res. Lett.* <https://doi.org/10.1002/2014GL059861>.
- Malin, M.C., Edgett, K.S., 2000. Evidence for recent groundwater seepage and surface runoff on Mars. *Science* 288:2330–2335. <https://doi.org/10.1126/science.288.5475.2330>.
- Mangold, N., 2003. Geomorphic analysis of lobate debris aprons on Mars at Mars Orbiter Camera scale: evidence for ice sublimation initiated by fractures. *J. Geophys. Res.* 108:8021. <https://doi.org/10.1029/2002JE001885>.
- Mangold, N., 2005. High latitude patterned grounds on Mars: classification, distribution and climatic control. *Mars Polar Sci. III* 174:336–359. <https://doi.org/10.1016/j.icarus.2004.07.030>.
- Mangold, N., Allemand, P., 2001. Topographic analysis of features related to ice on Mars. *Geophys. Res. Lett.* 28:407–410. <https://doi.org/10.1029/2000GL008491>.
- Mansfield, M., Kite, E.S., Mischna, M.A., 2018. Effect of Mars atmospheric loss on snow melt potential in a 3.5 Gyr Mars climate evolution model. *J. Geophys. Res. Planets*. <https://doi.org/10.1002/2017JE005422>.
- Marchant, D.R., Head, J.W., 2007. Antarctic dry valleys: microclimate zonation, variable geomorphic processes, and implications for assessing climate change on Mars. *Icarus* 192:187–222. <https://doi.org/10.1016/j.icarus.2007.06.018>.
- Massé, M., Bourgeois, O., Le Mouélic, S., Verpoorter, C., Le Deit, L., Bibring, J.P., 2010. Martian polar and circum-polar sulfate-bearing deposits: sublimation tills derived from the North Polar Cap. *Icarus* 209, 434–451.
- Matsuoka, N., Murton, J., 2008. Frost weathering: recent advances and future directions. *Permafrost. Periglacial Process.* 19:195–210. <https://doi.org/10.1002/ppp.620>.
- Mellon, M.T., 1997. Small-scale polygonal features on Mars: seasonal thermal contraction cracks in permafrost. *J. Geophys. Res. Planets* 102:25617–25628. <https://doi.org/10.1029/97JE02582>.
- Mellon, M.T., Jakosky, B.M., 1993. Geographic variations in the thermal and diffusive stability of ground ice on Mars. *J. Geophys. Res.* 98:3345. <https://doi.org/10.1029/92JE02355>.
- Mellon, M.T., Jakosky, B.M., 1995. The distribution and behavior of Martian ground ice during past and present epochs. *J. Geophys. Res.* 100:3367. <https://doi.org/10.1029/95JE01027>.
- Mellon, M.T., Arvidson, R.E., Sizemore, H.G., Searls, M.L., Blaney, D.L., Cull, S., Hecht, M.H., Heet, T.L., Keller, H.U., Lemmon, M.T., Markiewicz, W.J., Ming, D.W., Morris, R.V., Pike, W.T., Zent, A.P., 2009. Ground ice at the Phoenix Landing Site: stability state and origin. *J. Geophys. Res. Planets* 114, E00E07. <https://doi.org/10.1029/2009JE003417>.
- Michael, G.G., Neukum, G., 2010. Planetary surface dating from crater size-frequency distribution measurements: partial resurfacing events and statistical age uncertainty. *Earth Planet. Sci. Lett.* 294:223–229. <https://doi.org/10.1016/j.epsl.2009.12.041>.
- Milliken, R.E., Mustard, J.F., Goldsby, D.L., 2003. Viscous flow features on the surface of Mars: observations from high-resolution Mars Orbiter Camera (MOC) images. *J. Geophys. Res.* 108. <https://doi.org/10.1029/2002JE002005>.
- Moran, S.R., Clayton, L., Hooke, R.L., Fenton, M.M., Andriashek, L.D., 1979. Glacier-bed landforms of the prairie region of North America. *J. Glaciol.* 23:423–424. <https://doi.org/10.1017/S0022143000030161>.
- Moratto, Z.M., Broxton, M.J., Beyer, R.A., Lundy, M., Husmann, K., 2010. Ames Stereo Pipeline, NASA's Open Source Automated stereogrammetry Software. Presented at the 41st Lunar and Planetary Science Conference, LPI, The Woodlands, Texas, p. #1533.
- Morgan, G.A., Head III, J.W., Marchant, D.R., 2009. Lineated valley fill (LVF) and lobate debris aprons (LDA) in the Deuteronilus Mensae northern dichotomy boundary region, Mars: constraints on the extent, age and episodicity of Amazonian glacial events. *Icarus* 202:22–38. <https://doi.org/10.1016/j.icarus.2009.02.017>.
- Murton, J.B., Peterson, R., Ozouf, J.-C., 2006. Bedrock fracture by ice segregation in cold regions. *Science* 314:1127–1129. <https://doi.org/10.1126/science.1132127>.
- Mustard, J.F., Cooper, C.D., Rifkin, M.K., 2001. Evidence for recent climate change on Mars from the identification of youthful near-surface ground ice. *Nature* 412:411–414. <https://doi.org/10.1038/35086515>.
- Neukum, G., 1983. *Meteoritenbombardement und datierung planetarer oberflächen*, 186. Habilit. Ludwig Maximil. Univ, München.
- Neukum, G., Hoffmann, H., Hauber, E., Head, J.W., Basilevsky, A.T., Ivanov, B.A., Werner, S.C., van Gassel, S., Murray, J.B., McCord, T., The HRSC Co-Investigator Team, 2004. Recent and episodic volcanic and glacial activity on Mars revealed by the High Resolution Stereo Camera. *Nature* 432:971–979. <https://doi.org/10.1038/nature03231>.
- Oerlemans, J., 1984. Numerical experiments on glacial erosion. *Z. Für Gletscherkunde Glazialgeol.* 20, 107–126.
- Pasquon, K., Gargani, J., Massé, M., Conway, S.J., 2016. Present-day formation and seasonal evolution of linear dune gullies on Mars. *Icarus* 274:195–210. <https://doi.org/10.1016/j.icarus.2016.03.024>.
- Pasquon, K., Gargani, J., Nachon, M., Conway, S.J., Massé, M., Jouannic, G., Balme, M.R., Costard, F., Vincendon, M., 2017. Are the different gully morphologies due to different formation processes on the Kaiser dune field? *Geol. Soc. Lond. Spec. Publ.* 467.
- Pierce, T.L., Crown, D.A., 2003. Morphologic and topographic analyses of debris aprons in the eastern Hellas region, Mars. *Icarus* 163:46–65. [https://doi.org/10.1016/S0019-1035\(03\)00046-0](https://doi.org/10.1016/S0019-1035(03)00046-0).
- Plaut, J.J., Picardi, G., Safaeinili, A., Ivanov, A.B., Milkovich, S.M., Cicchetti, A., Kofman, W., Mouginot, J., Farrell, W.M., Phillips, R.J., Clifford, S.M., Frigeri, A., Orosei, R., Federico, C., Williams, I.P., Gurnett, D.A., Nielsen, E., Hagfors, T., Heggy, E., Stofan, E.R., Plettemeier, D., Watters, T.R., Leuschen, C.J., Edenhofer, P., 2007. Subsurface radar sounding of the south polar layered deposits of Mars. *Science* 316:92. <https://doi.org/10.1126/science.1139672>.
- Plaut, J.J., Safaeinili, A., Holt, J.W., Phillips, R.J., Head, J.W., Seu, R., Putzig, N.E., Frigeri, A., 2009. Radar evidence for ice in lobate debris aprons in the mid-northern latitudes of Mars. *Geophys. Res. Lett.* 36, 02203. <https://doi.org/10.1029/2008GL036379>.
- Putzig, N.E., Phillips, R.J., Campbell, B.A., Holt, J.W., Plaut, J.J., Carter, L.M., Egan, A.F., Bernardini, F., Safaeinili, A., Seu, R., 2009. Subsurface structure of Planum Boreum from Mars Reconnaissance Orbiter Shallow Radar soundings. *Icarus* 204:443–457. <https://doi.org/10.1016/j.icarus.2009.07.034>.
- Raack, J., Reiss, D., Appéré, T., Vincendon, M., Ruesch, O., Hiesinger, H., 2015. Present-day seasonal gully activity in a south polar pit (Sisyphi Cavi) on Mars. *Icarus* 251:226–243. <https://doi.org/10.1016/j.icarus.2014.03.040>.
- Richardson, M.L., Mischna, M.A., 2005. Long-term evolution of transient liquid water on Mars. *J. Geophys. Res. Planets* 110, 03003. <https://doi.org/10.1029/2004JE002367>.
- Richardson, M.L., Wilson, R.J., 2002. A topographically forced asymmetry in the martian circulation and climate. *Nature* 416:298. <https://doi.org/10.1038/416298a>.
- Rise, L., Bellec, V.K., Ottesen, D., Bøe, R., Thorsnes, T., 2016. Hill–hole pairs on the Norwegian continental shelf. *Geol. Soc. Lond. Mem.* 46:203–204. <https://doi.org/10.1144/M46.42>.
- Robbins, S.J., Hynes, B.M., 2012. A new global database of Mars impact craters ≥ 1 km: 1. Database creation, properties, and parameters. *J. Geophys. Res. Planets* 117. <https://doi.org/10.1029/2011JE003966>.
- Roberts, D.H., Long, A.J., 2005. Streamlined bedrock terrain and fast ice flow, Jakobshavn Isbrae, West Greenland: implications for ice stream and ice sheet dynamics. *Boreas* 34:25–42. <https://doi.org/10.1111/j.1502-3885.2005.tb01002.x>.
- Röthlisberger, H., Iken, A., 1981. Plucking as an effect of water-pressure variations at the glacier bed. *Ann. Glaciol.* 2:57–62. <https://doi.org/10.3189/172756481794352144>.
- Sass, O., 2005. Rock moisture measurements: techniques, results, and implications for weathering. *Earth Surf. Process. Landf.* 30:359–374. <https://doi.org/10.1002/esp.1214>.
- Scanlon, K.E., Head, J.W., Wilson, L., Marchant, D.R., 2014. Volcano–ice interactions in the Arsia Mons tropical mountain glacier deposits. *Icarus* 273:315–339. <https://doi.org/10.1016/j.icarus.2014.04.024>.
- Scanlon, K.E., Head, J.W., Marchant, D.R., 2015. Volcanism-induced, local wet-based glacial conditions recorded in the Late Amazonian Arsia Mons tropical mountain glacier deposits. *Icarus* 250:18–31. <https://doi.org/10.1016/j.icarus.2014.11.016>.
- Schon, S.C., Head, J.W., 2011. Keys to gully formation processes on Mars: relation to climate cycles and sources of meltwater. *Icarus* 213:428–432. <https://doi.org/10.1016/j.icarus.2011.02.020>.
- Schon, S.C., Head, J.W., 2012. Gasa impact crater, Mars: very young gullies formed from impact into latitude-dependent mantle and debris-covered glacier deposits? *Icarus* 218:459–477. <https://doi.org/10.1016/j.icarus.2012.01.002>.
- Schon, S.C., Head, J.W., Milliken, R.E., 2009a. A recent ice age on Mars: evidence for climate oscillations from regional layering in mid-latitude mantling deposits. *Geophys. Res. Lett.* 36. <https://doi.org/10.1029/2009GL038554>.
- Schon, S.C., Head, J.W., Fassett, C.I., 2009b. Unique chronostratigraphic marker in depositional fan stratigraphy on Mars: evidence for ca. 1.25 Ma gully activity and surficial meltwater origin. *Geology* 37:207–210. <https://doi.org/10.1130/g25398a.1>.
- Schon, S.C., Head, J.W., Fassett, C.I., 2012. Recent high-latitude resurfacing by a climate-related latitude-dependent mantle: constraining age of emplacement from counts of small craters. *Planet. Space Sci.* 69:49–61. <https://doi.org/10.1016/j.pss.2012.03.015>.
- Segura, T.L., Toon, O.B., Colaprete, A., 2008. Modeling the environmental effects of moderate-sized impacts on Mars. *J. Geophys. Res.* 113. <https://doi.org/10.1029/2008JE003147>.
- Shean, D.E., Alexandrov, O., Moratto, Z.M., Smith, B.E., Joughin, I.R., Porter, C., Morin, P., 2016. An automated, open-source pipeline for mass production of digital elevation models (DEMs) from very-high-resolution commercial stereo satellite imagery. *ISPRS J. Photogramm. Remote Sens.* 116:101–117. <https://doi.org/10.1016/j.isprsjprs.2016.03.012>.
- Shreve, R.L., 1984. Glacier sliding at subfreezing temperatures. *J. Glaciol.* 30:341–347. <https://doi.org/10.3189/S0022143000006195>.
- Sinha, R.K., Vijayan, S., 2017. Geomorphic investigation of craters in Alba Mons, Mars: implications for Late Amazonian glacial activity in the region. *Planet. Space Sci.* 144:32–48. <https://doi.org/10.1016/j.pss.2017.05.014>.
- Sizemore, H.G., Zent, A.P., Rempel, A.W., 2015. Initiation and growth of Martian ice lenses. *Icarus* 251:191–210. <https://doi.org/10.1016/j.icarus.2014.04.013>.

- Smith, C.A., Lowell, T.V., Caffee, M.W., 2009. Lateglacial and Holocene cosmogenic surface exposure age glacial chronology and geomorphological evidence for the presence of cold-based glaciers at Nevado Sajama, Bolivia. *J. Quat. Sci.* 24:360–372. <https://doi.org/10.1002/jqs.1239>.
- Soare, R.J., Conway, S.J., Dohm, J.M., 2014. Possible ice-wedge polygons and recent landscape modification by “wet” periglacial processes in and around the Argyre impact basin, Mars. *Icarus* 233:214–228. <https://doi.org/10.1016/j.icarus.2014.01.034>.
- Soare, R.J., Conway, S.J., Gallagher, C., Dohm, J.M., 2017. Ice-rich (periglacial) vs icy (glacial) depressions in the Argyre region, Mars: a proposed cold-climate dichotomy of landforms. *Icarus* 282:70–83. <https://doi.org/10.1016/j.icarus.2016.09.009>.
- Souness, C., Hubbard, B., 2012. Mid-latitude glaciation on Mars. *Prog. Phys. Geogr.* 36: 238–261. <https://doi.org/10.1177/0309133312436570>.
- Souness, C., Hubbard, B., Milliken, R.E., Quincey, D., 2012. An inventory and population-scale analysis of Martian glacier-like forms. *Icarus* 217:243–255. <https://doi.org/10.1016/j.icarus.2011.10.020>.
- Squyres, S.W., 1978. Martian fretted terrain: flow of erosional debris. *Icarus* 34:600–613. [https://doi.org/10.1016/0019-1035\(78\)90048-9](https://doi.org/10.1016/0019-1035(78)90048-9).
- Squyres, S.W., 1979. The distribution of lobate debris aprons and similar flows on Mars. *J. Geophys. Res. Solid Earth* 84:8087–8096. <https://doi.org/10.1029/JB084iB14p08087>.
- Svitek, T., Murray, B., 1990. Winter frost at Viking Lander 2 site. *J. Geophys. Res.* 95:1495. <https://doi.org/10.1029/JB095iB02p01495>.
- Thomas, P.C., Malin, M.C., Edgett, K.S., Carr, M.H., Hartmann, W.K., Ingersoll, A.P., James, P.B., Soderblom, L.A., Veverka, J., Sullivan, R., 2000. North-south geological differences between the residual polar caps on Mars. *Nature* 404:161. <https://doi.org/10.1038/35004528>.
- Thorn, C.E., Hall, K., 1980. Nivation: an Arctic-alpine comparison and reappraisal. *J. Glaciol.* 25:109–124. <https://doi.org/10.3189/S0022143000010339>.
- Toner, J.D., Catling, D.C., Light, B., 2014. The formation of supercooled brines, viscous liquids, and low-temperature perchlorate glasses in aqueous solutions relevant to Mars. *Icarus* 233:36–47. <https://doi.org/10.1016/j.icarus.2014.01.018>.
- Tornabene, L.L., Watters, W.A., Osinski, G.R., Boyce, J.M., Harrison, T.N., Ling, V., McEwen, A.S., 2018. A depth versus diameter scaling relationship for the best-preserved melt-bearing complex craters on Mars. *Icarus* 299:68–83. <https://doi.org/10.1016/j.icarus.2017.07.003>.
- Vaucher, J., Baratoux, D., Mangold, N., Pinet, P., Kurita, K., Grégoire, M., 2009. The volcanic history of central Elysium Planitia: implications for martian magmatism. *Icarus* 204: 418–442. <https://doi.org/10.1016/j.icarus.2009.06.032>.
- Vincendon, M., 2015. Identification of Mars gully activity types associated with ice composition. *J. Geophys. Res. Planets* 120:1859–1879. <https://doi.org/10.1002/2015JE004909>.
- Vincendon, M., Mustard, J., Forget, F., Kreslavsky, M., Spiga, A., Murchie, S., Bibring, J.-P., 2010. Near-tropical subsurface ice on Mars. *Geophys. Res. Lett.* 37. <https://doi.org/10.1029/2009gl041426>.
- Waller, R.I., 2001. The influence of basal processes on the dynamic behaviour of cold-based glaciers. *Quat. Int.* 86:117–128. [https://doi.org/10.1016/S1040-6182\(01\)00054-4](https://doi.org/10.1016/S1040-6182(01)00054-4).
- Watters, W.A., Geiger, L.M., Fendrock, M., Gibson, R., 2015. Morphometry of small recent impact craters on Mars: size and terrain dependence, short-term modification. *J. Geophys. Res. Planets* <https://doi.org/10.1002/2014JE004630> (2014JE004630).
- Werner, S.C., 2009. The global martian volcanic evolutionary history. *Icarus* 201:44–68. <https://doi.org/10.1016/j.icarus.2008.12.019>.
- Whalley, W.B., Azizi, F., 2003. Rock glaciers and protalus landforms: analogous forms and ice sources on Earth and Mars. *J. Geophys. Res. Planet.* 108. <https://doi.org/10.1029/2002JE001864>.
- Williams, K.E., Toon, O.B., Heldmann, J.L., McKay, C., Mellon, M.T., 2008. Stability of mid-latitude snowpacks on Mars. *Icarus* 196:565–577. <https://doi.org/10.1016/j.icarus.2008.03.017>.
- Williams, K.E., Toon, O.B., Heldmann, J.L., Mellon, M.T., 2009. Ancient melting of mid-latitude snowpacks on Mars as a water source for gullies. *Icarus* 200:418–425. <https://doi.org/10.1016/j.icarus.2008.12.013>.
- Willmes, M., Reiss, D., Hiesinger, H., Zanetti, M., 2012. Surface age of the ice-dust mantle deposit in Malea Planum, Mars. *Planet. Space Sci.* 60:199–206. <https://doi.org/10.1016/j.pss.2011.08.006>.